AD-A097 426 UNION CARBIDE CORP OAK RIDGE TENN Y-12 PLANT F/G 11/2
MATERIALS FOR HIGH-TEMPERATURE HYDROGEN FLUORINE ENVIRONMENTS.(U)
MAR 81 C E HOLCOMBE, L KOVACH W-7405-ENG-26
UNCLASSIFIED Y-2201 NL

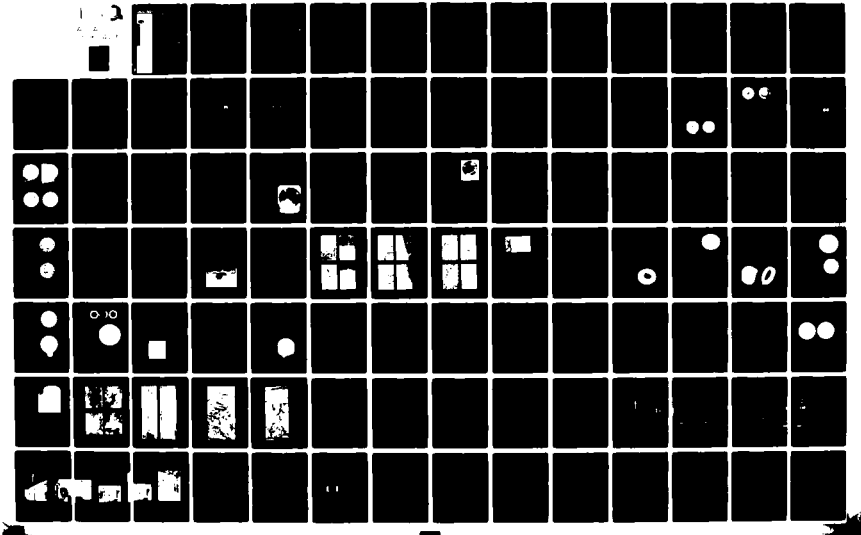

1 OF 2
AD A
097426
1.0
1.1
1.25
1.4
1.6
2.8
3.2
3.6
2.5
2.2
2.0
1.8
MICROCOPY RESOLUTION TEST CHART

UCC-ND

NUCLEAR DIVISION

UNION CARBIDE

Y-2201

LEVEL II

MATERIALS FOR HIGH-TEMPERATURE HYDROGEN FLUORINE ENVIRONMENTS

(Final Report, AFWL Project Order 78-002
June 1976 - December 1978)

C. E. Holcombe, Jr.
L. Kovach

March 1981

AD A097426

DTIC
ELECTE
APR 7 1981
C

DTIC FILE COPY

DISTRIBUTION STATEMENT A
Approved for public release;
Distribution Unlimited

81 4 3 026

Printed in the United States of America
Available from
National Technical Information Service
U. S. Department of Commerce
5285 Port Royal Road
Springfield, VA 22161

NTIS price codes
Printed copy: A07
Microfiche copy: A01

DISCLAIMER

This report was prepared as an account of work sponsored by an agency of the United States Government. Neither the United States Government nor any agency thereof, nor any of their employees, makes any warranty, express or implied, or assumes any legal liability or responsibility for the accuracy, completeness, or usefulness of any information, apparatus, product, or process disclosed, or represents that its use would not infringe privately owned rights. Reference herein to any specific commercial product, process, or service by trade name, trademark, manufacturer, or otherwise, does not necessarily constitute or imply its endorsement, recommendation, or favoring by the United States Government or any agency thereof. The views and opinions of authors expressed herein do not necessarily state or reflect those of the United States Government or any agency thereof.

Date of Issue: March 4, 1981
Distribution Category: UC-25

Y-2201

MATERIALS FOR HIGH-TEMPERATURE HYDROGEN FLUORINE ENVIRONMENTS

Final Report, AFWL Project Order 78-002
June 1976 - December 1978

C. E. Holcombe, Jr.
L. Kovach
Metals and Ceramics Department
Y-12 Development Division

DTIC
ELECTE
APR 7 1981
C

Prepared for Department of the Air Force
Air Force Weapons Laboratory
Kirtland Air Force Base, New Mexico

DISTRIBUTION STATEMENT A
Approved for public release;
Distribution Unlimited

Oak Ridge Y-12 Plant
P. O. Box Y, Oak Ridge, Tennessee 37830

Prepared for the Department of Energy
Under US Government Contract W-7405-eng-26

2

ABSTRACT

A determination has been made of the stability of 35 materials under high-temperature, fluorine rich, hydrogen fluoride torch testing. Refractory materials tested included 4 borides, 3 carbides, 3 nitrides, 12 oxides, 1 oxynitride, 1 sulfide, 10 metals, and carbon (10 types). Three materials distinctly performed better than nickel: lanthanum hexaboride, calcium hexaboride, and lanthanum silicon oxynitride. Of these, lanthanum hexaboride is the best candidate tested since it has an estimated upper use temperature > 1726 K, which is above the melting point and more than 300 K above the upper use temperature of nickel.

Accession For
NTIS GRA&I ☐
DTIC TAB ☐
Unannounced ☐
Justification
By
Distribution/
Availability Codes
Dist | Avail and/or Special
A

CONTENTS

SUMMARY 4

INTRODUCTION 5

MATERIALS FOR HIGH-TEMPERATURE HYDROGEN FLUORINE ENVIRONMENTS 7

Material Test Facility 7
- Design and Construction 7
- Operation of the Facility 10

Experimental Work 15
- Materials Selection Criteria 15
- Materials Characterization 16
- Material Test Runs 16
- General Discussion of Test Results 55

Further Materials Considerations 61
- Impregnation or Coating of Carbon with Fluoride 61
- Thermal Analyses of Fluorides 61
- Tetrafluoromethane Addition Experiments 62
- Fluorine to Hydrogen Ratio Change 64

CONCLUSIONS 70

REFERENCES 71

ACKNOWLEDGMENTS 73

APPENDIX A 75

Facility Drawings and Photos 75

APPENDIX B 79

Summary of Test Conditions During the Exposure of Specimens to a Hydrogen Fluorine Flame 79

APPENDIX C 116

Observations on Test Specimens Exposed to a Hydrogen Fluorine Flame 116

APPENDIX D 131

Tables, Figures, and Bibliography 131

SUMMARY

This investigation includes characterization of the behavior of 35 different compounds, solid solutions, and elements in an environment containing a controlled, high-temperature, hydrogen (H_2) fluorine (F_2) (generally $2F_2$ and H_2 or 2HF and F_2 torch. The design, construction, and operation of the test facility is discussed. Materials for testing included ordinary cylindrical specimens, cylindrical specimens with embedded thermocouples to determine sample temperature profiles, and test plates for a configuration test chamber.

Stability of a material in this corrosive environment is determined by the properties of the fluoride coating that forms on the surface of the material. Materials with volatile fluorides are unprotected, whereas fluoride film formers exhibit near zero corrosion below the breakpoint or film failure temperature, T_f. The T_f depends on the melting, vaporizing, and mechanical properties of the film.

T_f values were determined for 16 fluoride film formers including (in order of decreasing stability): lanthanum hexaboride (LaB_6), calcium hexaboride (CaB_6), lanthanum silicon oxynitride ($La_2O_3 \cdot Si_3N_4$), scandium (Sc), Nickel (Ni), strontium oxide (SrO), lanthanum chromite ($LaCrO_3$), yttrium (Y), yttrium oxide (Y_2O_3), nickel aluminide (NiAl), Y_2O_3 doped Ni, magnesium oxide (MgO), aluminum oxide (Al_2O_3), titanium aluminide (TiAl), beryllium oxide (BeO), and carbon (C). This work established that three materials had maximum use temperatures for near zero corrosion which were considerably greater than that for nickel [the standard material used for high-temperature hydrogen fluoride (HF) environments] : (1) LaB_6, 1800 K; (2) CaB_6, 1700 K; and (3) $La_2O_3 \cdot Si_3N_4$, 1500 K, as compared with nickel, 1400 K.

Since LaB_6 was the best material tested for stability, its fabrication and machining properties were further explored; particularly, the feasibility to form plasma-sprayed layers of LaB_6 on substrates or to form entire thin-walled structures of plasma-sprayed LaB_6. The performances of LaB_6 and other materials as test plates were also studied.

INTRODUCTION

One of the laser systems that is currently being developed by the Air Force Weapons Laboratory (AFWL), the Defense Advanced Research Projects Agency (DARPA), and the Missile Research and Development Command (MIRADCOM) is the HF chemical laser. The lasing action in this system is based on the excitation of HF molecules to an elevated vibrational state as a consequence of the highly exothermic chemical reaction between hydrogen and fluorine in the presence of helium (He) and the rapid expansion of the resultant hot gases in the laser machine.

Nickel metal has become the principal nozzle material to be used in the HF laser because of its superior resistance to attack by fluorine. However, there are some problems associated with the use of nickel; eg, the nozzles must be internally cooled, and the special machining (that is required) results in a relatively high cost per nozzle. More importantly, lasing efficiencies are penalized because of high energy losses through the flowing coolants. The AFWL was, therefore, interested in developing nozzle materials that would function without the use of liquid or gaseous coolants and would have the potential to be less expensive. This activity is referred to by the AFWL as the Advanced Low-Heat-Loss Nozzle Research Program.

At the request of the AFWL, a test facility was constructed at the Oak Ridge Y-12 Plant[a] for screening materials to be used as uncooled nozzles for an HF laser system. The facility permits the testing of candidate materials in a high-temperature (1650 to $\geq$ 2850-K) corrosive environment containing hydrogen, fluorine, HF, and helium gases. Material recommendations for this program were made on the assumption that a protective fluoride layer would be formed on usable materials, and they are detailed in the **Material Selection Criteria** section of this report. The candidate materials for high-temperature ($>$ 1000-K-surface-temperature) stability were solicited from private vendors with expertise in the field, selected from materials offered by specialty ceramic companies, or fabricated at the Y-12 Plant.

This report discusses the design, construction, and operation of the HF facility with the goal of evaluating material compatibility with a controlled hydrogen fluorine flame at atmospheric pressure. The objective was to determine the surface temperature at the onset of rapid reaction and material loss (or the surface temperature below which little or no reaction could occur) for each candidate material—thereby providing a ranking of all candidate materials in the order of their performance.

Included are the results of tests on 177 specimens in the form of: (1) cylindrical specimens, (2) cylindrical specimens with embedded thermocouples, and (3) flat plates tested in the configuration-test-chamber assembly involving 35 different materials. The upper use temperatures for near zero corrosion are presented for 16 different materials.

(a) Operated by the Union Carbide Corporation's Nuclear Division for the Department of Energy.

After initial assessment of material behavior, several tests were conducted in an attempt to improve performance and/or fabrication of the best candidate, LaB_6. The effect of gas composition (specifically the F_2:H_2 ratio) was only cursorily investigated, ie, for LaB_6; generally, all tests were done with a $2F_2$ and H_2 or a 2HF and F_2 flame to yield a most corrosive enrivonment.

MATERIALS FOR HIGH-TEMPERATURE HYDROGEN FLUORINE ENVIRONMENTS

MATERIAL TEST FACILITY

Design and Construction

In order to rank various candidate materials, a test environment closely duplicating the final end use HF laser environment with respect to gas compositions, gas flows, and temperature was required. To accomplish this, the design of the material test facility was based on a technology (to process uranium) that has been in use at the Oak Ridge Y-12 and Oak Ridge Gaseous Diffusion Plants for several years; namely, flame-reactor technology. In one specific application (the cold-wall-reactor process), the highly exothermic reaction between hydrogen and fluorine supplies the energy and temperature to initiate and sustain the hydrogen reduction of gaseous uranium hexafluoride (UF_6) to solid UF_4 (green salt).[1] This reaction was conducted in a vertical Monel[(b)] pipe reactor provided with externally wound cooling coils.

Figure 1 is an as-built flow diagram of the material test facility as designed by the Y-12 Engineering Division. The test reactor, which is the center of the facility, is made of 20-cm (8-in)-diameter Monel pipe, approximately 1.2 m (4 ft) long, with externally wound cooling coils. Drawings showing fabrication details of the reactor, the flame nozzle, and sight ports are presented in the Appendix A. Monel was used in most cases as the material of construction where a contact with fluorine gas was expected. Teflon[(c)] and Viton[(c)] were used as gasket materials, and recessed soft copper (Cu) rings were employed as gaskets with the larger flange connections. Wherever possible, all connections were welded in order to minimize the possibility of leaks and the escape of fluorine. Photographs of the facility, which include the Lexan[(d)] enclosure around the test reactor and the gas cylinder storage area, are also presented in the Appendix A.

Process gases enter the top of the reactor through a concentric-type Monel nozzle. Hydrogen flows through the core, and the helium and fluorine mixture enters through the annulus. It is possible to position the nozzle so that the distance between the nozzle tip and the test specimens can be varied. An ignition device, spark-discharge-type, was initially installed in the reactor to ensure instantaneous burning of the hydrogen and fluorine gases. Under the operating conditions subsequently employed, the use of the igniter was found to be unnecessary. Gas flows are controlled by hand-operated valves, and the rates are observed on panel-mounted flow meters. Gas flow and pressure controllers, which were to be part of the instrument controls, were not installed because of long-term delivery schedules. Automatic valves are included in the facility; but these are used only during start-up, shutdown, for purging operations, or for emergencies. The fluorine gas is supplied from a low pressure "pig," shown in Figure 1, having a capacity of about 1.3 m^3 (45 ft^3) and maintained at pressures between 0.1 to 0.3 MPa (15 to 50 psig). This distribution system minimizes the exposure of the piping, valves, gaskets, and regulators to highly pressurized fluorine in order to reduce the possibility of a fluorine release. The "pig" is refilled from a 2.8-MPa (400-psig) cylinder, as required. A chemical trap containing soda lime and a vacuum pump are employed to facilitate the transfer process.

(b) The International Nickel Company, Inc., Huntington Alloy Products Division.
(c) E.I. du Pont de Nemours & Co., Inc.
(d) General Electric Co.

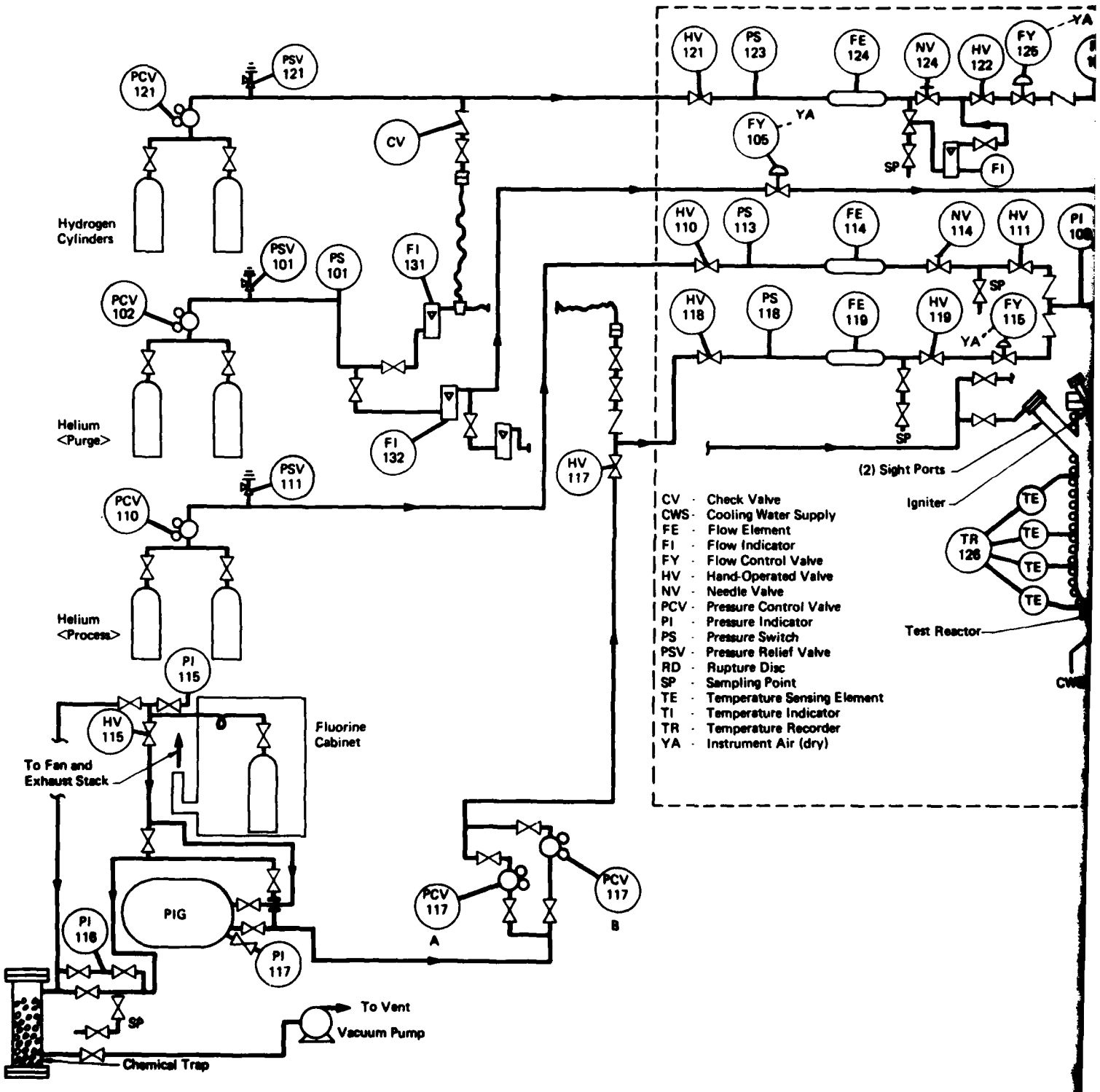

Figure 1. MATERIAL TEST FACILITY FLOW DIAGRAM.

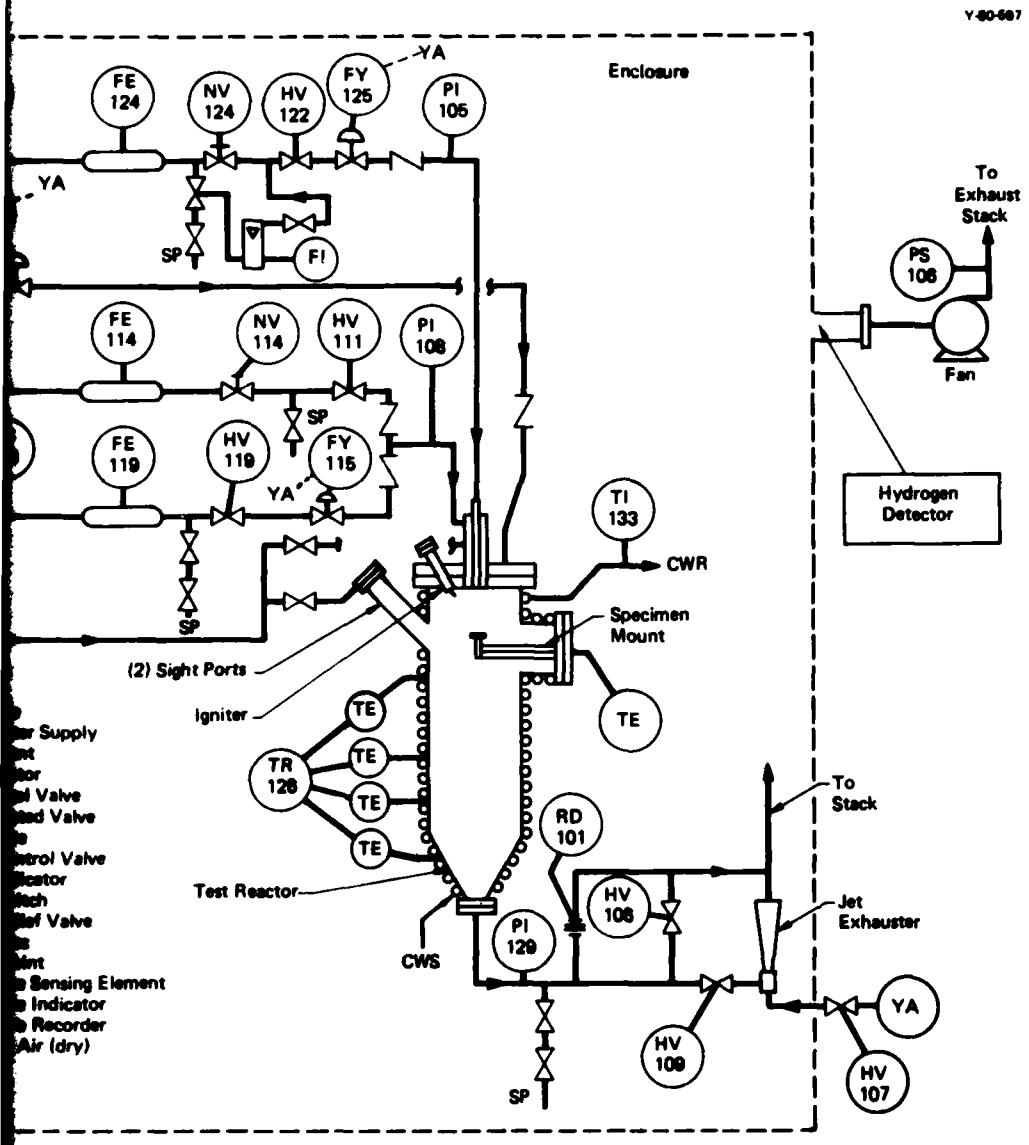

CILITY FLOW DIAGRAM.

Exhaust gases from the test reactor are discharged directly into the plume of a ventilation stack. Sampling tests conducted during a typical run gave results of less than one-half of the threshold limit value (TLV) for fluorides; namely, 2.5 mg/m^3. The jet exhauster shown in the flow diagram, Figure 1, plays no part during a test run and is used only for purging operations.

Consideration was also given to safety in the design of the facility. In order to eliminate the possibility of fluorine or hydrogen escaping into the building area, the test reactor was contained within a ventilated Lexan enclosure. Operation is not possible if the enclosure fan is not running. Any leakage of hydrogen inside the enclosure is monitored with a hydrogen detector. If a hydrogen leak occurs during a run, the hydrogen and fluorine flows are automatically shut off. Gas flows are monitored so that an audible flow alarm is sounded when a gas flow failure occurs. In the event of malfunctions or emergencies, it is possible, by means of a single emergency shutdown button to immediately shut off all process gas flows and to maintain a flow purge of helium through the reactor. The accumulation of hydrogen in the test reactor is avoided by an operating procedure which will not permit the flow of hydrogen until the helium and fluorine flows are established. Redundant valving is employed, and the manual valves that control gas flows are operated by extension handles which protrude through the Lexan enclosure.

The anticipated gas flow rates that were employed in the design of the facility are tabulated in Table 1. Total flow rates, as shown, amount to 5.7×10^{-3} m^3/s or 12 ft^3/min (standard). Design criteria called for operating temperatures between 1400 and 2400 K, which were to be attained by controlling flame temperatures. Flame temperatures were to be controlled by varying the mol ratios of the helium employed while maintaining a fluorine-to-hydrogen ratio of 2:1. A plot of flame temperatures versus mol fraction

Table 1

DESIGN GAS FLOWS IN THE MATERIALS TESTING FACILITY(1)

	Flow Rate				
	(g/min)	(g mol/min)	[$m^3s \times 10^{-3}$ (ft^3/min)]		Mol Ratio
		Inlet Gas Flows			
Helium	36.9	9.2	3.4	(7.3)	0.609
Fluorine	150.3	3.96	1.5	(3.1)	0.261
Hydrogen	3.97	1.97	0.76	(1.6)	0.130
	191.17	15.13	5.7	(12.0)	1.000
		Exit Gas Flows			
Helium	36.9	9.2	3.4	(7.3)	0.608
Fluorine	75.6	1.99	0.76	(1.6)	0.132
Hydrogen	0.0	0.0	0.0	(0.0)	0
Hydrogen Fluoride	78.8	3.94	1.5	(3.1)	0.260
	191.3	15.13	5.7	(12.0)	1.000

(1) Based on: dew point of exit gas [255 K (-17.8°C)], nozzle flow [core, hydrogen, 732 m/s (2400 ft/s); annulus, helium and fluorine, 183 m/s (600 ft/s)], and reaction temperature [(calculated) 2200 K].

reactants is presented in Figure 2; this data, which is calculated, was supplied by the AFWL. In the actual testing operations, total gas flow rates were in the order of 2.4×10^{-3} m^3/s (5 ft^3/min); and the flame temperatures ranged between 1650 and 2850 K. Attempts to use flame temperatures below 1650 K resulted in flameouts.

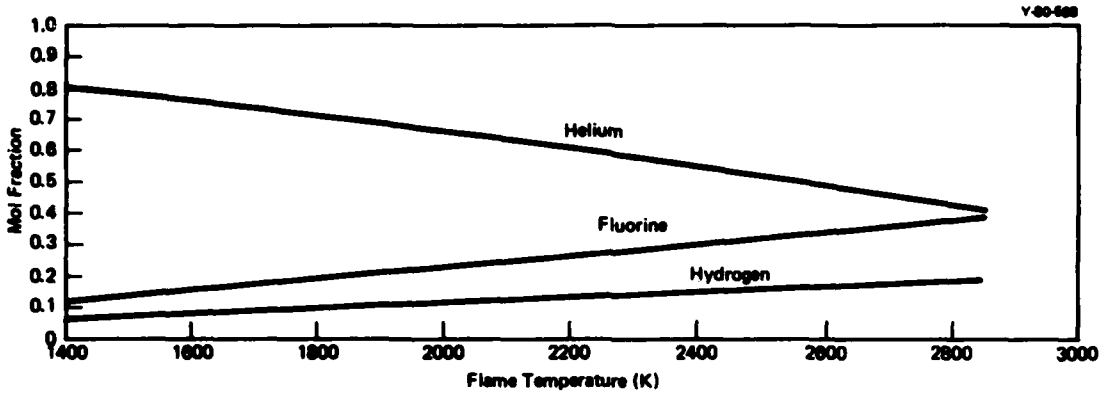

Figure 2. FLAME TEMPERATURES VERSUS MOL FRACTION REACTANTS.

Provision had been made in the design and construction of the facility to monitor the temperature profiles inside the test reactor by means of four thermocouples, each inserted into the reactor to a depth of 51 mm (2 in). After a period of operation, it was found that the thermocouple located approximately 143 mm (5.6 in) below the test specimen registered the highest readings; and the reactor wall normally became hottest in this general location. These thermocouple measurements were discontinued after Run HF-88, since it was felt that the data was not significant in our investigations.

Operation of the Facility

Passivation and Start-Up - Prior to the first operation, it was necessary to passivate the component surfaces that would contact the fluorine. Passivation involves exposing the components to gaseous fluorine under controlled conditions, thereby stabilizing the components so that they will not react catastrophically when fluorine is introduced under normal operating conditions. During construction of the facility, care was taken to ensure that no contaminants would be present to react with fluorine; the components were degreased and washed with trichlorotrifluoroethane [TF Freon(c)] and the workmen used clean gloves. Apparently, the cleanliness procedures were appropriate since the passivation step was conducted without incident.

The next essential step, prior to the testing of specimens, was to demonstrate the operability of the facility and to establish operating parameters. The chief variables that needed to be considered were: (1) the distance between the nozzle tip and test specimen, (2) the total gas flow rates, (3) gas ratios, and (4) specimen exposure time. Several exploratory runs were made with nickel specimens mounted 14 cm (5-1/2 in), 17.3 cm (6.8 in), and then 10.2 cm (4 in) from the nozzle tip. Total gas flow rates were also varied, and they ranged as high as

6.17 X 10^{-3} m^3/s (13 ft^3/min). It was found that, with a nozzle distance of 10.2 cm (4 in) and total gas flow rates of 2.3 X 10^{-3} m^3/s to 2.5 X 10^{-3} m^3/s (4.8 to 5.2 ft^3/min), a test specimen could be heated to 1900 K. Observing the test specimens during the initial runs showed that the impinging bluish flame did not make a uniform pattern on the specimen surface. By modifying the nozzle tip and replacing the single 1.1-mm-diameter hydrogen core opening with eight uniformly spaced holes which were 0.4 mm (17 mils) in diameter, a more uniform impingement pattern was established.

Test Run Procedures - The procedures were divided into five categories:

Cylindrical Specimens - The majority of the specimens tested were 25.4 mm (1 in) in diameter by 12.7 mm (1/2 in) thick. Specimens were tested singly and were supported under the HF torch by an uncooled flange-mounted fixture, as illustrated in Figure 3. A nickel support was used to hold low thermal conductivity specimens, and a graphite support plus an insulating spacer, such as Al_2O_3 (alumina) or lanthanum fluoride (LaF_3) was used for high thermal conductivity specimens. A thermocouple, sheathed in 6.4-mm (1/4-in) OD nickel tubing terminating underneath the test specimens, was used to measure the back face temperatures.

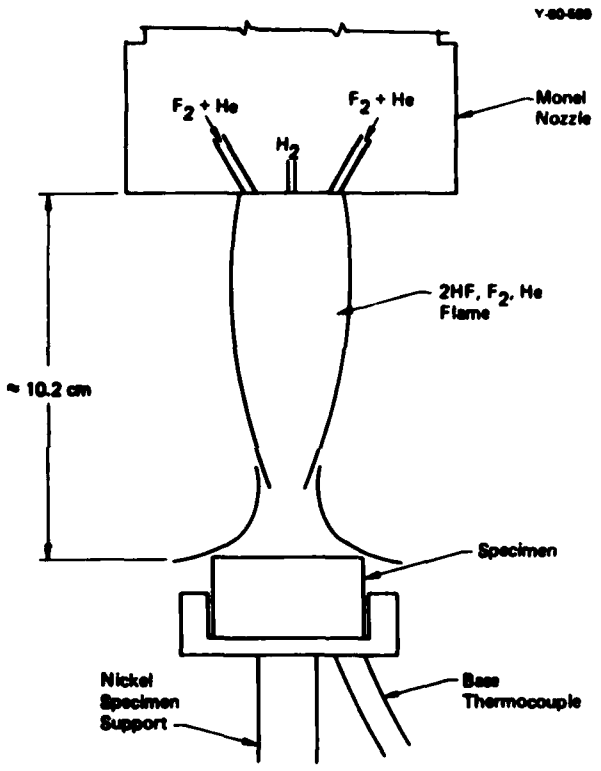

Figure 3. SCHEMATIC OF TORCH TESTER. (Cylindrical samples were tested on a nickel holder with gas temperatures determined by the exothermic hydrogen fluorine reaction and the amount of helium diluent.)

Specimen surface temperatures were determined with a calibrated automatic optical pyrometer (Leeds and Northrup,(e) Model M-9633) by sighting through one of the two sight ports installed in the side of the reactor. A 3-mm-thick sapphire window and a 12.7-mm (1/2-in)-thick quartz window were used in the sight port for the pyrometer. Calibration of the two windows (together) indicated that corrections, to be applied to the pyrometer readings, ranged from +15 to +45 K with the surface temperature range from 1175 to 2173 K (900 to 1900°C). The sapphire window

(e) Leeds and Northrup Corporation, North Wales, Pennsylvania.

which faced the reactor environment was a replacement for a second quartz window which required frequent change. The sapphire window allowed operation for a year without apparent clouding or reaction.

Although not previously mentioned, the design of the sight ports did provide for a flow of helium between the two sight windows; and it was then directed across the exposed face of the sapphire.

From test Runs HF-79 to HF-171, specimen surface temperatures were determined with both a manual and an automatic optical pyrometer. Temperature readings were made as low as 1050 K with the manual pyrometer, while automatic pyrometer readings could not be made below 1138 K. Readings made with the manual pyrometer were done with the aid of a mirror, which entailed an additional temperature correction estimated to be +20 K. The manual pyrometer permitted the operator to take temperature readings on any selected surface region (ie, hot spots); whereas, the automatic pyrometer—sighted on the center of the specimen—remained in a fixed position and used an overall average emission from the specimen center.

Thermocouple Experiments - Uncertainty existed as to the temperature corrections needed (to be added to the optical pyrometer readings) to arrive at true surface temperatures. This results from the large uncertainties in the specific emissivity values to be employed, particularly when nonblackbody specimens are involved. In an effort to approach true surface temperatures, experiments were devised whereby thermocouples were inserted into the specimens being tested. In these experiments, three platinum (Pt) [Pt-10 wt % rhodium (Rh)] thermocouples [1.0 mm (0.040 in) in diameter and sheathed with nickel] were placed into 1.5-mm (0.060-in)-diameter holes drilled into the usual 25.4-mm (1-in) diameter, 12.7-mm (0.5-in)-high test specimen; a fourth thermocouple monitored the specimen backface temperature. A typical specimen showing the thermocouple locations is presented in Figure 4. The thermocouples were monitored with a multipoint recorder, which was capable of making 10 measurements per minute for each thermocouple.

During the course of the experimental runs, in addition to the thermocouple measurements, both manual and automatic pyrometer readings were taken along with visual observations.

Configuration Test Chamber - Upon completion of the screening phase encompassing the testing of 25.4-mm (1-in)-diameter cylindrical specimens, another testing phase was initiated for the purpose of evaluating the erosion effects as well as the chemical and temperature effects of the HF torch gases on candidate test materials. This investigative phase was conducted in a configuration-test-chamber assembly shown in Figure 5. As designed, the chamber is threaded onto the existing nozzle assembly within the reactor to permit easy installation and removal. In this threading operation, the spacing between the nozzle tip and the test plate is adjusted (within limits) to the desired distance. The sight port, which has a sapphire window,

permits visual observation of the HF flame and its effect on the test material and also permits scanning with the automatic optical pyrometer. The deflection ring, shown in *Figure* 5, was included for the purpose of reducing eddy currents and the possibility of accelerated corner corrosion. Although not shown, a pressure tap connected to a pressure gage was provided to monitor the chamber pressure. Initially, the chamber was fabricated from ATJ graphite because of its low cost, easy machinability, and low corrosion rate in a fluorine environment at temperatures below 975 K (700°C). Test materials were fabricated as test plates, 3.8 mm (0.150 in) thick, which were fastened to the bottom of the chamber; the plates were removed from the Monel reactor without disturbing the chamber.

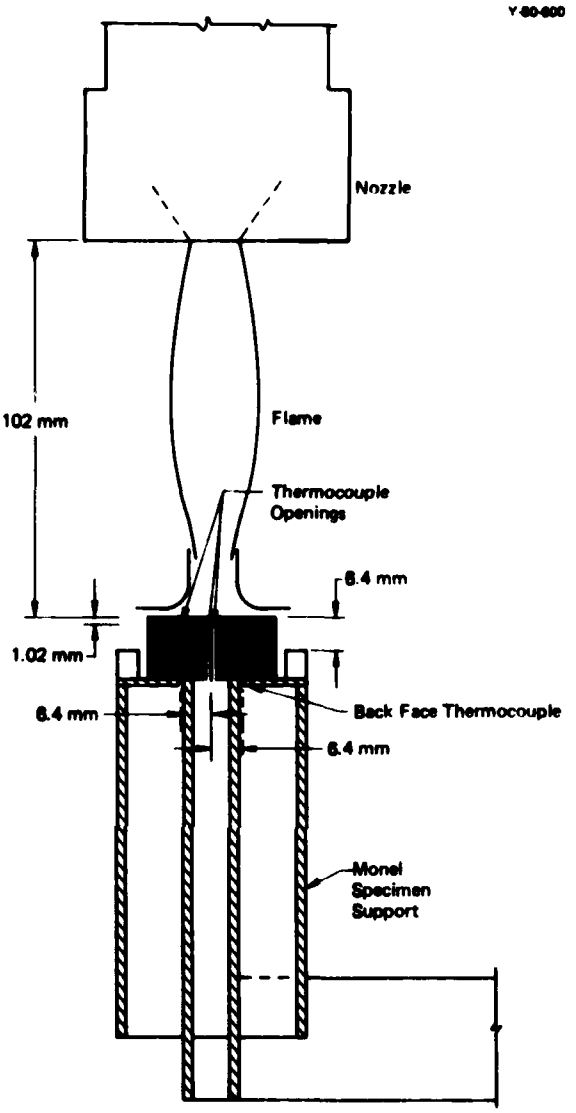

Figure 4. THERMOCOUPLE LOCATIONS.

A redesign of the nozzle normally used for specimen testing was also undertaken. Instead of a tapered coaxial converging flame, it was desired to have a broader flame front to equalize temperatures and exposure on the test plates with larger surfaces. Design details of the redesigned nozzle may be found in Appendix A.

Beryllium Oxide Tests - As previously mentioned, in the operation of the facility, exhaust gases from the reaction chamber are discharged directly into the plume of the building's ventilation stack. Because of the toxicity of finely divided beryllium (Be) compounds, it was necessary to meet specific industrial hygiene requirements to permit testing of BeO in this device. A stainless steel filter unit with a porous Monel element having 930 cm^2 of filter area and a removal rating of 100% for 1.0-μm-sized particles was installed in the 5-cm exhaust line. During the specimen testing runs, the filter performed satisfactorily; and there was no observable

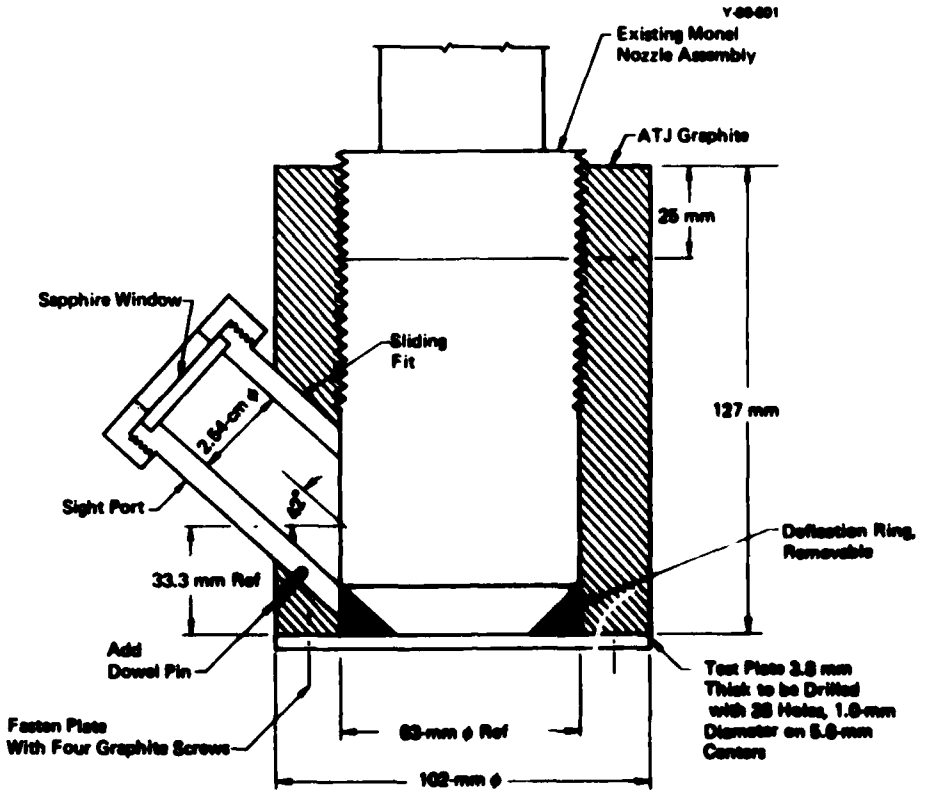

Figure 5. CONFIGURATION-TEST-CHAMBER ASSEMBLY.

differential pressure. Upon completion of the runs, the reaction chamber was determined to be highly contaminated with Be. However, the contamination in the exhaust piping (adjacent to the filter and at the filter) was found to be acceptable (well below the maximum allowable working limit). After a complete cleaning of the chamber with TF Freon and water and after additional contamination tests, the equipment was deemed acceptable to permit resumption of normal operations.

Observations on Test Specimens - Specimens were cleaned with TF Freon, dried, weighed, and dimensionally inspected before each test. Behavior during the tests was visually observed, and posttest weight and dimensions were recorded. By monitoring sample behavior after exposure at a particular temperature and by examining automatic pyrometry measurements (which gave instant recording of rapid reactions), it was possible to correlate sample stability with temperature. The torch test procedure was developed to the point of an intermittent thermogravimetric analysis of material behavior in $2F_2$ and H_2.

Fluoride film morphology was examined on selected specimens by scanning electron microscopy (SEM), and fluorides were identified by X-ray diffraction.

EXPERIMENTAL WORK

Materials Selection Criteria

In order to select materials that might perform well in the corrosive $2F_2$ and H_2 environment, certain criteria were initially used. Since fluorides are quite stable (ΔG_f in the range -30 to -140 kcal per gram-atom of fluorine),[2] fluoride formation on any refractory surface was considered ensured in a high-temperature fluorine rich environment; ie, none of the nonfluorides would be unreactive to the excess fluorine in the torch gas. Therefore, a material should form a protective fluoride layer in order to restrict reaction with the substrate candidate.

The optimum candidate should have a high-melting-point low-vapor-pressure fluoride film that forms on a substrate material with good mechanical strength, thermal shock resistance, and a high melting point. Arbitrarily, it was desired that the fluoride layer remain protective (allowing near zero corrosion of the substrate) above 1400 K. Low-melting eutectics between the substrate and the fluoride film were avoided. The possibility was considered of finding an unknown mixed fluoride with a higher melting point and a lower vapor pressure than the known pure fluorides. These requirements dictated alkaline-earth or rare earth fluoride formers as primary candidates [consisting of magnesium (Mg), calcium (Ca), strontium (Sr), barium (Ba), scandium (Sc), yttrium (Y), lanthanum (La), and cerium (Ce) as well as nickel].

A low heat-of-reaction to form the fluoride film (with a correspondingly lower surface-temperature rise on fluoride formation) was believed to increase the possibility of film stability; thus, a preliminary thermodynamic ranking gave oxides, nitrides, sulfides, carbides, and borides in the order of their decreasing stability.

Initially, fluoride film stability was thought related to the coefficients of thermal expansion (CTE) of the fluoride layer and the substrate as well as the lattice matching of fluoride layer and substrate. Having a minimal CTE difference between layer and substrate and having similar lattices should reduce any tendency of the fluoride layer to microcrack or spall. As fluorides typically have a high CTE, the substrate should either have a high CTE or be capable of plastic flow or deformation (as metals or some intermetallics).

Thermal shock resistance of the substrate would be greatest for a material with low CTE, high thermal conductivity, high strength, and low modulus of elasticity. Metals, graphite, and loaded carbon were accordingly expected to have the best thermal shock resistance.

Multicomponent systems such as intermetallics, binaries, cermets, and impregnated materials were also considered, although a greater potential for eutectics was surmised.

Water reactivity of specimens, based on alkaline-earth or rare earth elements, was recognized as a handling problem; but samples were tested, since this could be controlled to some extent by proper procedures (eg, argon filled glove boxes and low-humidity rooms).

Materials Characterization

The ceramic materials employed in this investigation are characterized by the data presented in Table 2. Most samples were procured as hot-pressed cylinders, nominally > 99% pure and > 90% dense. Sapphire ($01\bar{1}0$ exposed surface) and magnesia (100 exposed surface) single crystals in the typical cylindrical shape were also obtained. Lanthanum chromite, a candidate material for magnetohydrodynamic (MHD) generator channels, was purchased as a pressed-and-sintered cylinder. Sintered Al_2O_3 [Coors[f] AD-995] specimens were also used. The materials containing silicon nitride (Si_3N_4) were hot-pressed at Y-12: for Si_3N_4 (+5 wt % MgO), conditions were 1925 K, 1 hour, 13.8 MPa (2000 psi); for La_2O_3·Si_3N_4, conditions were 1875 K, 1 hour, 20.7 MPa (3000 psi). At Y-12, one calcium aluminate ($CaAl_4O_7$) specimen (P-31) was sintered (1675 K, 1 hour) and one (HF-51) was hot-pressed: 1500 K, 1.25 hours, 24.1 MPa (3500 psi). One BeO specimen (HF-134) was also hot-pressed at Y-12 with conditions: 1325 K, 0.5 hour, 6.9 MPa (1000 psi).

The fluorine gas used in the runs had a specified purity of 98.5% with a maximum carbon compound content of 0.1% and a maximum sulfur, as sulphur hexafluoride (SF_6), content of 0.01%. The hydrogen gas was designated as an ultrapure grade with a specified total impurity level of ≤ 10 ppm. The purity of the helium used as diluent in the HF flame was 99.9995%.

Material Test Runs

Some 35 different materials were investigated in 177 separate runs in the HF test facility. A compilation of the materials tested, the type of test conducted with each material, and the respective run numbers are itemized in Table 3. A summary of the run data which includes pyrometer and thermocouple temperature readings, flame temperatures, gas flows, and time periods may be found in Appendix B. Additional data, including dimensional and weight changes in the test specimens plus visual observations, are presented in Appendix C.[g]

Early in the investigation, it was observed that most of the ceramic specimens had low thermal shock resistance. It was necessary to employ a modified heating cycle to successfully evaluate these materials. By gradually increasing and, during cool down, decreasing the temperature of the HF torch (generally in ≤ 200 K incremental steps), cycles were developed which ensured material survival. As previously mentioned, torch temperatures were controlled by varying the helium flow rates.

Midway in the investigative program, after about 40 different tests, a preliminary ranking of the best candidates for an uncooled laser nozzle was established: namely, LaB_6, MgO, Al_2O_3, and carbon. Work with these materials (and also nickel and NiAl) was extended to

---

(f) Coors Porcelain Co.

(g) All data gathered for this report were recorded in English units (ie, standard cubic feet per minute, mils, inches) and have subsequently been converted to centimeter-gram-second units.

Table 2

CHARACTERIZATION OF REFRACTORY CERAMIC SAMPLES

Materials	Supplier or Vendor	Determined by Mercury Porosimeter: Bulk Density (g/cm^3)	Theoretical Density (%)	Open Porosity (%)	Impurity Level Information: Impurities (wt % level)[1]	Remarks[2]
BeO (HF-134)	Y-12	3.00	99.3	0.6	None detected	MS indicated > 99.99% pure, contains 390 wt ppm Li or 0.22 wt % Li_2O.
BeO (Berlox K-150:HF-133)	National Beryllia[3]	2.87	95.0	0.1	Mg (0.15), Si (0.2)	MS indicated > 99.54% pure; 0.08 wt % Al, probably clay-bonded.
MgO (HF-7, 9, 155)	Norton[4]	2.77	76.9	22.7	Ta (< 0.15), Cs (< 0.6), Rb (< 0.15), P (< 1), Si (0.15), U (< 0.3)	ES.
MgO (HF-67, 72-74, 138)	Research Chemicals (Haselden)[5]	3.50	97.2	0	Ta (< 0.15), Cs (< 0.6), Rb (< 0.15), P (< 1), U (< 0.3)	ES.
MgO Single Crystal (HF-137, 147)	Materials Research[6]	3.60	100.0	0	None detected	No impurities > 35 wt ppm, VC.
Al_2O_3 (P-23-24; HF-5, 21, 22, 24, 38, 39, 58, 69, 71, 79, 89, 90, 126, 130-132, 135, 159)	Coors[7]	3.91	98.0	0	Si (0.1)	MS indicated 99.75% pure.
Sapphire Single Crystal (Al_2O_3: HF-120, 121)	Electronic Space Products[8]	3.99	100.0	0	None detected	MS indicated > 99.93% pure.
CaO (HF-48)	Cerac[9]	2.62	78.4	16.5	Fe (0.1), Mg (0.2), Si (0.1)	VC by ES, typically 99.8% pure.
Sc_2O_3 (HF-93)	Research Chemicals (Haselden)	3.43	88.9	8.9	Ta (< 0.15), Cs (< 0.6), Rb (0.2) P (< 1), Cd (1.5), U (0.3)	ES.
SrO (HF-14, 47, 83, 88)	Cerac	4.48	88.4	6.6	Ta (< 0.15), Cs (< 0.6), Rb (< 0.15), P (< 1), Ba (0.5), U (< 0.3)	ES.
Y_2O_3 (P-19, 36; HF-53, 54)	Cerac	3.04	60.4	37.5	None detected	No impurities detected at a level > 50 ppm, VC by ES, typically 99.9% pure.
Y_2O_3 (HF-162, 163)	Ceradyne[10]	4.98	99.0	0	Ta (< 0.15), Al (0.3), Cs (< 0.6), Rb (< 0.15), P (< 1), U (< 0.3)	ES.
BaO (HF-2, 46, 62)	Cerac	5.02	87.8	8.8	Al (0.1), Ca (0.1), Sr (0.1)	VC by ES, typically 99.5% pure.
CeO_2 (P-14, 35; HF-52, 61)	Cerac	6.48	90.0	8.1	Na (0.15)	VC by ES, typically 99.9% pure.
$CaAl_4O_7$ (HF-51) (P-31)[11]	Y-12	2.87	97.6	2.6	Fe (0.21), Na (0.13), Mg (0.9)	VC by unspecified chemical analyses, typically 97% pure.
$CaZrO_3$ (HF-81)	Research Chemicals (Haselden)	4.44	95.5	0.1	Hf (0.20), Mg (0.15), Ta (< 0.15) Cs (< 0.6), Rb (< 0.15), P (< 1), Fe (0.12), Si (0.15), Li (0.15), U (< 0.3)	ES.
$LaCrO_3$[12] (HF-122,123)	A-T Research[13]	6.08	89.8	2.9	Ta (< 0.15), Cs (< 0.6), Rb (< 0.15), P (< 1), Th (< 0.3)	ES.
ATJ Graphite (HF-3, 11, 17, 28, 30-36, 70, 77, 129, 139, 144-146, 148, 156, 168, 172, 176)	Union Carbide[14]	1.55	68.6	29.1	None detected	No impurities detected at a level > 125 ppm, ES.
SiC (HF-68)	Research Chemicals (Haselden)	2.95	91.6	0.1	Ta (< 0.15), Al (5), Cs (< 0.6), Rb (< 0.15), P (< 1), Ti (0.15), B (0.15), U (< 0.3)	ES, ~ 5% Al as a hot-pressing aid.
80TaC-20HfC (HF-19, 20)	Cerac	10.90	77.3	21.3	Fe (0.18) Ti (0.1)	VC by ES, note Zr not measured, typically 99% pure.

ATJ Graphite (HF-3, 11, 17, 28, 30-36, 70, 77, 129, 138, 144-148, 148, 188, 188, 172, 176)	Union Carbide[14]	1.86	68.6	29.1	None detected	No impurities detected at a level > 125 ppm, ES.
SiC (HF-68)	Research Chemicals (Haselden)	2.95	91.6	0.1	Ta (< 0.15), Al (5), Cs (< 0.6), Rb (< 0.15), P (< 1), Ti (0.15), B (0.15), U (< 0.3)	ES, ≈ 5% Al as a hot-pressing aid.
80TaC·20HfC (HF-19, 20)	Cerac	10.90	77.3	21.3	Fe (0.18) Ti (0.1)	VC by ES, note Zr not measured, typically 99% pure.
64WC·36HfC (P-20, HF-6)	Cerac	10.22	70.4	28.0	Ta (0.1), Ti (0.1), Nb (0.1)	VC by ES, note Zr not measured, typically 99% pure.
CaB_6 (HF-87)	Cerac	1.97	81.1	20.8	Mg (0.6), Ta (< 0.15), Cs (< 0.6), Rb (< 0.15), P (< 1), Fe (0.3), Si (0.15) Li (0.25), U (< 0.3)	ES.
CaB_6 (HF-165, 167, 169)	Ceradyne	2.43	100.0	0.1	Mg (0.9), Ta (< 0.15), Cs (< 0.6), Rb (< 0.15), P (< 1), Fe (0.15), Li (0.12)	ES.
LaB_6 (Dense Cylinders: HF-69, 75, 76, 78, 98-103)	Research Chemicals (Haselden)	4.66	96.8	0.2	None detected	MS indicated > 99.84% pure.
LaB_6 (Dense Cylinders: HF 141-143, 171)	Research Chemicals (Haselden)	4.68	99.4	0.7	None detected	MS indicated > 99.84% pure.
LaB_6 (Dense Plates: HF-188, 200)	Ceradyne	4.69	97.5	0	None detected	MS indicated > 99.89% pure.
LaB_6 (Plasma-Sprayed Plates: HF-173, 175)	Y-12	3.85	81.7	18.9	None detected	MS indicated > 99.94% pure.
LaB_6 (Plasma-Sprayed Plates: HF-174)	Y-12	3.97	84.3	15.8	None detected	MS indicated > 99.95% pure.
LaB_6 (Plasma-Sprayed Liner)	Y-12	4.00	84.9	7.4	Not determined	
BN (HF-12)	Union Carbide	1.93	85.0	15.7	Not given	VC greater than 97.5% wt % BN.
Si_3N_4[15] (Nominal 5 wt % MgO: HF-127)	Y-12	3.16	99.1	0.9	Mg (5), Ta (< 0.15), Al (0.3), Cs (< 0.6) Rb (< 0.15), P (< 1), Ca (0.15)	ES.
YN (HF-49)	Cerac	4.72	80.1	11.8	Ta (0.8)	VC by ES, typically 99% pure.
$La_2O_3·Si_3N_4$[12] (HF-125)	Y-12	3.75	80 est	20.3	Ta (< 0.15), Cs (< 0.6), Rb (< 0.15) P (< 1), Th (< 0.3)	ES.
CaS (P-29, HF-55)	Cerac	5.31	88.8	7.4	None detected	No impurities detected at a level > 150 ppm, VC by ES, typically 99.5% pure.

(1) Determined at a detection level > 0.1 wt %.
(2) Spark source mass spectrographic analysis (MS); emission spectrographic analysis (ES), vendor certification (VC).
(3) National Beryllia Corporation, Haskell, New Jersey.
(4) Norton Company, Worcester, Massachusetts.
(5) Research Chemicals Division of Nucor Corporation, Phoenix, Arizona (samples prepared by Haselden Corporation, San Jose, California).
(6) Materials Research Corporation, Orangeburg, New York.
(7) Coors Porcelain Company, Golden, Colorado.
(8) Electronic Space Products, Inc., Los Angeles, California.
(9) Cerac, Inc., Milwaukee, Wisconsin.
(10) Ceradyne, Inc., Santa Ana, California.
(11) Density information and impurity levels apply for HF-51, only impurity levels apply for P-31.
(12) X-ray diffraction indicated single phase.
(13) A-T Research Company, Vichy, Missouri.
(14) Union Carbide Corporation, Carbon Products Division, Chicago, Illinois.
(15) X-ray diffraction indicated: major phase = $\beta - Si_3N_4$
intermediate phase = $\alpha - Si_3N_4$.

the thermocouple experiments to determine breakpoint or film failure temperatures[h] and to the experiments in the configuration test chamber.

It became evident that the machining of LaB_6 into prescribed shapes was difficult and slow. Hence, investigative efforts which are still underway[i] turned to find materials containing lanthanum with the capability of surviving in the HF flame environment and of having good machining characteristics.

The latter portion of the investigative work was concerned with testing plasma-sprayed LaB_6, the fabrication and testing of specimens containing lanthanum, and the testing of other materials of interest to the program.

Carbon and Graphite - Graphite has a maximum use temperature, which depends upon the formation of a carbon monofluoride (CF_x) type film, CF_x ($X \approx 1$). An X-ray diffraction analysis showed this film to have the CF_x type diffraction pattern,[3] (copper K_α radiation) Figure 6, with reflections at 6.0, 2.23, and 1.30 A. Graphite materials consistently exhibited a performance pattern related to film formation. At the beginning of an experimental run, sparks fly from the surface of the graphite specimen. This is attributed to loose carbon particles not removed by cleaning which react rapidly to go from carbon to CF_4 (tetrafluoromethane) because of the high surface area. Before the surface temperature of the specimen reaches red heat ($\approx$ 1075 K or 800°C), a gray-to-white film forms. No overall corrosion is observed as long as the film is adherent and continuous. As the substrate heats, a breakpoint temperature is reached at which the CF_x film is no longer intact, and the highly exothermic substrate reaction of carbon to CF_4 is initiated. Film breakdown normally occurs at an edge (for cylindrical specimens) and can be visually observed as a rapid peeling or burn-off action, which sweeps across the top and side of the specimen. A wide spectrum of carbon and graphite specimens (11) were tested, and they displayed similar characteristics; there were no discernible trends in behavior. An attempt was

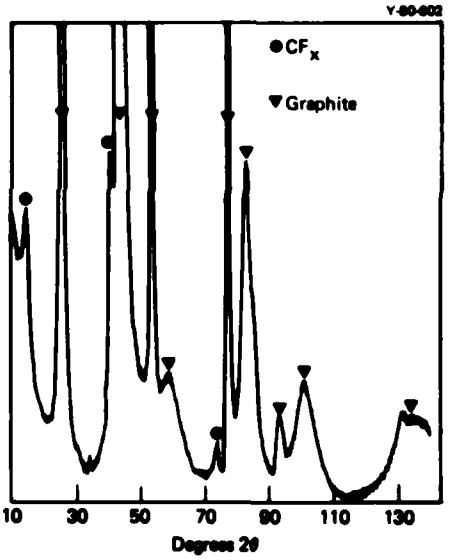

Figure 6. THE X-RAY DIFFRACTION PATTERN OF A GRAY FILM (ON A POCO GRAPHITE BLOCK) RESULTING FROM TREATMENT WITH A HYDROGEN FLUORIDE TORCH. THE SCAN SHOWS THE PRESENCE OF CARBON MONOFLUORIDE LINES.

(h) The authors define breakpoint or film failure-point temperature as: the surface temperature of a specimen at which the fluoride film effectively loses its protective characteristics and rapid reaction takes place; little or no corrosion takes place below the breakpoint temperature.

(i) DARPA Order No. 3565.

made to determine corrosion rates for essentially all the carbon and graphite cylindrical specimens tested in this program. From visual observations or recorded data, it was possible to establish when the (CF_x) film (0.08 mm or ≈ 0.003 in thick) left a specimen so as to have a time basis for making calculations. The resultant data are presented in Figure 7, in which percent weight loss per second is plotted versus specimen surface temperatures. Since the specimen surface temperatures varied during each test, the plotted temperature values are the centroid temperatures, determined from the areas under the curves of time versus temperature. Though the results are scattered, they do indicate a trend; namely, corrosion rates increase with rising temperatures.

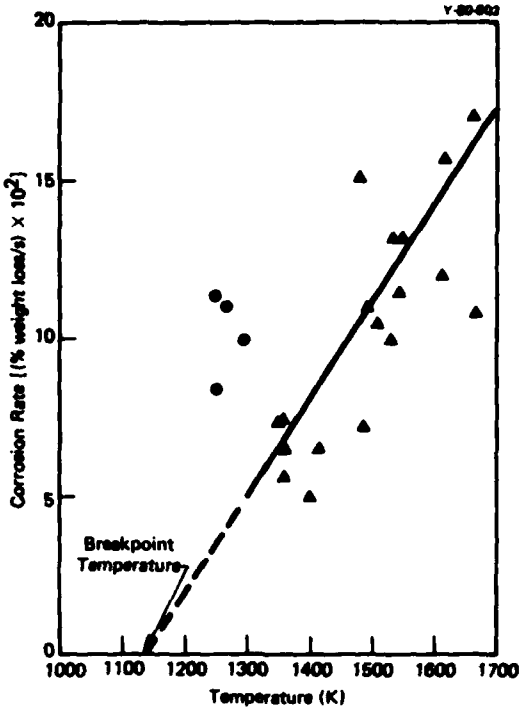

Figure 7. CORROSION RATE FOR CARBON AND GRAPHITE SPECIMENS.

The thermal behavior of a graphite specimen during a test run was graphically depicted by the thermocouple experiments. Two runs, HF-139 and HF-144, were made with an ATJ graphite specimen; time-versus-temperature data for Run HF-144 are plotted in Figure 8. It is seen that the specimen reached a breakpoint temperature of 1138 K, according to the top thermocouple reading, and then experienced another rapid temperature rise to reach a maximum surface temperature of 1543 K. Automatic and manual pyrometer readings are included in Figure 8, and these show the specimen surface temperature, in the temperature region of 1500 K, to be about 40 K higher than the TC 3 (top) thermocouple reading.

Runs were made in the configuration test chamber with two ATJ graphite test plates which were 3.81 mm thick, drilled with 36 1.0-mm (0.040-in)-diameter holes, set in a square array on 5.59-mm (0.220-in) centers. In the first run, HF-145, a flame temperature of 1700 K was employed. After 5.6 min, the run was terminated. At no time did the plate get hot enough to enable pyrometer readings to be taken.

In the second run, HF-146, the flame temperature was 1900 K. After about 4.25 min, the test plate started to react, as evidenced by the rapid rise in both thermocouple and pyrometer temperature readings. The holes in the test plate were observed to increase in size, and the pressure in the test chamber dropped to 0.103 MPa (0 psig).

Figures 9 and 10 show the conditions of the test plates that were exposed to the HF flame during Runs HF-145 and HF-146. For Run HF-145, the test plate shows that the protective

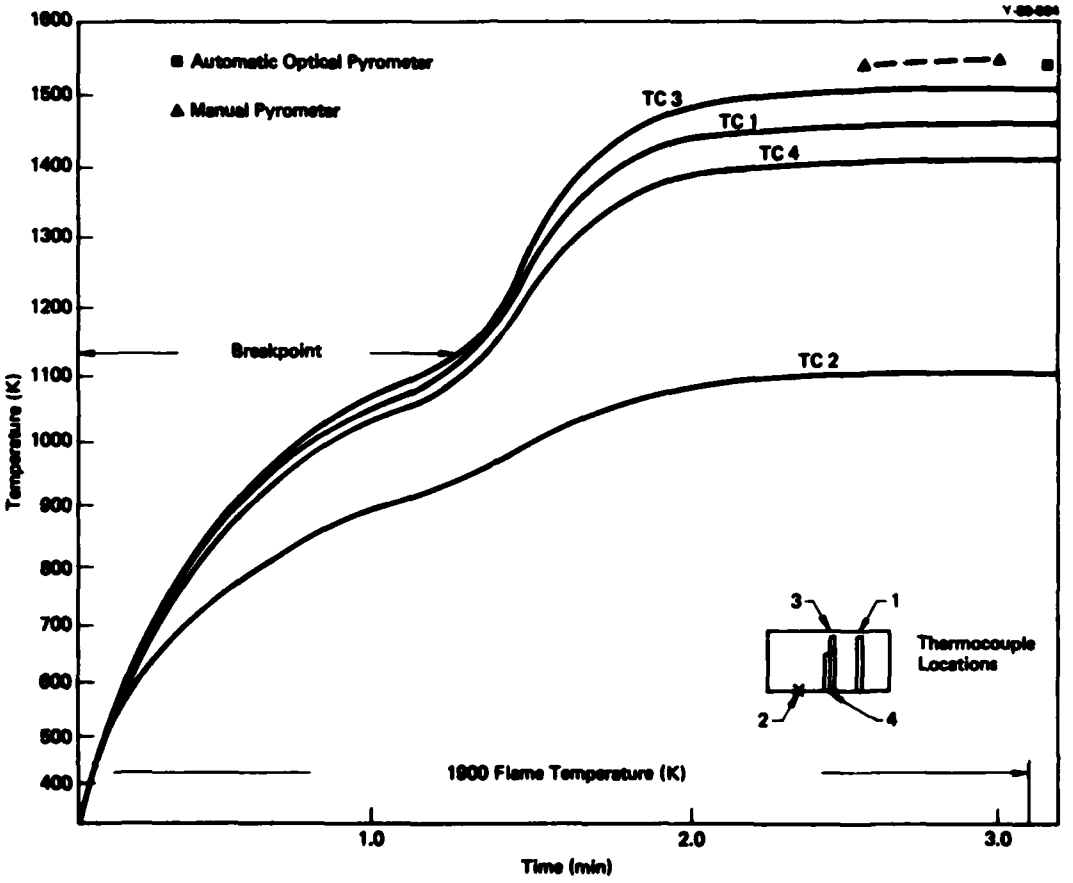

Figure 8. TEMPERATURE-VERSUS-TIME CURVE FOR ATJ GRAPHITE EXPOSED TO HYDROGEN FLUORIDE FLAME. (Run HF-144).

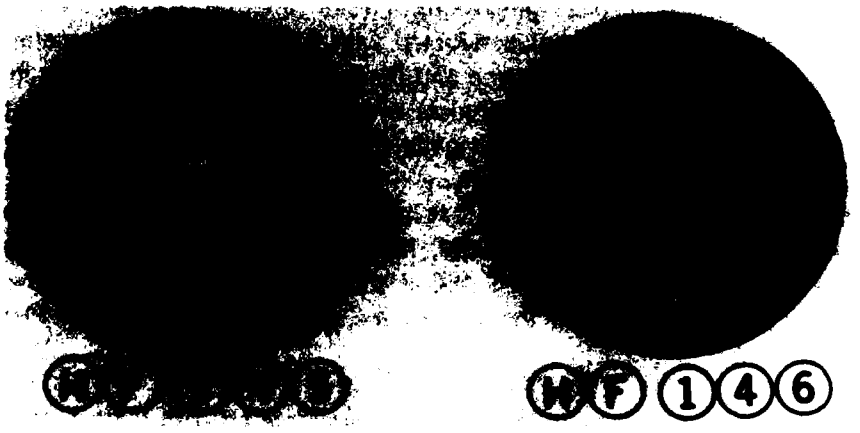

176378

Figure 9. THE ATJ GRAPHITE TEST PLATE FACES EXPOSED TO HYDROGEN FLUORIDE FLAME. (Runs HF-145 and HF-146.)

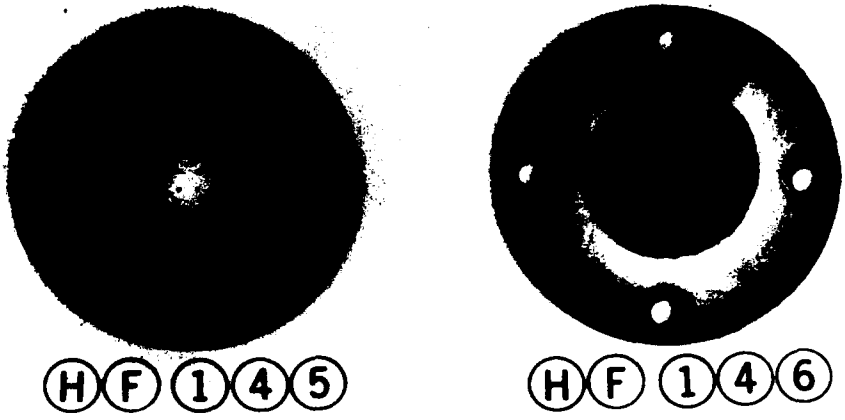

179375

Figure 10. THE ATJ GRAPHITE TEST PLATE BACK FACES. (Runs HF-145 and HF-146.)

CF_x film was retained and that there was no evidence of corrosion. For Run HF-146, the protective film in the center area with the holes is gone, and enlargement of the holes and corrosion in this area is evident. Figure 10 shows the faces of the plates that were directed away from the HF flame. One comment to be made in regard to Plate HF-146 (back face) is that the temperature in the white outer ring area was lower (<1138 K) than the temperature in the center.

Examination of the test-chamber assembly, upon completion of both runs, showed that the interior was still black and unaffected and had, therefore, experienced no appreciable temperature rise. Two additional ATJ graphite plates, 3.8 mm (0.150 in) thick, were fabricated for testing in the chamber; but the openings in the plates were slots instead of holes. Each plate had five slots, 12.7 mm (0.500 in) long, spaced 5.6 mm (0.220 in) apart with tapered cross sections. Typical dimensions of a slot (for Run HF-156) are shown by the sketch, Figure 11. Run HF-156 was conducted with a 1900 K flame temperature. In an interval of 38 s, the graphite plate reacted and its surface temperature rapidly increased to 1635 K. Figure 12 shows the face of the plate that had been exposed to the HF flame, and Figure 13 shows the back face of the test plate (HF-156). It is apparent that corrosion had occurred in the immediate area of the slots, and the slots had increased in width. A second run, HF-158, was conducted with a 1700 K flame temperature. Here, too, the graphite plate reacted and temperatures increased rapidly; however, not until 4.3 min of the run had elapsed. The exposed face of Plate HF-158 is shown in Figure 14. Again, the corrosive action is seen to have occurred in the area of the slots. The back face of Plate HF-158 appears in Figure 15.

Evidently there was a difference in behavior between Plate HF-146 (with holes) and Plate HF-156 (with slots) in that—under the same operating conditions—the plate with the slots reacted much more rapidly, 38 s versus 4.25 min. This behavior is explained by differences in configuration. The sharp thin edges within the slots protruded into the hot gas stream and

heated up more rapidly to the temperature at which the protective film failed and corrosion began.

Alumina - The behavior of Al_2O_3 under the HF flame proved to be similar to that of graphite, except that it required a slower heating cycle. At low temperatures, a stable aluminum fluoride (AlF_3) film forms, which inhibits corrosion as long as it remains intact. Above the breakpoint temperature, the film sublimes and corrosion is rapid.

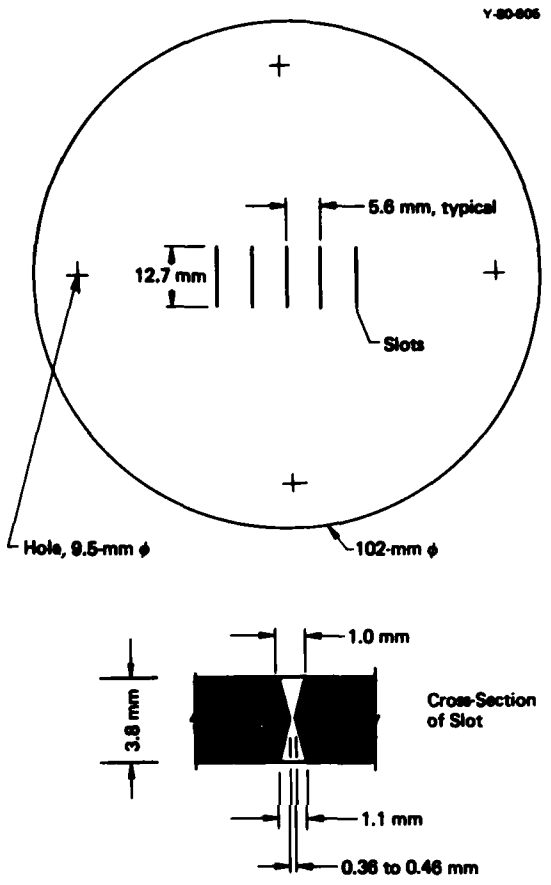

Figure 11. GRAPHITE TEST PLATE. (Run HF-156.)

Four experiments were conducted with Al_2O_3 in attempts to determine true specimen surface and breakpoint temperatures. Temperature readings taken during the course of the first experiment (Run HF-90) which included thermocouple, manual, and automatic pyrometer readings are shown in Figure 16. The difference in temperature, ΔT, between the top and bottom thermocouples increased from zero to over 300 K after approximately 7 min of flame exposure. Apparently the ΔT was not great enough to cause catastrophic thermal shock cracking at elevated temperatures. The calculated true surface temperature of the specimen was determined from the thermocouple measurements employing a transient heat conduction equation with consideration for surface recession. Up to approximately 1148 K, the calculated true surface temperature is observed to be 5 to 15 K higher than the TC 2 (top) thermocouple reading. Above 1148 K, the pyrometer readings exceed the TC 2 thermocouple readings by 55 to 115 K.

Two of the experiments (HF-130 and HF-131) were conducted under conditions in which specimen surface temperatures were below the breakpoint temperature. In Figure 17, temperature-versus-time data are shown for Run HF-131. In this plot, the surface temperatures, as determined by manual pyrometer readings, differ from the TC 3 (top center) thermocouple readings by 10 to 30 K. Run HF-132 was conducted so that specimen surface temperatures extended beyond the Al_2O_3 breakpoint temperature; temperature-versus-time data are presented in Figure 18. Here, the manual pyrometer readings correspond closely to the top center thermocouple readings (ΔT being 10 to 30 K) until the breakpoint is reached. Then, as a result of rapid exothermic reaction, specimen surface and thermocouple temperatures rise sharply; and the ΔT between them increases to as much as

181359

Figure 12. THE ATJ GRAPHITE TEST PLATE FACE EXPOSED TO HYDROGEN FLUORIDE FLAME. (Run HF-156.)

181362

Figure 13. THE ATJ GRAPHITE TEST PLATE BACK FACE. (Run HF-156.)

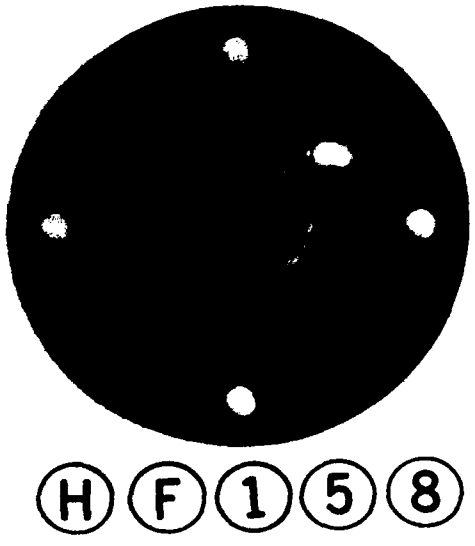

181360

Figure 14. GRAPHITE TEST PLATE FACE EXPOSED TO HYDROGEN FLUORIDE FLAME. (Run HF-158.)

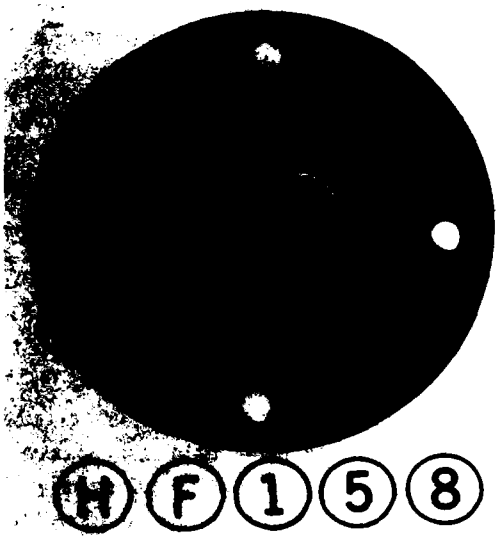

181361

Figure 15. GRAPHITE TEST PLATE BACK FACE. (Run HF-158.)

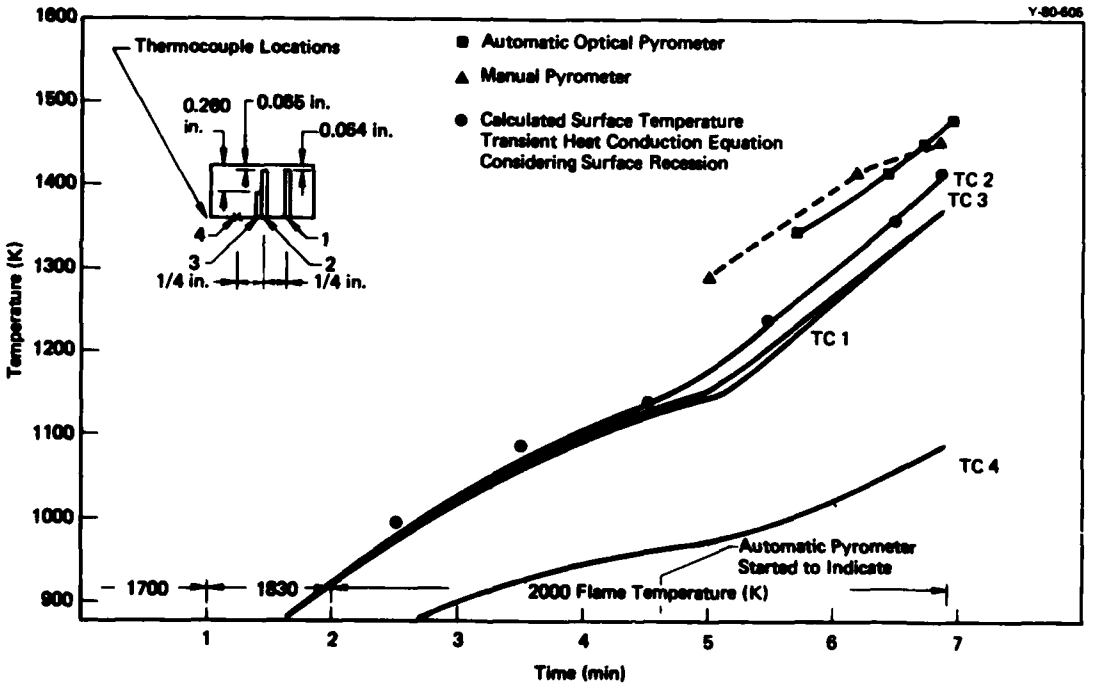

Figure 16. TEMPERATURE-VERSUS-TIME CURVE FOR THERMOCOUPLE EXPERIMENT WITH ALUMINA EXPOSED TO HYDROGEN FLUORIDE FLAME. (Run HF-90.)

1200
1100
1000
900
800
700
600
500
400
Temperature (K)

Figure 17.
MAXIMU

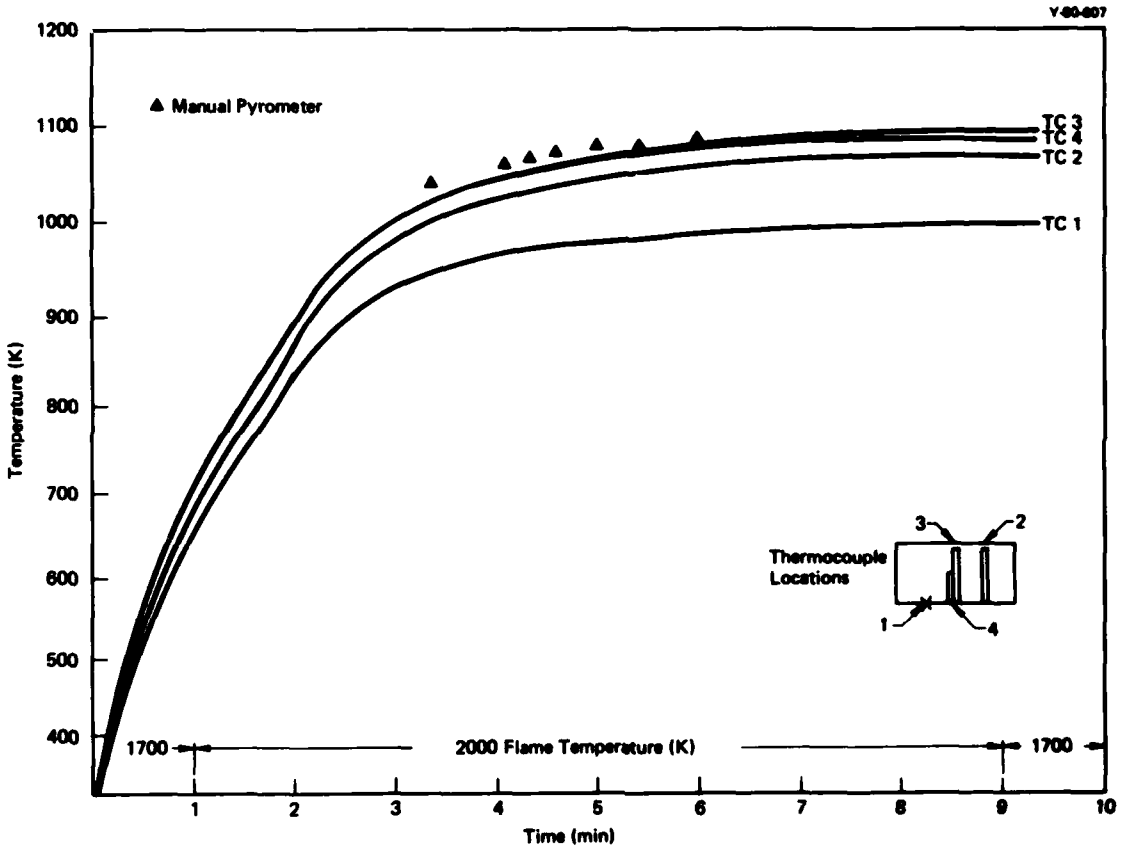

Figure 17. TEMPERATURE-VERSUS-TIME CURVES FOR THERMOCOUPLE EXPERIMENT WITH ALUMINA BELOW MAXIMUM SURFACE TEMPERATURE FOR NEAR ZERO CORROSION. (Run HF-131.)

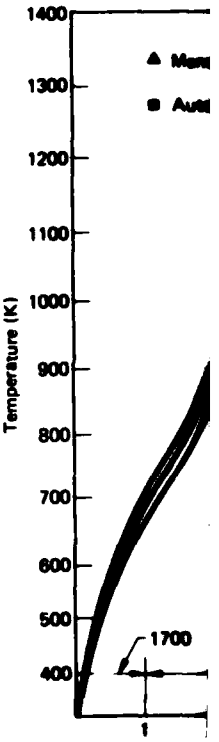

Figure 18. TEMPERA
TEMPERATURE EX
HF-132.)

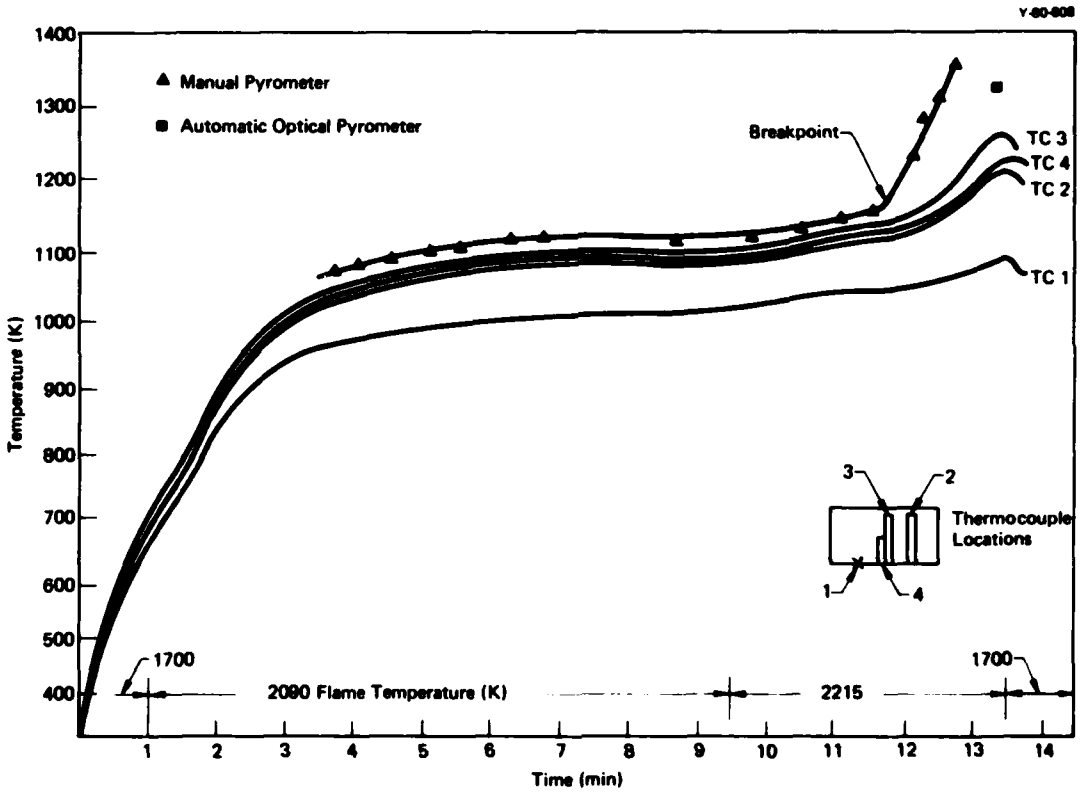

A BELOW

Figure 18. TEMPERATURE-VERSUS-TIME CURVES FOR THERMOCOUPLE EXPERIMENT WITH ALUMINA WITH TEMPERATURE EXCEEDING THE MAXIMUM SURFACE TEMPERATURE FOR NEAR ZERO CORROSION. (Run HF-132.)

150 K. In this instance, HF-132, the breakpoint temperature was 1178 K. A breakpoint occurred during another run (HF-135), which was indicated by the automatic pyrometer recorder; this value was 1183 K. Recorded breakpoints were seldom seen with Al_2O_3 specimens, since the point at which the automatic pyrometer starts to record is close to the AlF_3 film failure point.

A single crystal specimen of Al_2O_3 was tested (Runs HF-120 and HF-121) and appeared to behave like the polycrystalline material except with a possibly higher corrosion rate. By X-ray diffraction, the index of the face of the sapphire single crystal which was exposed to the torch was the $(01\bar{1}0)$. Thus, this orientation may result in more favorable reaction kinetics from the atomic packing arrangement.

An experiment (Run HF-159) conducted in the configuration test chamber with a specimen plate of Al_2O_3 was not successful in that a section of the plate cracked and fell away; this was not evident until the run was completed. With a flame temperature of 1700 K, the surface of the Al_2O_3 reached a maximum of 1416 K as determined by the automatic pyrometer. No temperature breakpoints were noted on either the pyrometer recorder or thermocouple recorder charts. Figure 19 shows the exposed side of the plate, which evidently experienced some corrosion.

181383

Figure 19. ALUMINA TEST PLATE FACE EXPOSED TO HYDROGEN FLUORIDE FLAME.

Similarly, as with graphite, calculations were made to ascertain corrosion rates for Al_2O_3. Again, as presented in Figure 20, corrosion rates expressed as percent weight loss per second are plotted versus specimen surface temperatures. A trend is also observed in the data, in that corrosion rates increase with rising temperatures.

Magnesia - An early test (Run HF-7) of MgO indicated that an adherent protective coating of magnesium fluoride (MgF_2) formed on exposure to the HF flame at a recorded specimen surface temperature of 1233 K and remained intact. This coating was

estimated to be in excess of 2μm thick by ion microprobe and X-ray diffraction.

Several experiments were conducted to determine the maximum temperature use limit for MgO. In one of the experiments (Run HF-74), the specimen was observed to start melting at the edge after a 3-min and 50-s exposure to a 2320 K flame; the surface melted rapidly after initiation, with the molten region moving across the specimen. Analysis, afterward, by X-ray diffraction of a melted droplet showed major constituents of MgO and MgF_2, as would be expected for the eutectic.

Examination of the recorded automatic pyrometer temperature data for Run HF-74 showed that a breakpoint of 1248 K was attained, after which the temperature rapidly rose to 1757 K. This breakpoint temperature is lower than the eutectic temperature for MgO-MgF_2, which is reported to be 1485 K.[4]

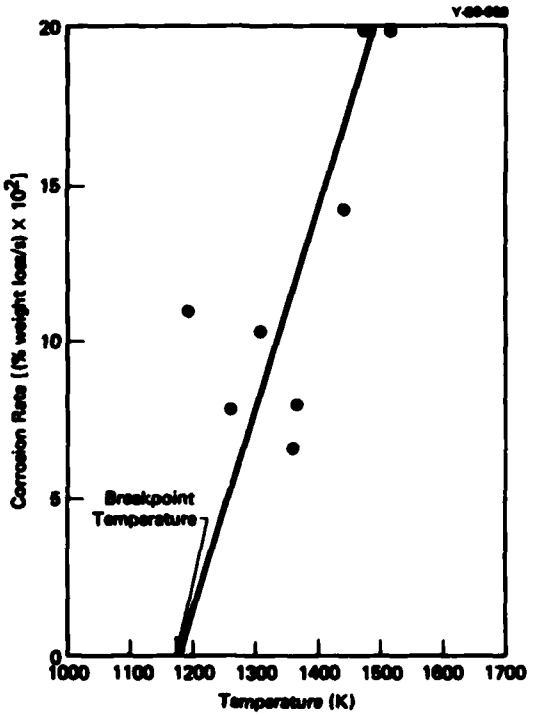

Figure 20. CORROSION RATE OF ALUMINA.

A test run (HF-137) was also conducted with a single crystal specimen of MgO oriented in the [100] direction; this run was almost identical to the polycrystalline MgO run. A breakpoint occurred at 1241 K, after which the temperature rapidly rose to 1375 K (with no emissivity corrections) where a characteristic endothermic temperature drop was recorded which indicated the melting of the MgO-MgF_2 eutectic. This cooling was observed visually for a few seconds. The temperature then continued to rise to a maximum of 1692 K. Temperature-versus-time data for Run HF-137 are shown in Figure 21. The ΔT between the reported MgO-MgF_2 eutectic (1485 K)[4] and that recorded at the endotherm in Figure 21 is 110 K; this is indicative of the amount of emissivity correction for this specimen (≈ 0.3).

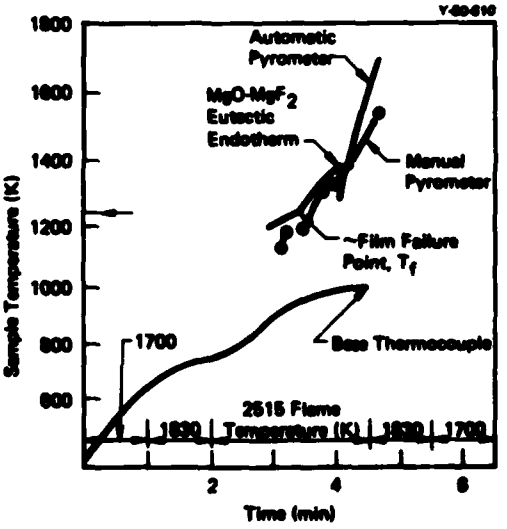

Figure 21. TEMPERATURE-VERSUS-TIME CURVE FOR MAGNESIA (SINGLE CRYSTAL) EXPOSED TO HYDROGEN FLUORIDE FLAME. (Run HF-137.)

An attempt to conduct a thermocouple experiment with a dense polycrystalline MgO

specimen was unsuccessful in that the specimen split in a plane running through the three drilled thermocouple holes. A second run was attempted with a single crystal MgO specimen having only two thermocouple holes. After operating for 5.25 min, the run was aborted because the flame was off center. Upon adjustment of the nozzle, the run (HF-147) was continued with the same specimen even though it had developed visible cracks. The run was terminated after 17.05 min, during which time it was observed that a portion of the specimen had melted and the center thermocouple hole had become visible.

Temperature-versus-time data for Run HF-147 are plotted in Figure 22. The data indicate that a breakpoint occurred at about 1279 K, after which there was a rapid temperature rise to 1421 K (per automatic pyrometer scan). Up to and beyond the breakpoint, the pyrometer readings are higher than the TC 3, top thermocouple, temperatures by some 30 to 70 K.

A MgO plate, having multiple holes and the same configuration as the graphite plate (HF-145), described in the Carbon and Graphite section, was fabricated and tested in the

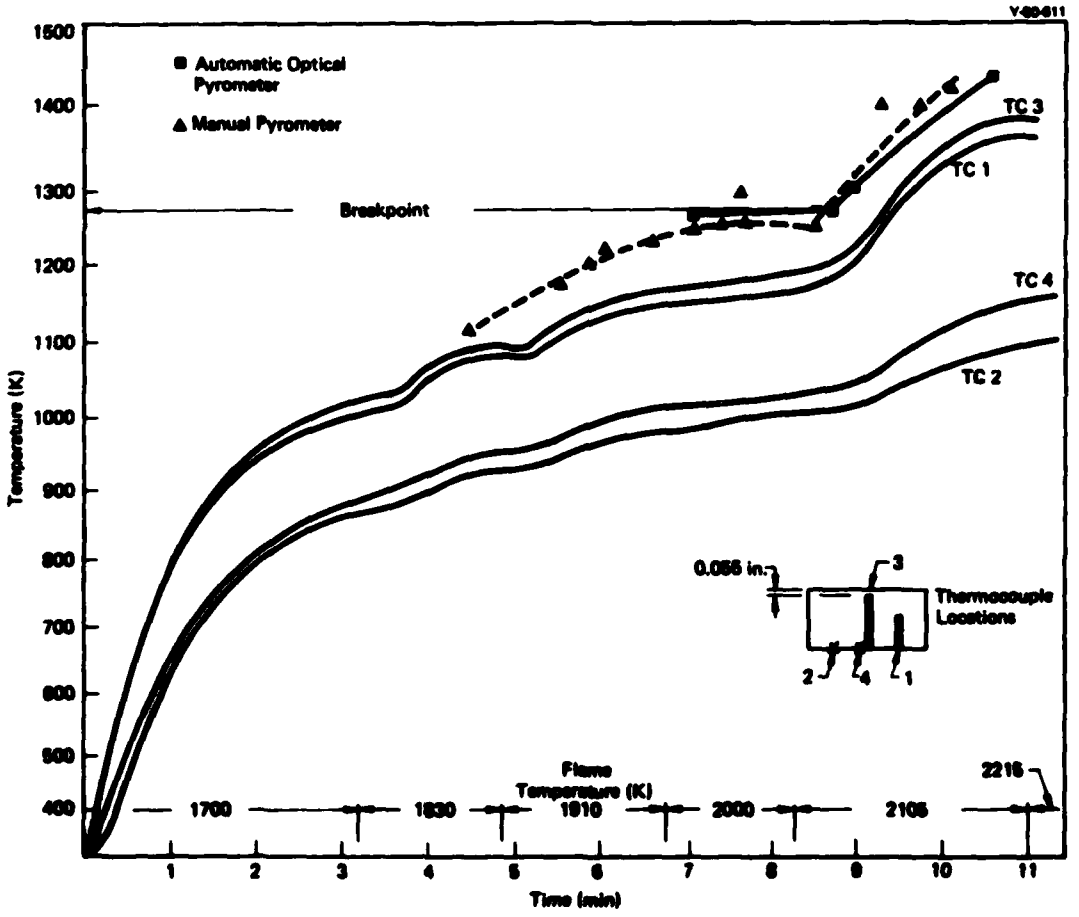

Figure 22. TEMPERATURE-VERSUS-TIME CURVE FOR MAGNESIA (SINGLE CRYSTAL) EXPOSED TO HYDROGEN FLUORIDE FLAME. (Run HF-147.)

configuration test chamber. During the run (HF-155), the plate cracked into several pieces, which may have occurred at the start. After 3.93 min, a breakpoint temperature of 1247 K was attained, as observed on the pyrometer recorder chart. This value compares well with the other breakpoint data reported above for MgO. The exposed face of the MgO plate after the test is shown in Figure 23, where it is seen that the center area with the holes did experience some corrosion. An additional observation was made in this run; namely, that the interior of the graphite chamber had reacted with the HF flame gases since a higher flame temperature was needed to test the MgO plate to the failure point.

181389

Figure 23. THE MAGNESIA FACE PLATE EXPOSED TO HYDROGEN FLUORIDE FLAME. (Run HF-155.)

From the tests conducted with MgO, it appears that: (1) there is little effect from grain boundaries or purity on the upper use temperature, and (2) fluoride film protection on MgO ceases at 125 K below the eutectic (MgF_2 and MgO) temperature of 1485 K. The loss of film protection is probably the result of vaporization of the fluoride which could be appreciable below its melting point. Microcracking or spalling of the fluoride film is not likely since the CTE values of MgO and MgF_2 are similar.[5]

Beryllia - Two grades of BeO were obtained—Berlox K-150,[(j)] and a high-purity Y-12 material. From Table 2, it can be seen that the Y-12 grade contained < 400 wt ppm lithium as its main impurity, whereas the Berlox material has approximately 0.5% impurities (apparently from a clay hot-pressing aid).

Test runs were made on the two oxides using cylindrical specimens. Figure 24 shows the temperature-versus-time data (Run HF-133) for the Berlox specimen. The data for the Y-12 material (Run HF-134) is shown in Figure 25. For Berlox, the film created an initially darker appearance on the top surface of the sample, during the run, as compared to the edges. This is attributed to the thicker film on top as compared to the edge. Because of this initial darker appearance, it was possible to note when the top and edges appeared equally hot. The temperature where this occurred coincided with the point where surface temperature began to rapidly rise or where film protection ceased. The darker film phenomenon did not occur for the Y-12 BeO, so this darkness may be related to the higher level of impurities in Berlox. The Y-12 grade appeared to survive higher surface

(j) National Beryllia Corporation, Haskell, New Jersey.

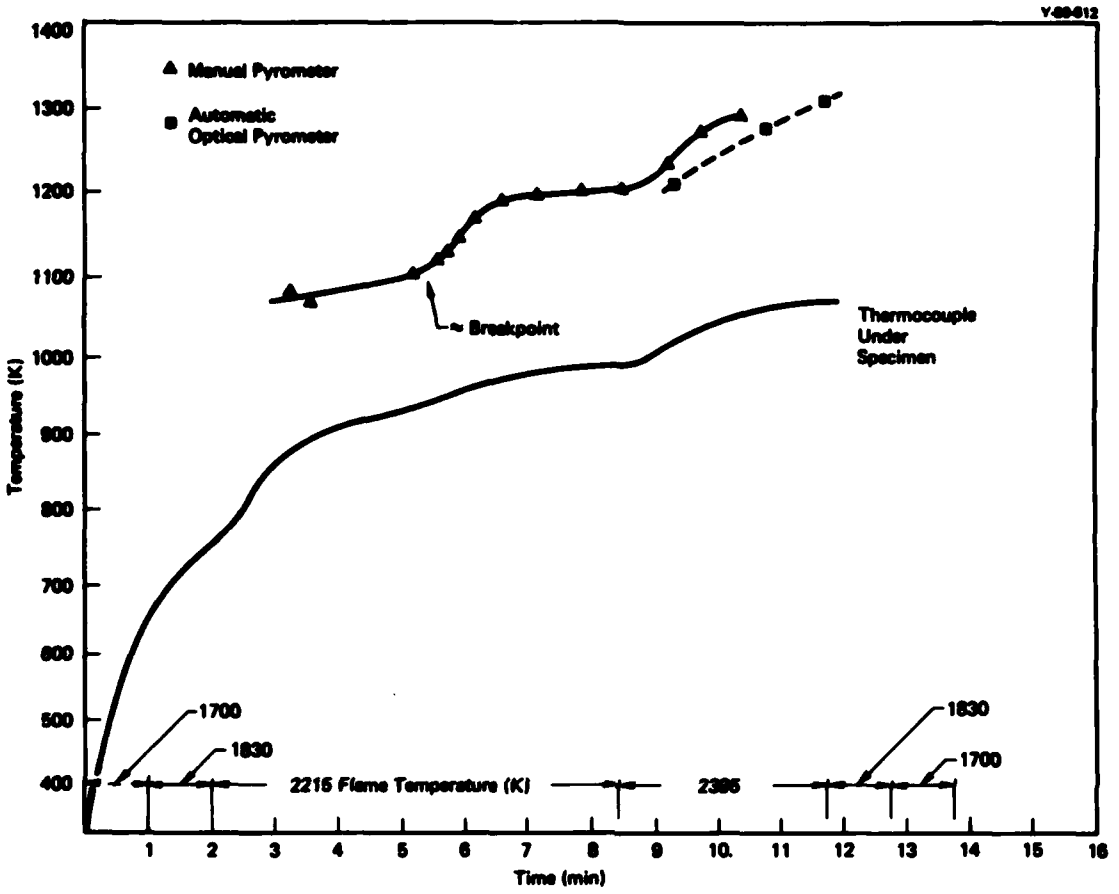

Figure 24. TEMPERATURE-VERSUS-TIME CURVE FOR BERYLLIA (BERLOX K-150) EXPOSED TO A HYDROGEN FLUORIDE FLAME. (Run HF-133.)

temperatures (approximately 65 K) before failure. Apparent breakpoints, as determined from the plotted data, are 1093 K for the Berlox specimen and 1158 K for the Y-12 specimen.

The melting temperature of beryllium fluoride (BeF_2) is from 825 to 1075 K,[6,7] and an oxyfluoride ($2BeO \cdot 5BeF_2$) may[7] or may not[8] exist—melting at 1025 K.[7] Therefore, the maximum surface temperature for near zero corrosion (or breakpoint) of BeO is reasonable, especially since both the fluoride and oxyfluoride would be present as a glass with its viscosity decreasing with increasing temperature past its melting range. That BeO reacts rapidly at 1273 K with fluorine had also been established in an earlier study[9] of refractories in halogen environments.

Other Oxides - On the basis of fluoride melting-point criteria alone, barium oxide (BaO), calcium oxide (CaO), and strontium oxide (SrO) might be suitable materials in a HF flame environment; however, such is not the case. These materials cracked when they were tested, and the resultant fluoride layers on the specimens were flaky and nonadherent after testing

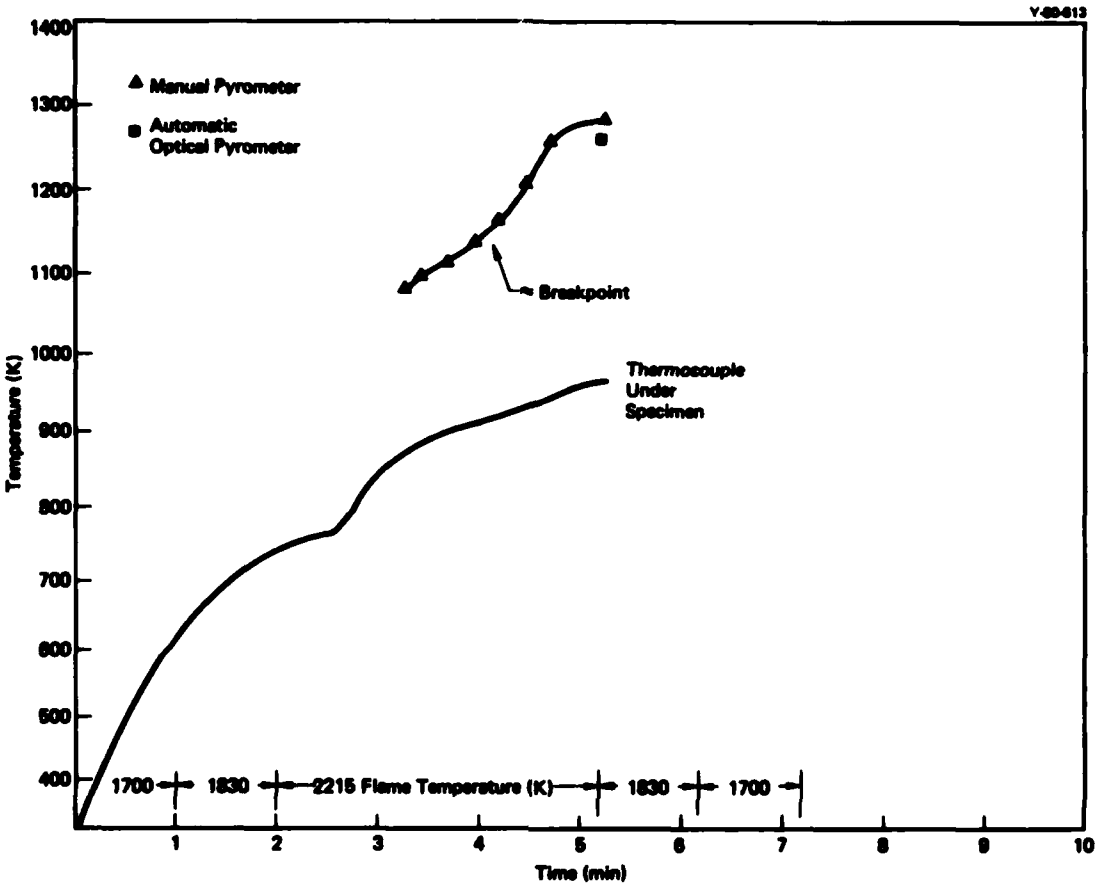

Figure 25. TEMPERATURE-VERSUS-TIME CURVE FOR BERYLLIA (Y-12) EXPOSED TO A HYDROGEN FLUORIDE FLAME. (Run HF-134.)

(possibly from moisture reactivity). In addition, their hygroscopicity would introduce complicated fabrication problems, since they react readily with the water vapor in the atmosphere.

Exposure of a high-porosity (38%-open-pore) yttria (Y_2O_3) to the HF flame resulted in disintegration of the specimens. Dense material was obtained with zero open porosity corresponding to 99% theoretical density. This material remained thermal shock-sensitive but could be tested using programmed gas flows (Runs HF-162, HF-163). A temperature-versus-time curve for Run HF-163 is presented in Figure 26. As shown, a breakpoint occurs at 1340 K (1422 K with assumed emissivity correction), nearly identical to the reported[10] yttrium fluoride YF_3 melting point of 1421 K and there is an additional temperature rise to a maximum of 1486 K. The specimen did, however, split into three parts after its temperature exceeded the breakpoint temperature.

Since the breakpoint temperature for Y_2O_3 apparently represents the fluoride melting point, the following is indicated: (1) that either no oxide/fluoride eutectic occurs or the

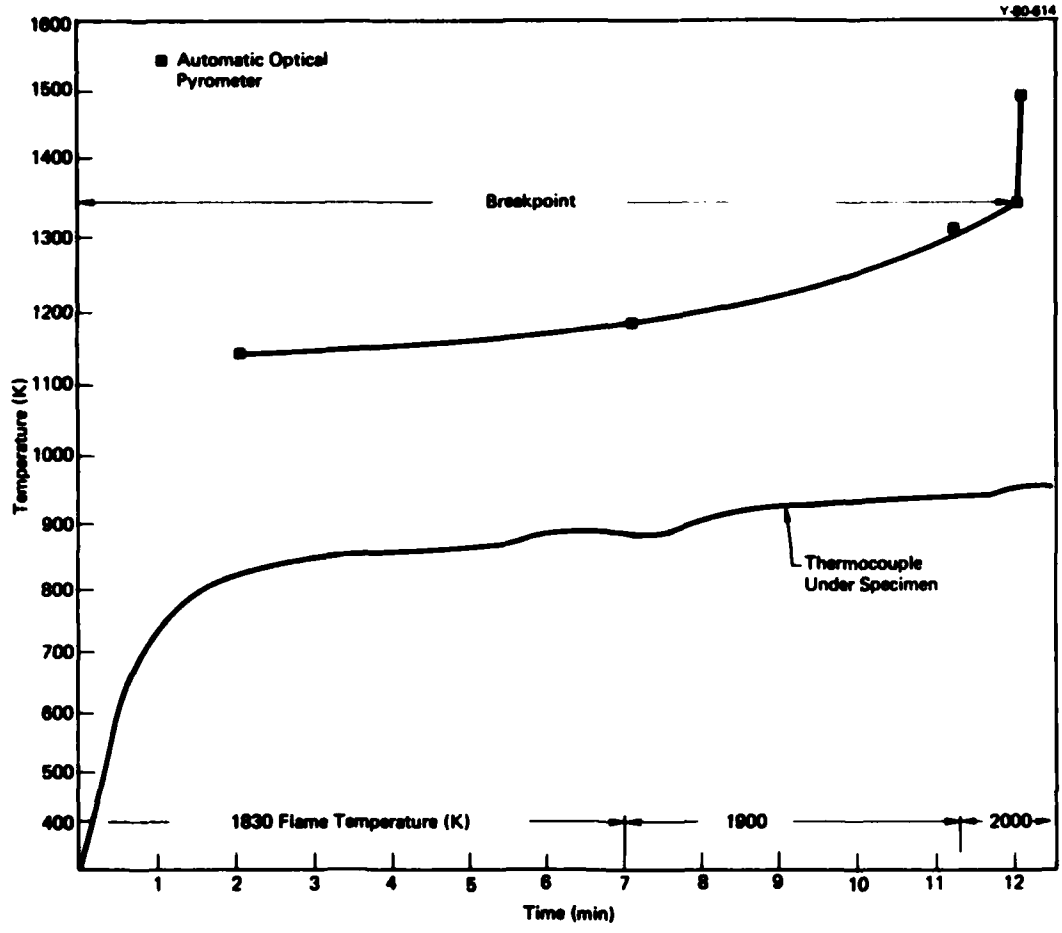

Figure 28. TEMPERATURE-VERSUS-TIME CURVE FOR YTTRIA EXPOSED TO HYDROGEN FLUORIDE FLAME. (Run HF-163.)

eutectic is close to the fluoride melting point, (2) that film failure is predominantly caused by melting, and (3) that fluoride vaporization is a minor consideration.

The testing of a scandium oxide (Sc_2O_3) specimen, which was >90% dense, was unsuccessful in that the specimen disintegrated (Run HF-93); and no surface temperature data could be obtained. Thus, such poor thermal shock resistance would eliminate Sc_2O_3 as being suitable for nozzle application.

Ceria (CeO_2) also behaved poorly when tested in the HF flame; it cracked, corroded severely, and—in one instance (Run HF-61)—the fluoride layer was flaky and nonadherent. This is not surprising when it is realized that two cerium fluorides (CeF_3, mp = 1733 K and CeF_4, mp = 1250 K) exist.[2] Thus the melting point of CeF_4 would be rapidly reached, and a CeF_3-CeF_4 eutectic temperature could significantly lower the fluoride film failure temperature.

Two $CaAl_4O_7$ specimens were tested (Runs P-31 and HF-41), and they exhibited very poor performance. This behavior can be explained by the formation of a low melting point (1095 K) eutectic of calcium fluoride (CaF_2) and AlF_3.[11] A calcium zirconate ($CaZrO_3$) specimen, nearly 100% dense, fragmented during test (Run HF-81). Approximately one-half of the specimen remained in position which made it possible to complete a 4-min run. No height losses were detected on the pieces which had remained on the holder. The surface film was scraped away for X-ray diffraction (XRD) analysis, which showed an unidentified phase (possibly a Ca-Zr-F composition). It was noted that the film was physically similar to soap, which denotes that it was highly capable of plastic flow or deformation.

Lanthanum chromite, while not reacting rapidly with $2F_2$ and H_2, forms a very thick, poorly adherent fluoride film (Run HF-122). This film measured 0.7 mm (0.029 in) thick on the top, 0.8 mm (0.031 in) thick on the side of the cylinder near the top, and is readily flaked off. The film was identified as LaF_3 by X-ray diffraction. This indicates that the chromium fluorides volatilize. Since some melting of the film occurred, possibly the chromium fluorides[2] (CrF_2 mp = 1375 K; CrF_3 mp = 1375 K; CrF_4 subl = 640 K; or CrF_5 bp = 390 K) may initiate liquid formation to cause film failure at 1365 K (or 1450 K including assumed emissivity correction which is approximately 400 K below the LaF_3 melting point). Thus, the nature (and protectiveness) of the fluoride film that forms is dependent on the substrate precursor. It should be noted that $LaCrO_3$ appears to have excellent thermal shock resistance since it withstood, with no apparent cracking, direct heating with a 2400 K flame followed by subsequent rapid cooling (Run HF-123). The $LaCrO_3$ is also not water reactive.

Carbides, Sulfides, and Nitrides - Two mixed carbides (64WC·36HfC and 80TaC·20HfC) were found to react rapidly in the HF flame. Since these materials form volatile fluorides, there is no possibility of substrate protection. The melting temperature of the substrate has no effect on its stability in fluorine, as illustrated by the behavior of the mixed carbide 80TaC·20HfC, which has the highest reported[12] melting point (4215 ± 150 K) of any refractory.

Silicon carbide (SiC) behaved similarly to the two carbides and for the same reason, volatile fluoride formation (Run HF-68).

Cerium sulfide (CeS), similar to CeO_2, behaved poorly when tested in the HF flame. As previously mentioned, the low melting CeF_4 (mp = 1250 K)[2] or the possibly lower melting CeF_3-CeF_4 eutectic results in a low fluoride film failure temperature.

Boron nitride (BN) was heated to a relatively high surface temperature, 1908 K, and—as a result—was severely corroded. The fact that volatile fluorides are formed from BN precludes the possibility of a protective fluoride film forming.

A yttrium nitride (YN) specimen (approximately 12% porous) fragmented almost immediately upon exposure to the HF flame which indicated it to be a thermal-shock-sensitive material. Whether or not a near 100% dense specimen would behave more favorably would require further investigation.

A silicon nitride (Si_3N_4) specimen with approximately 5% MgO additive reacted at all observable temperatures when tested (Run HF-127). According to the pyrometer recorder data, a breakpoint temperature apparently occurred at 1365 K (presumably from the MgF_2 formed with MgO additive); and the specimen reached a maximum surface temperature of 1631 K. The specimen lost 29.3% weight and had a thin, friable, lacelike coating which was identified by X-ray diffraction as MgF_2.

Because of its low thermal expansion and good mechanical properties, Si_3N_4 is considered to be a high-toughness ceramic and is under study for turbine blade applications. For rigorous thermal changes, it would appear to be a good candidate material. For a $2F_2$ and H_2 environment, however, it reacts rapidly—presumably to form nitrogen fluoride (NF_3) or nitrogen and silicon fluoride (SiF_4). These species are noneutectic-forming volatile fluorides. Thus, an increased dopant level with a fluoride film former could yield a very promising material with the good properties of Si_3N_4 while forming a protective fluoride layer. The previously reported[13] oxynitride $La_2O_3 \cdot Si_3N_4$ was considered for improving the properties of the constituents with lanthanum oxide (La_2O_3) being extremely water reactive but forming the stable LaF_3 and with Si_3N_4 being relatively inexpensive with its excellent thermal shock properties but not a fluoride film former. The compound $La_2O_3 \cdot Si_3N_4$ was prepared by reactive hot-pressing a 1:1 molar mixture of calcined La_2O_3 and Si_3N_4 at 1600°C at 21 MPa (approximately 3 ksi) for 1 hour. The oxynitride was only 80% dense. On testing in $2F_2$ and H_2 (Run HF-125), the specimen developed cracks even with programmed heating. Nevertheless, the maximum surface temperature for near zero reaction appears quite high, 1493 K (or 1595 K with assumed emissivity correction). Because of the porosity, the specimen appeared to be reacted throughout to some extent but was well protected from complete destruction considering its high porosity. The upper use temperature seems to be 150 K less than the LaF_3 melting point,[10] but the apparent coating failure could have been influenced by the surface cracking and specimen porosity. It should be noted that $La_2O_3 \cdot Si_3N_4$ is apparently not very reactive with water, since no weight change resulted when a sample was immersed in water for 1 week.

The cracking failure of $La_2O_3 \cdot Si_3N_4$ may be caused either by a high thermal expansion coefficient or by buildup of SiF_4 vapor in the pores followed by pore blockage. A more dense specimen should be examined to resolve the cause of the cracking. Additionally, the compound $La_2O_3 \cdot 2Si_3N_4$ has been reported[13] and could exhibit good behavior in the $2F_2$ and H_2 environment. Further testing along these lines is in progress.(i)

Metals and Metallics -

Nickel - Three test runs (HF-43, 44, and 110) were made on nickel 270 cylindrical specimens to determine maximum use temperature. In Run HF-110, the specimen was exposed to flame temperatures ranging from 2400 to 2840 K for a period of 16 min. After about 15-1/4 min, a film which formed on the specimen appeared to wash away. The recorded specimen surface temperature at this point was approximately 1390 K, which could be considered a breakpoint. By the end of the run, the specimen had fused to both the nickel support and the thermowell, which

indicated that its temperature was higher than the maximum recorded surface temperature of 1545 K.

The testing of nickel 270 was continued with a thermocouple experiment, Run HF-140, to determine true surface temperature. Time-versus-temperature data for the run are plotted in Figure 27. A breakpoint occurred at 1418 K. Up to the breakpoint, the pyrometer readings are higher than the TC 4, top thermocouple, readings by 10 to 30 K. Beyond 1418 K, the readings diverge and then converge. The maximum thermocouple (TC 4) and pyrometer readings attained are 1698 and 1680 K, respectively. Actually, the temperature of the specimen was higher, since the specimen did melt and the melting point of nickel is 1726 K. Based on this data, the emissivity of this specimen, at a 1700 K temperature level, would be $\epsilon = 0.7$.

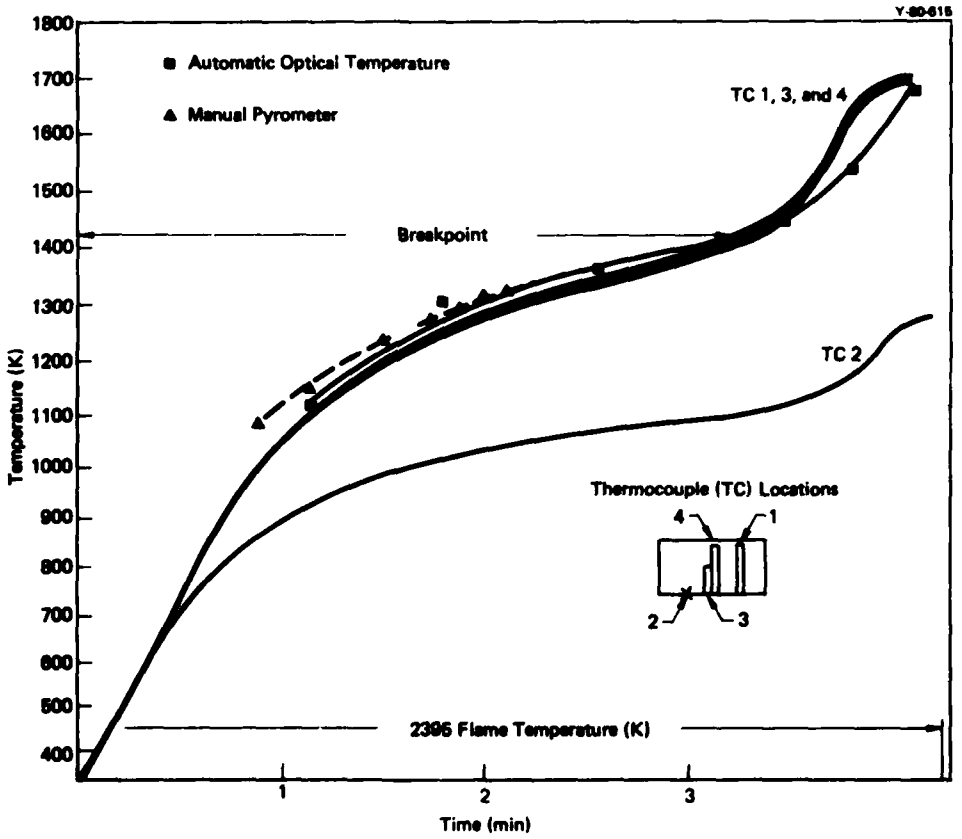

Figure 27. TEMPERATURE-VERSUS-TIME CURVE FOR NICKEL 270 EXPOSED TO HYDROGEN FLUORINE FLAME. (Run HF-140.)

A chamber experiment was conducted with a nickel 200 test plate having a 36-hole configuration similar to the plate described in the Carbon and Graphite section for a test (Run HF-145). In this run, there was a steady rise in the specimen surface temperature to a maximum of 1437 K, at which time the run was terminated; no breakpoint temperature was indicated. The front and back faces of the tested plate

are shown in Figures 28 and 29. The plate did experience some corrosion, particularly in the center; the hole diameters were enlarged from 1.0 mm (0.040 in) to 1.1 to 1.2 mm (0.042 to 0.048 in).

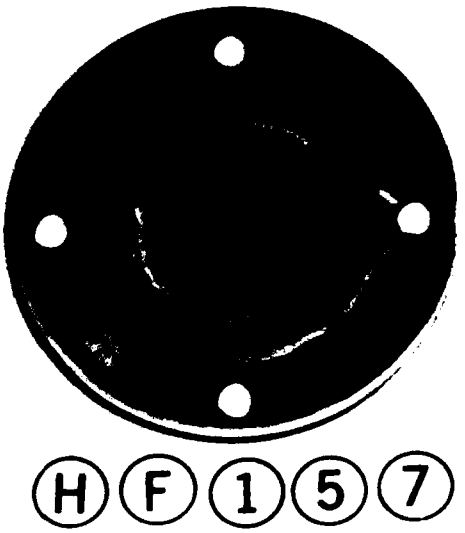

181360
Figure 28. NICKEL 200 TEST PLATE FACE EXPOSED TO HYDROGEN FLUORIDE FLAME. (Run HF-157.)

Nickel Aluminide - Another of the metallic materials tested was NiAl which is essentially an equimolecular compound of aluminum and nickel. One advantage of NiAl over nickel is that NiAl melts at 1920 K while nickel melts at 1726 K. Several test runs were made on NiAl cylindrical specimens to determine its maximum use temperature. In one run, HF-109, an apparent breakpoint was estimated to be 1319 K. In a subsequent run, HF-149, which was a thermocouple experiment, the apparent breakpoint was estimated to be 1279 K; time-versus-temperature data for the run are presented in Figure 30. Examination of the pyrometer recorder charts for the two runs shows that the breakpoints are not readily distinguishable. The curves have a double slope such that the breakpoints lie within a range of values. The conclusion derived from the data is that the breakpoint of NiAl is between that of Al_2O_3 and nickel and that the gradual breakpoint is probably related to volatilization of AlF_3 and nickel fluoride (NiF_2).

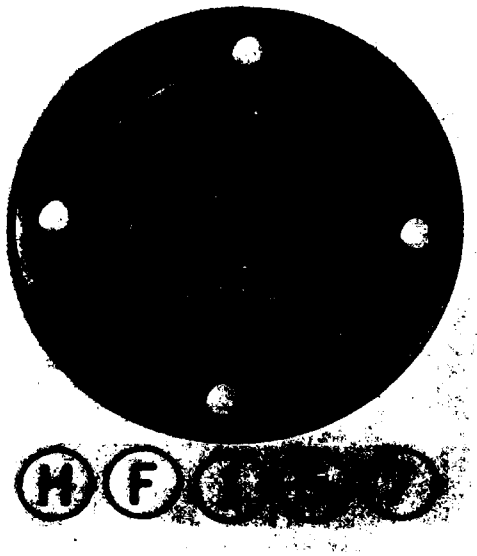

181361
Figure 29. NICKEL 200 TEST PLATE BACK FACE AFTER EXPOSURE TO HYDROGEN FLUORIDE FLAME. (Run HF-157.)

Other Metallics - Three of the metals tested [tungsten (W), tantalum (Ta), and molybdenum (Mo) coated with tungsten] are materials whose fluorides are volatile and, hence, provide no protection from the HF flame. As expected, they performed poorly when exposed to the HF flame.

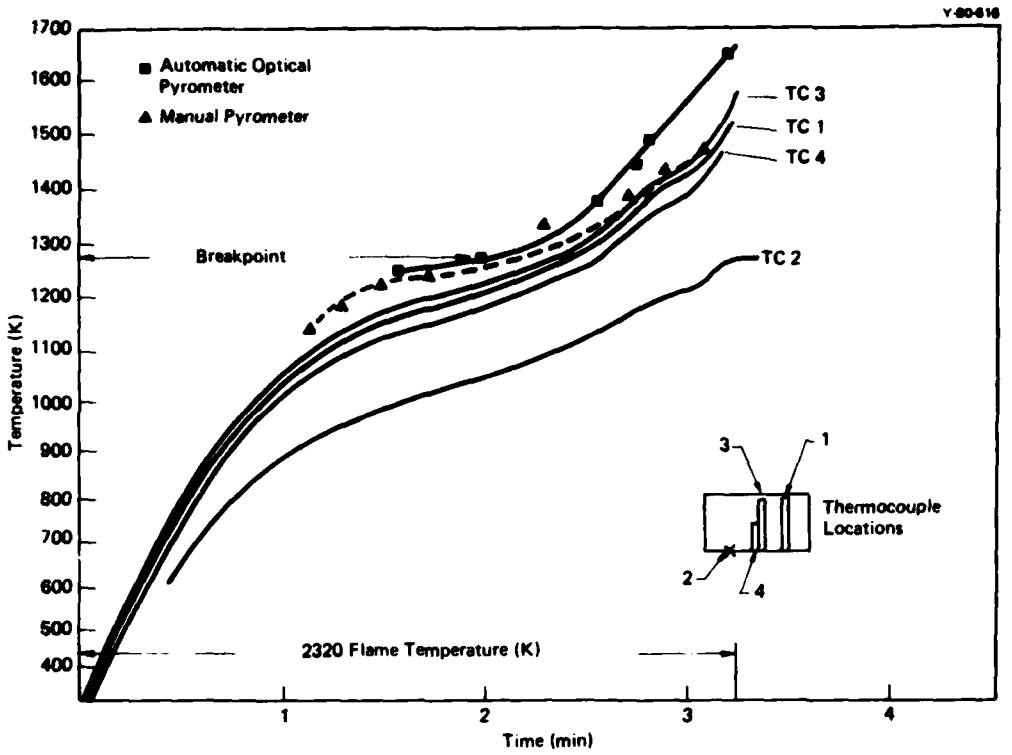

Figure 30. TEMPERATURE-VERSUS-TIME CURVE FOR NICKEL ALUMINIDE EXPOSED TO HYDROGEN FLUORIDE FLAME. (Run HF-149.)

Scandium (Sc) was considered as a possible candidate material, because scandium fluoride (ScF_3) has the highest melting point of the metal fluorides.[14] Test results were unexpected in that (in an interval of 46 s) the specimen heated up, started to fail at 1395 K, and then melted (Run HF-119), having reached a maximum surface temperature of 1576 K. With a breakpoint of 1395 K (or 1465 K with assumed emissivity correction), it appears that ScF_3 ceases to be protective at approximately 300 K below its reported melting point, 1788 K. The X-ray analysis of the droplets on the specimen detected the metal only. This behavior can probably be explained by the rather high vapor pressure of ScF_3 (10.1 Pa or 1×10^{-4} atm at approximately 1445 K)[15] with the ScF_3 film volatilizing from the surface of the specimen.

Yttrium metal is a fluoride former; the yttrium fluoride (YF_3) has a reported melting point of 1425 K.[14] When Run HF-111 was tested, the specimen heated up rapidly, started to melt at approximately 1365 K (or 1424 K with assumed emissivity correction), and then reacted catastrophically. The breakpoint temperature of Y_2O_3 (Run HF-163) was found to be 1340 K; and both breakpoints, considering assumed emissivities, are nearly identical to the YF_3 melting point. Film failure is predominantly by melting.

Yttria doped specimens of nickel were tested in two runs (HF-41 and HF-42) in which surface temperatures never exceeded 1138 K; and the specimens experienced no corrosion. In two subsequent tests (Runs HF-201 and HF-202), Al_2O_3 insulating wafers were placed under the specimens, and specimen surface temperatures above 1400 K were attained. From visual observations, a fluid spot appeared on the top surface of the specimen at approximately 1289 K. Molten drops were rolling over the edge of the specimen (Run HF-202) at 1561 K, and gross melting took place at approximately 1671 K. The breakpoint is, therefore approximately 1289 K for yttria doped nickel—very similar to yttrium metal and Y_2O_3.

Titanium aluminide, another material of interest to the program, has a melting point of 1743 K. Visual observation of the specimen during test (Run HF-124) noted a film burn-off at virtually the same temperature at which Al_2O_3 fails, 1163 K. This is plausible, since AlF_3 is the protective layer for both the Al_2O_3 and TiAl. The maximum surface temperature attained by the specimen was 1732 K with a 10% loss in weight.

A composite was considered: combining the stable, high-melting LaF_3 with a ductile metal (tantalum) that forms a volatile fluoride, tantalum fluoride (TaF_5), with the prospect of reacting the tantalum away on the surface and leaving the protective LaF_3. The mixture (15.3 wt % LaF_3 + 84.7 wt % tantalum) was designed to have approximately 33 vol % LaF_3. Two samples were prepared: the first, about 72% dense (9.3 g/cm^3 bulk density), isostatically pressed at 206.8 MPa (30 ksi), and sintered at 1725 K for 15 min in argon (Ar); and the second, about 90% dense (from bulk dimensions and corrected for one-half of the LaF_3 content vaporization) and hot-pressed at 26.2 MPa (3.8 ksi) for 1 hour at 1725 K. Both specimens reacted vigorously with the HF flame, as demonstrated in Runs HF-150, 151, and 152. The LaF_3 film was poorly adherent, thick, and quite porous. It is doubtful that a fully dense composite would have performed much better since the large surface voids created throughout the LaF_3 film by the TaF_5 evaporation diminishes the protection.

Lanthanum Hexaboride -

Dense, Hot-Pressed Lanthanum Hexaboride - One hot-pressed LaB_6 cylindrical specimen was tested in a series of 10 runs—in which the flame temperature was programmed and increased in approximately 100 K increments for each run from 2000 to 2770 K (Runs HF-69, 75, 76, 78, and 96 through 101). After the first run, it was observed that a white adherent fluoride film (identified as LaF_3 by X-ray diffraction) formed on the LaB_6 upon exposure to the HF flame. Only a small portion of the bottom surface was not coated. The white film is a strong contrast to the bluish purple LaB_6. After 34 min of exposure (Runs 69, 75, 76, and 78) to HF flame temperatures $>$ 1700 K, an electron microscopy scan showed the film to be approximately 100 μm (0.004 in) thick. Upon completion of the 10 runs, after an 87-min exposure at flame temperatures $>$ 1700 K, the cumulative weight loss was

0.57%; losses in height and diameter were only 0.1 mm (4 mils) or 0.79% and 0.02 mm (1 mil) or 0.10%, respectively. The maximum specimen surface temperature 1486 K was attained in the tenth run (HF-101).

In a test (Run HF-102) continued with the same specimen, efforts were made to increase flame and specimen surface temperatures. With no observable corrosion after a 10.75-min exposure to a 2840 K flame, the temperature was increased by decreasing the fluorine flow to 5.7×10^{-4} m^3/s (1.2 ft^3/min) fluorine and to 4.7×10^{-4} m^3/s (1.0 ft^3/min) hydrogen. At this point, some flowing of the LaF_3 film was observed, and the film appeared to be viscous. This flowing action occurred at a surface temperature of 1656 to 1671 K. A further attempt to increase flame temperatures by reducing the fluorine flow to 4.7×10^{-4} m^3/s (1.0 ft^3/min) resulted in flameout. Even after initial liquid formation, the specimen had retained its configuration and had not corroded catastrophically.

A further experiment (HF-103) with the same specimen demonstrated the thermal shock resistance of the material. Direct heating of the specimen in a 2840 K flame and subsequent rapid cooling after equilibration by instantaneously extinguishing the flame showed no indication of thermal shock cracking. Conventional nonmetallic specimens require a programmed heating cycle to avoid fragmentation. Other than graphite, LaB_6 and $LaCrO_3$ are the only nonmetallics that have withstood direct heating with a flame temperature > 2000 K. Figure 31 shows a close-up of the LaB_6 specimen after the 12 test runs. The retention of shape is readily seen as well as the LaF_3 film and the teardrops of clear melted LaF_3. There was sufficient movement of the film to create these small drops.

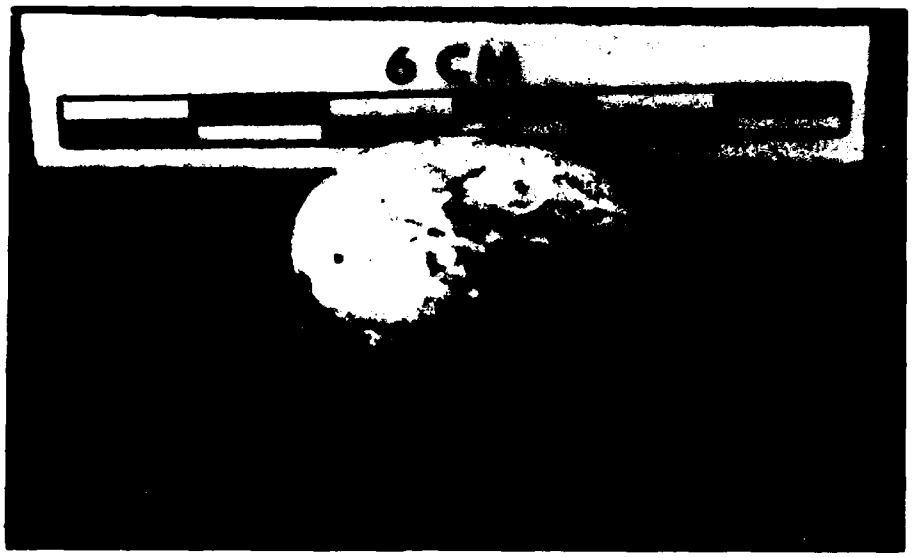

177108

Figure 31. LANTHANUM HEXABORIDE SAMPLE CLOSE-UP SHOWING MELTED LANTHANUM FLUORIDE SURFACE AND TEARDROPS.

The morphology of the LaF_3 film on LaB_6 exposed to $2F_2$ and H_2 was determined by examining the specimen after Run HF-78. Figure 32 illustrates an edge view of the LaF_3 coating (left side at 100X). The 1000X view of Figure 32 illustrates that: (1) the film was approximately 100 μm thick, (2) the growth adjacent to the LaB_6 (right side) was rapid-forming elongated grains and probably occurred during the first run (HF-69), (3) no growth layers appeared (these may heal by grain growth during each successive run), and (4) the LaF_3 film density increased toward the outer region (left side).

An edge view of the side (or rim) coating on the cylinder is shown in Figure 33. The morphology is very similar to that of Figure 32; however, in the 1000X view, a crack occurs through the film (approximately one-third of the distance from the left side of the photo). The crack contains grains on either side that fit together. As there is no apparent corrosion of the LaF_3 grains, rounding of edges, or grain growth, this crack appears to have occurred after the last run was made.

Figure 34 shows a region which had been chipped prior to the Run HF-78. Thus, this region is recently reacted to LaF_3. Note, in the 300X and 1000X views, the appearance of columnar grains when viewed from the top. When compared with Figure 32, the early formed LaF_3 columnar grains adjacent to LaB_6 readily show in the edge view of the LaF_3 coating but would appear as in Figure 34 if viewed from the top. The grains of Figure 34 are obviously microcracked (or contain grain boundary separations). This behavior is a common method of stress relief in ceramic bodies. While such microcracks are often seen in Figure 34, it should be noted that grain-to-grain bonding also always occurs. The apparent sintering of the top surfaces of the columnar grains can be seen in Figures 32 through 34 but is illustrated dramatically in Figure 35, where grain growth is apparent as are circular pores (upper right of photo) denoting sintering.

Thus, this SEM study revealed: (1) the LaF_3 coating appears to form rapidly, with elongated grains; (2) later growth of the coating probably occurs by diffusion of fluorine through the film to the LaB_6 substrate; (3) sintering (or densification) probably occurs when high-temperature long runs are used; (4) microcracking appears to be the stress relief mechanism which allows this LaF_3 coating (CTE approximately 14×10^{-6} from 298 to 450 K)[16] to adhere to LaB_6 (CTE approximately 8.9×10^{-6} from 295 to 1275 K).[17] It is also indicated that a higher temperature pretreatment of LaB_6 with $2F_2$ and H_2 should form a denser outer coating and further reduce the continued LaF_3 growth rate.

Two thermocouple experiments were conducted with a dense, hot-pressed LaB_6 specimen. The specimen was mounted on Al_2O_3 grit, in each instance, to reduce the amount of heat conducted away by the nickel specimen support. In Run HF-141, in which the highest flame temperature was 2690 K, a maximum specimen surface temperature of only 1571 K was attained. The second run, HF-142, was made with the same specimen with higher flame temperatures employed. Figure 36 presents the

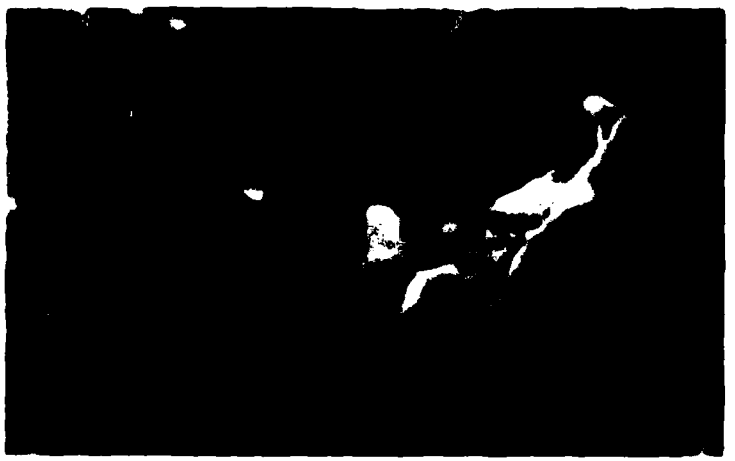

(a) 3000X; 1 mm equals 0.33 μm. SM-65795

(b) 1000X; 1 mm equals 1 μm. SM-65796

(c) 300X; 1 mm equals 3.3 μm. SM-65797

(d) 100X; 1 mm equals 10 μm. SM-65798

Figure 32. SCANNING-ELECTRON-MICROSCOPE PHOTOGRAPH OF LANTHANUM FLUORIDE COATING ON LANTHANUM HEXABORIDE. (Edge view of top coating on cylinder.)

(a) 3000X. SM-65782

(b) 1000X. SM-65783

(c) 300X. SM-65784

(d) 100X. SM-65785

Figure 33. SCANNING-ELECTRON-MICROSCOPE PHOTOGRAPH OF LANTHANUM FLUORIDE COATING ON LANTHANUM HEXABORIDE. (Edge view of side coating on cylinder.)

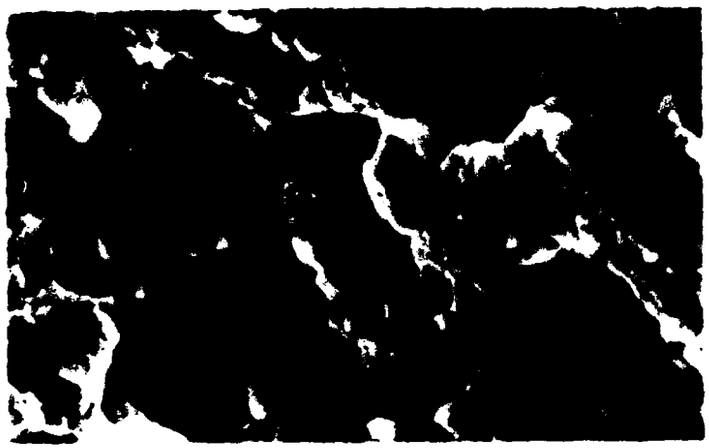

(a) 3000X. SM-65777

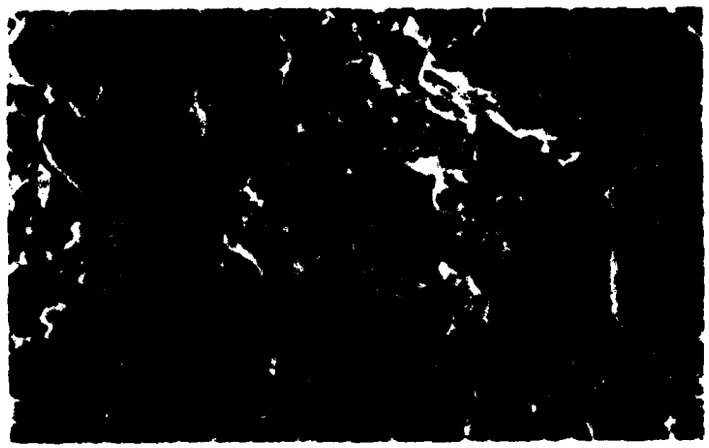

(b) 1000X. SM-65778

(c) 300X. SM-65779

(d) 100X. SM-65780

Figure 34. SCANNING-ELECTRON-MICROSCOPE PHOTOGRAPH OF LANTHANUM FLUORIDE COATING ON LANTHANUM HEXABORIDE. (Top view of coating on cylinder.)

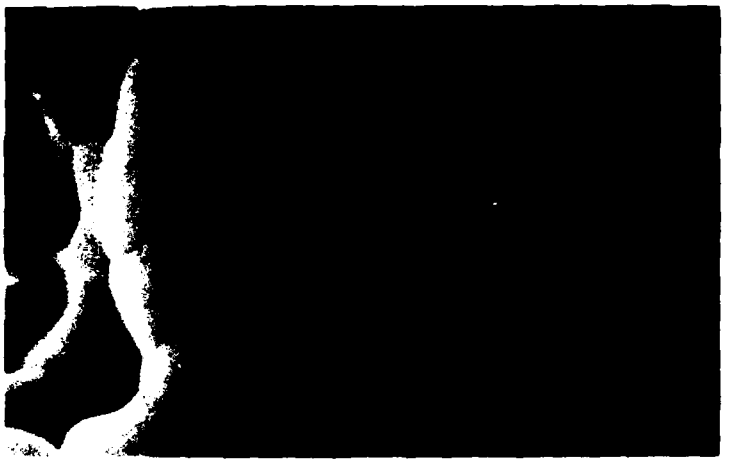

SM-65786

Figure 35. SCANNING-ELECTRON-MICROSCOPE PHOTOGRAPH OF LANTHANUM FLUORIDE COATING ON LANTHANUM HEXABORIDE. (Top view of coating on cylinder; 10,000X; 1 mm equals 0.1 μm.)

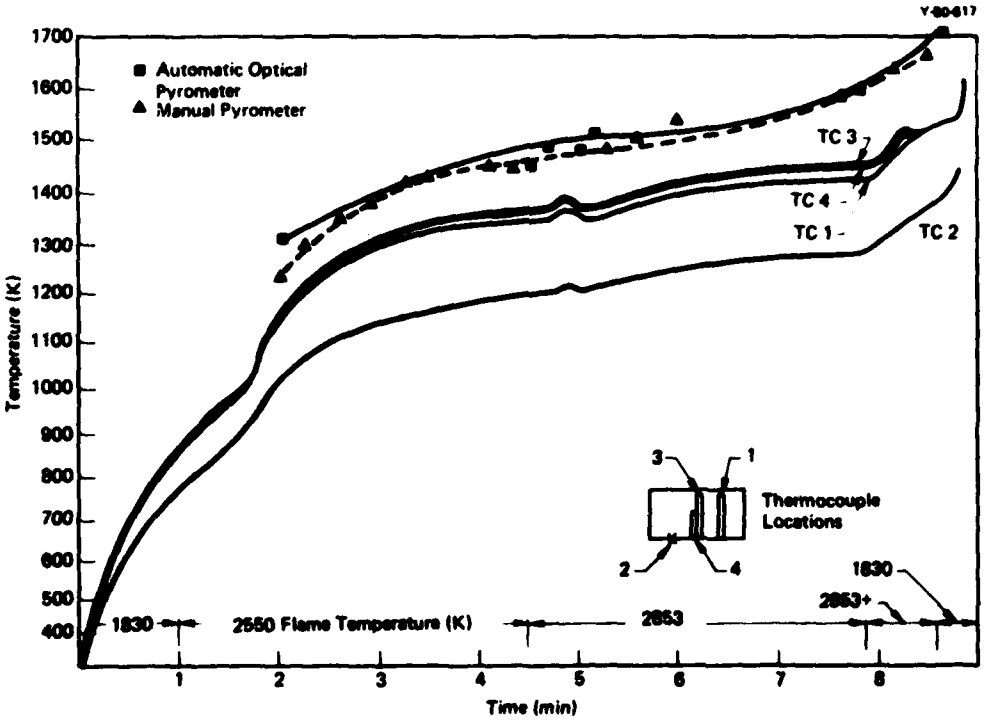

Figure 36. TEMPERATURE-VERSUS-TIME CURVE FOR LANTHANUM HEXABORIDE EXPOSED TO HYDROGEN FLUORIDE FLAME. (Run HF-142.)

temperature-versus-time data for Run HF-142. Employing flame temperatures to above 2853 K, a maximum specimen surface temperature of 1720 K was reached, as indicated by the automatic optical pyrometer. At this point, thermocouple readings became erratic; and, in fact, TC 4 (inserted in the center of the specimen) failed. The

nickel thermocouple sheath had melted which indicated that the temperature had reached the melting point of nickel, 1726 K. After these two runs, the specimen looked relatively untouched except for a grayish film on top and a whitish film on the bottom. Examination of these failures by SEM (after Run HF-142) revealed morphology similar to that shown in Figures 32 to 35 for the LaF_3 film on the top of the specimen. The bottom film, however, appeared as a eutectic microstructure (in the system LaF_3-AlF_3-Al_2O_3 because of the Al_2O_3 grit); thus, LaF_3 was used henceforth when the insulation of a LaB_6 specimen was desired.

The temperature plot of Figure 36 also shows that the ΔT between the pyrometer readings and the specimen temperature (TC 3) increases from approximately 60 to 150 K as the specimen gets hotter. A low-thermal-conductivity fluoride layer (LaF_3) could account for this ΔT.

The preceding experiments on LaB_6 failed to reach a breakpoint where the LaF_3 film would fail. The initial liquid formation point (where some flowing of the LaF_3 film occurs) is at 1656 to 1671 K (no emissivity correction); initially, this was thought to represent failure even though the fluoride was still highly viscous and protective.

By thermally insulating the underside of a specimen with a porous LaF_3 layer and by a slow continual reduction of fluorine from the $2F_2$ and H_2 ratio to 1.6 F_2 and H_2 to increase the flame temperature above 2853 K, a characteristic film failure was noted which was followed by rapid exothermic reaction. A temperature-versus-time curve for the run (HF-171) is presented in Figure 37. According to the optical pyrometer data, a breakpoint occurs at 1738 K (or 1875 K with assumed emissivity corrections); and there is an additional temperature rise to 2041 K. The run was terminated when the specimen support and the thermocouple tip had melted and the specimen had fallen to the bottom of the test reactor. The recovered specimen, still intact, had no LaF_3 film and had lost 9.2% of its weight. From these data, it appears that the melting point of the LaF_3 may be exceeded by approximately 100 K before film failure. Loss of LaF_3 may result from two effects: (1) the viscosity of the LaF_3 becomes low enough to allow rapid flow, and (2) rapid vaporization of the LaF_3 occurs simultaneously.

Two runs (HF-188 and HF-200) were conducted in the configuration test chamber with perforated plate specimens fabricated from dense, hot-pressed LaB_6. In the first run, HF-188, the plate specimen was annealed in argon to 1275 K prior to test. Upon initiation of the flame, the plate cracked immediately; and, upon further examination, it was observed to have several cracks in it, two of which originated at a bolt hole. Figures 38 and 39 are photographs of the front and rear faces of the tested plate. In the second run, HF-200, the experiment was modified; whereby, the bolt holes in the specimen were eliminated, and the specimen was supported under the flame, unrestrained, by a recessed graphite plate bolted to the chamber. Here again, the specimen split into two pieces, almost instantly, upon initiation

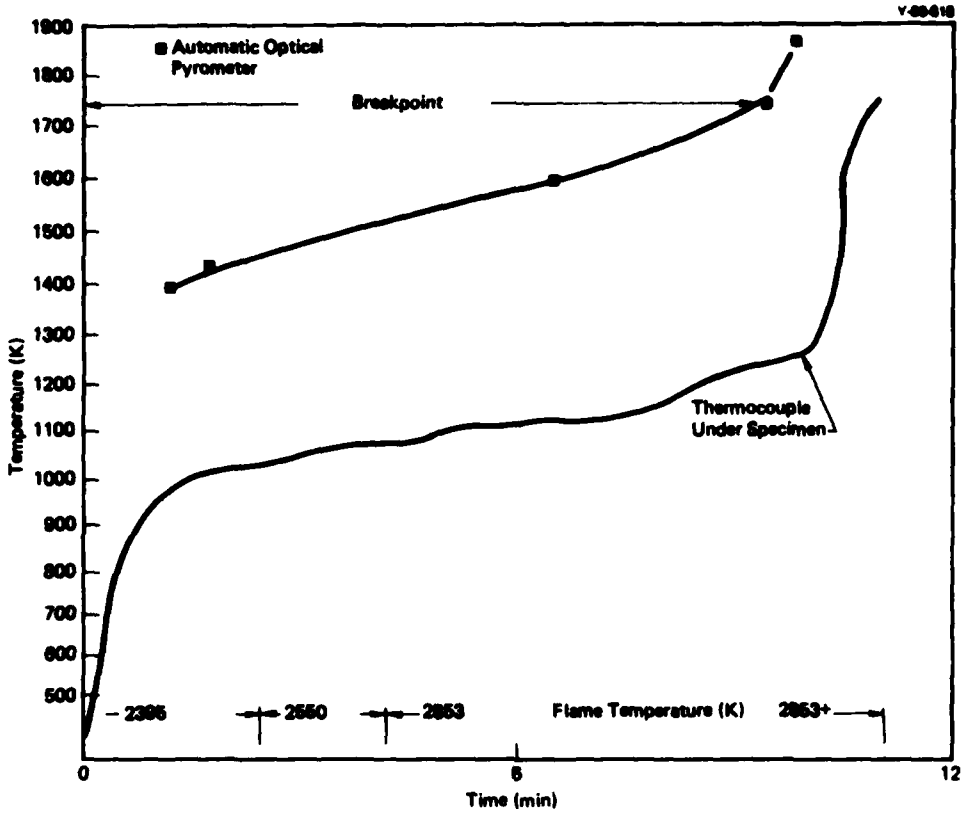

Figure 37. TEMPERATURE-VERSUS-TIME CURVE FOR LANTHANUM HEXABORIDE EXPOSED TO HYDROGEN FLUORIDE FLAME. (Run HF-171.)

of the HF flame. Based on the results of these last two runs, even the specimens fabricated from dense, hot-pressed LaB_6 are subject to thermal shock under the prevailing conditions in the configuration test chamber. A third experiment is planned,[(i)] wherein the plate specimen will first be exposed to the HF flame prior to being tested in the chamber.

Lanthanum Hexaboride Plasma-Sprayed Substrates - Since LaB_6 is a very hard material that requires either expensive

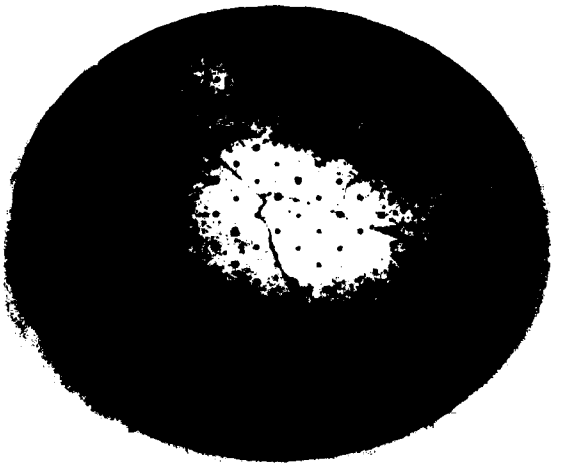

189885

Figure 38. DENSE LANTHANUM HEXABORIDE TEST PLATE FRONT FACE AFTER EXPOSURE TO HYDROGEN FLUORIDE FLAME. (Run HF-188.)

diamond tool grinding or less familiar nonconventional machining techniques—electrodischarge machining (EDM), electrochemical machining (ECM), or electrochemical grinding (ECG), consideration was given to fabricating the compound by plasma spraying. Plasma-sprayed (PS) material is approximately 85 to 95% dense with flat grains that are not as strongly bonded as hot-pressed, more equiaxed grains. Thus, the PS grains would pull out more readily in conventional machining, which would enable the rapid shaping of relatively dense PS layers [generally of 0.25 to 2.5-mm (0.010 to 0.100-in) thickness]. Additionally, PS coatings can be used to provide protection for materials with less stringent performance requirements than, for example, nozzles. An instance would be the graphite configuration-test-chamber assembly described in the **Configuration Test Chamber** section.

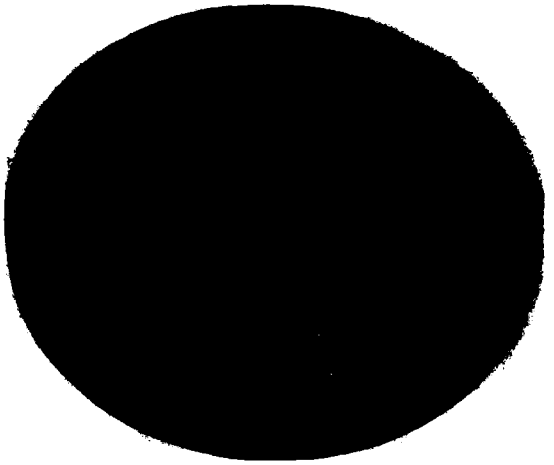

186886

Figure 39. DENSE LANTHANUM HEXABORIDE TEST PLATE BACK FACE AFTER EXPOSURE TO HYDROGEN FLUORIDE FLAME. (Run HF-188.)

By using -44 to +25-μm-sized powder,(k) it was possible to plasma spray LaB_6 successfully. Cylinders of nickel (CTE of 17.1×10^{-6}/K in the range of 298 to 1273 K), W-Ni-Fe alloy (CTE of 5.2×10^{-6}/K), and POCO(l) graphite (CTE of approximately 7.5×10^{-6}/K) were PS coated with LaB_6 (CTE of 9.0×10^{-6}/K). The LaB_6 layers were all ≥ 0.18 mm (or ≥ 0.007 in) and did provide a measure of protection for all substrates; however, cracking of the LaF_3 film layer occurred on shutdown for all except for one POCO graphite specimen, which has a very close CTE match to the LaB_6. It is likely that by plasma spraying mixed powders as an interlayer (ie, a nickel + LaB_6 interlayer on nickel followed by a pure LaB_6 layer) an expansion gradient may be achieved. From the tests with different thicknesses of LaB_6 on POCO graphite, it appears, at this time, that a 0.7-mm (0.028-in) coating will give the best protection. The LaB_6 coatings that were applied to these test specimens were nonuniform in thickness, and this may have been a factor in the performance of the tested specimens.

Three experiments were conducted with LaB_6 plasma sprayed onto POCO graphite; namely, Runs HF-153, 154, and 168. Runs HF-164 and HF-170 were conducted with a nickel 270 specimen and with a W-Ni-Fe alloy specimen, respectively, plasma sprayed with LaB_6. In reviewing the results of the tests, consideration must be given

(k) Nominally >99% pure lanthanum hexaboride, -44 to +25 μm powder; purchased from Hermann C. Starck, Inc, Berlin, West Germany.

(l) Poco Graphite, Inc.

to the fact that the specimens were sprayed on the top and peripheral surfaces only; and, as a consequence, they did suffer added corrosion on the bottom surface.

Plasma-Sprayed Lanthanum Hexaboride Test Specimens - In attempting to plasma spray LaB_6 on substrate materials, it was found possible to form the LaB_6 into various shapes and thicknesses. Accordingly, a PS plate [without substrate, 102 mm in diameter by 3.8 mm (0.150 in) thick, and provided with 36 1.0-mm (0.040-in)-diameter holes] was made for testing in the configuration test chamber. The test plate was prepared by plasma spraying the LaB_6 onto an aluminum mandrel plated with nickel, and a complete separation of the LaB_6 occurred when spraying was completed.

Expecting higher temperatures of operation in the chamber, the interior of the graphite chamber and the graphite deflection ring were plasma sprayed with LaB_6 for added protection. Photographs of the chamber, deflection ring, and test plate prior to testing are shown in Figures 40, 41, and 42. During the early part of the run (HF-173), the LaB_6 plate cracked. Upon subsequent examination, Figure 43, it appeared that the crack had initiated at one of the bolt holes. In addition, most of the diameters of the drilled holes had enlarged to 1.1 mm (0.043 in) (approximately 7.5% increase). A view of the back face of the tested plate is shown in Figure 44.

Figure 45 shows the configuration test chamber after test. The resultant LaF_3 layer, for the most part, did adhere to the graphite and protect it; however, in the area near the threaded section of the chamber and where the initial LaB_6 coating was

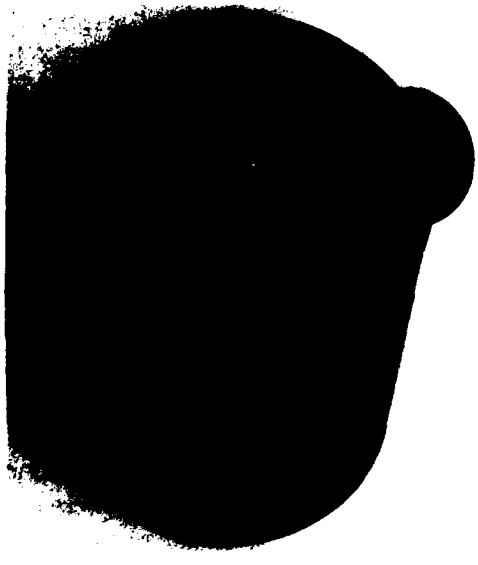

182663

Figure 40. GRAPHITE CONFIGURATION TEST CHAMBER PLASMA SPRAYED WITH LANTHANUM HEXABORIDE. (Prior to Run HF-173.)

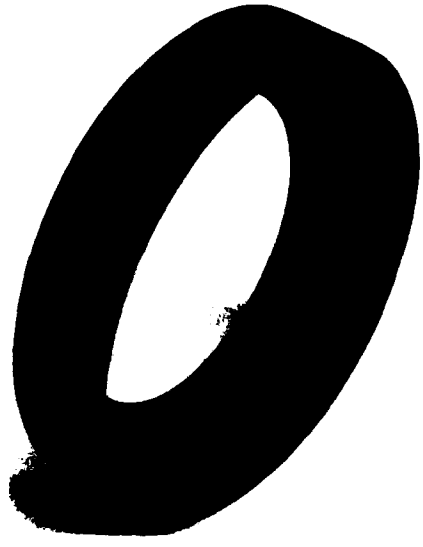

182665

Figure 41. GRAPHITE DEFLECTION RING PLASMA SPRAYED WITH LANTHANUM HEXABORIDE. (Prior to Run HF-173.)

thinnest, the LaF_3 layer did peel away from the graphite. A view of the deflection ring, Figure 46, shows the two LaB_6 layers (two right views) that had popped off the graphite ring (left view) during the run; only the top surface of the top LaB_6 layer (center view) had reacted to form LaF_3. Even with some peeling of the PS coating on the chamber or with delamination of the PS layers on the deflection ring, the PS LaB_6 allowed complete protection of these graphite parts.

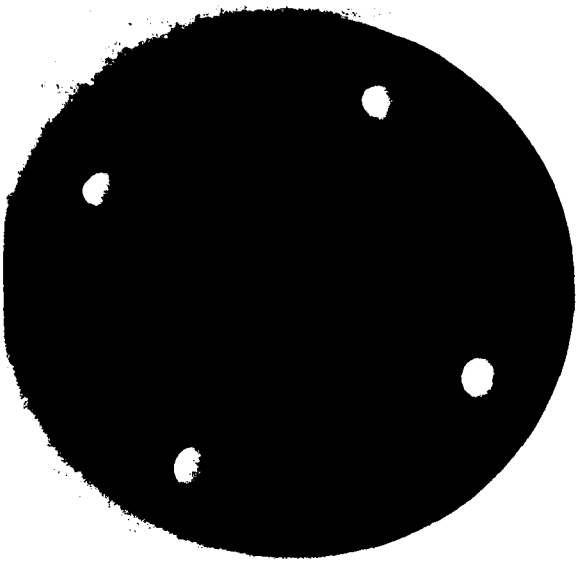

182668

Figure 42. PLASMA-SPRAYED LANTHANUM HEXABORIDE TEST PLATE. (Prior to Run HF-173.)

The behavior of the test plate of Run HF-173 was unexpected; however, the plate had not been annealed and was only 81.1% dense (99.94% pure by spark-source mass spectrometry). The plate was retested in the configuration chamber in Run HF-175 to see if it would undergo additional changes. Changes did take place. The crack in the plate increased in size. There was corrosion in the center of the plate, and most of the matrix hole diameters had enlarged (again approximately 7%) to about 1.2 mm (0.046 in). Figure 47 is a photograph of the exposed face of this plate.

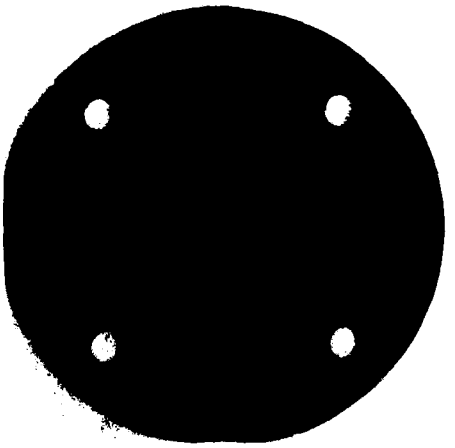

182910

Figure 43. PLASMA-SPRAYED LANTHANUM HEXABORIDE TEST PLATE EXPOSED TO HYDROGEN FLUORIDE FLAME. (Run HF-173.)

Another PS test plate was made (excluding the bolt holes) of a smaller diameter (75.8 mm or 3 in) than the previously tested plate. It was mounted and attached to the bottom of the graphite test chamber so that it would not be restrained during a heat-up and run cycle. After about 4 min into the run (HF-174), this test plate (which was 84.2% dense, 99.95% pure by spark-source mass spectrometry) cracked; and portions of it fell to the bottom of the Monel reactor. The cracking problem may be solved by annealing the PS material prior to test to relieve the residual stresses after forming. However, the fact that the holes in the PS

plates did corrode and increase in size would need further evaluation to deem PS LaB_6 suitable for use as laser nozzles. A trade-off may be necessary between a density high enough to allow near zero corrosion and a density low enough to take advantage of the relative ease of machining of PS material.

Plasma-Sprayed Lanthanum Hexaboride Structures - Based on the results shown in Figure 45, it was felt that the interior of the configuration test chamber could be protected more effectively by the use of a LaB_6 liner. Accordingly, a PS liner, 51 mm (2 in) long X 64 mm (2.5 in) OD X 2.5 mm (0.100 in) thick was fabricated by depositing the boride onto a graphite mandrel and then oxidizing the graphite at 1075 K in air. This heat treatment served to anneal the liner as well as to permit its removal from the graphite mandrel. A photograph of the liner prior to test is presented in Figure 48; the whitish appearance is a result of the annealing operation (presumably a thin oxide layer). Density of this liner (from mercury porosimetry of a rim section) was 78.6% of theoretical with 7.4% open porosity.

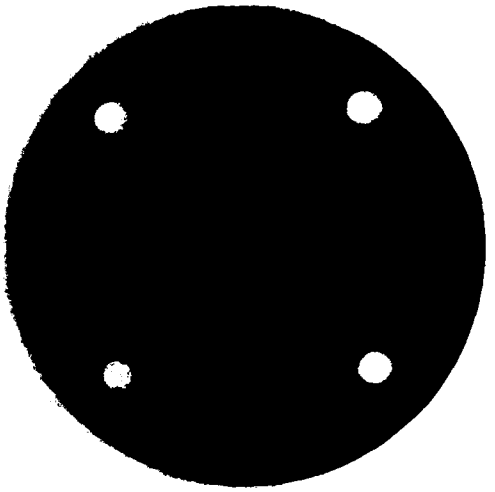

182909

Figure 44. PLASMA-SPRAYED LANTHANUM HEXABORIDE TEST PLATE BACK FACE EXPOSED TO HYDROGEN FLUORIDE FLAME. (Run HF-173.)

182911

Figure 45. CONFIGURATION TEST CHAMBER EXPOSED TO HYDROGEN FLUORIDE FLAME. (Run HF-173.)

A test run (HF-187) was conducted with the LaB_6 liner plus a used graphite deflection ring that had been initially plasma sprayed with LaB_6 on its top and bottom surfaces. A nickel 200 plate, 3.8 mm (0.150 in) thick, provided with 36 1.0-mm (0.040-in)-diameter holes drilled on 5.6-mm (0.220-in) centers served as a test specimen. Smoking was observed inside the chamber during the run,

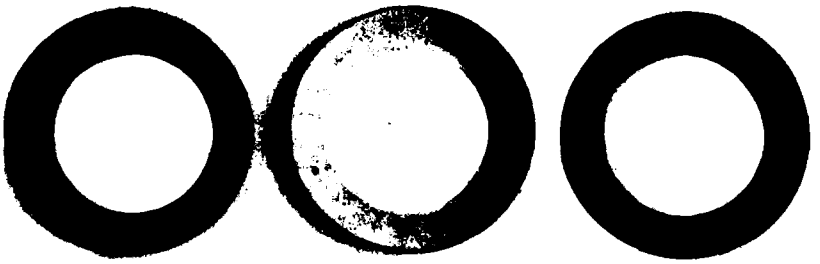

182912

Figure 46. DEFLECTION RING AFTER EXPOSURE TO HYDROGEN FLUORIDE FLAME. (Run HF-173.)

which eventually fogged the sight glass and led to incorrect readings by the automatic optical pyrometer. Apparently, the surface temperature of the nickel specimen was 1726 K, since the specimen showed signs of melting as well as extensive corrosion. Examination of the chamber after the run showed that the LaB_6 liner had cracked (completely through) in one area, and there was partial cracking elsewhere; however, the liner did stay in position inside the chamber. Essentially, the deflection ring had not changed. In areas where the interior of the chamber had not been shielded by the liner and deflection ring, there were signs of a reaction with the HF flame gases.

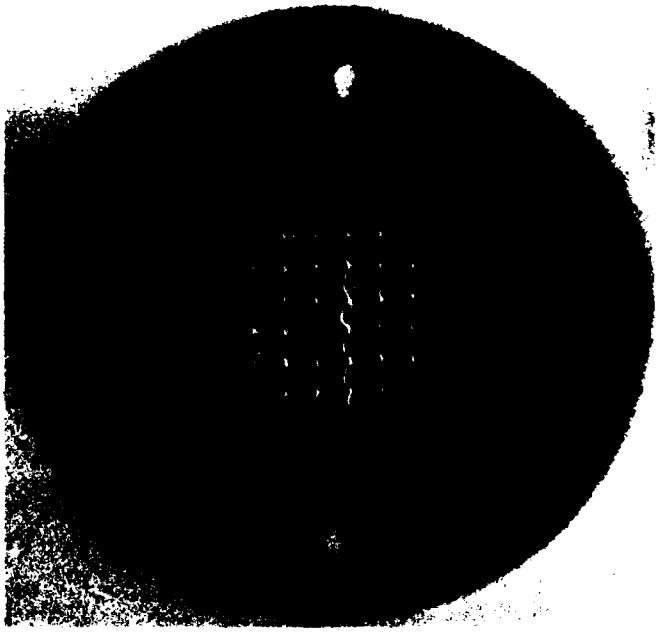

183085

Figure 47. RETEST OF PLASMA-SPRAYED LANTHANUM HEXABORIDE PLATE. (Run HF-175.)

The liner was used in two subsequent runs (HF-188 and HF-200) described in the **Dense, Hot-Pressed Lanthanum Hexaboride** section. Though the liner had been cracked, it still remained in position inside the chamber throughout the runs to serve as a protective shield.

Properties of Lanthanum Hexaboride - In view of the fact that LaB_6 is generally unfamiliar to people in the materials field, a compilation of its properties is presented in Appendix D. Thermal diffusivity,[18] thermal conductivity,[18] and

Table 4

MATERIALS WITH SIGNIFICANT WEIGHT LOSS ABOVE 1050 K[1]

Material[2]	Run	Anticipated Reaction-Product Fluoride[3]
Boron-Silicon-Carbide (Boride V)	HF-82	BF_3 (mp = 144 K, bp = 172 K); SiF_4 (subl = 184 K); CF_4 (mp = 89 K, bp = 145 K)
Si_3N_4 (MgO doped)[4]	HF-127	SiF_4; NF_3 (mp = 66 K; bp = 144 K); MgF_2 (mp = 1536 K; bp = 2500 K); OF_2 (mp = 49 K, bp = 128 K)
80TaC·20HfC	HF-20	TaF_5 (mp = 370 K, bp = 503 K); CF_4
SiC	HF-68	SiF_4; CF_4
W	P-30, HF-15	WF_6 (mp = 274 K; bp = 571 K)
Mo (coated)	HF-16, 18, 40	MoF_6 (mp = 291 K; bp = 370 K)
Ta	HF-60	TaF_5
64WC·36HfC	P-20, HF-6	WF_6; CF_4; HfF_4 (subl = 1200 K)
CeO_2	P-35, HF-52, 61	CeF_4 (mp = 1250 K, bp = 2000 K); OF_2
$CaAl_4O_7$ (CA-25)	P-31, HF-51	AlF_3 (subl = 1545 K); OF_2; CaF_2-AlF_3 (mp = 1095 K) CaF_2 (mp = 1675 K; bp = 2145 K)
BN	HF-12	BF_3; NF_3
CeS	P-29, HF-55	CeF_4; SF_6 (mp = 222 K; bp = 337 K)

(1) The temperature, 1050 K, represents the lower limit of pyrometry used.
(2) Listed qualitatively in order of decreasing stability based on loss in height with time.
(3) Assuming highest valence fluoride forms, the mp (melting point), bp (boiling point), and/or subl (sublimation point) are shown when a particular fluoride is first listed. Obtained from References 2, 10, 11, 14, and 22.
(4) X-ray diffraction analyses indicated: major phase = β-Si_3N_4, intermediate phase = α-Si_3N_4.

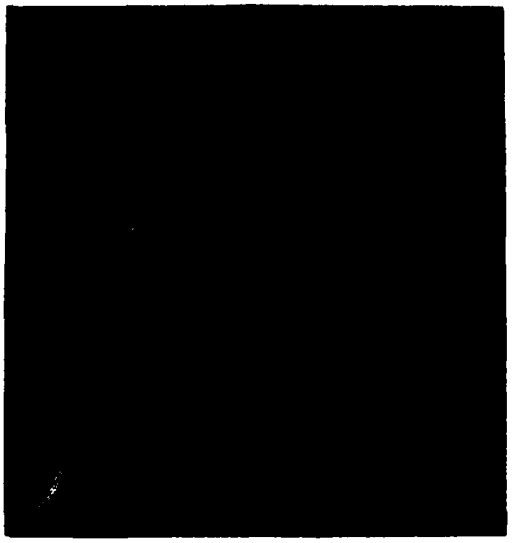

184543

Figure 48. PLASMA-SPRAYED LANTHANUM HEXABORIDE LINER OXIDIZED IN AIR.

thermal expansion data on LaB_6[17] (plotted as a function of temperature) are also presented along with comparison information on MgO, Al_2O_3, and BeO.[12,19] In addition to the properties listed, LaB_6 is not water reactive and has rather good resistance to thermal shock, presumably resulting from its unusually high thermal conductivity[18] since both its strength[20] and thermal expansion[17] are moderate. However, while LaB_6 cylindrical samples withstood rapid flame heat-up, LaB_6 test plate performance was poor; this indicates that a rather extreme thermal shock condition exists with the test plates. Poor performance was probably the result of a suspected presence of free boron.

Machining of Lanthanum Hexaboride - Attempts to fabricate a specimen—for testing in the configuration test chamber—from a dense, hot-pressed LaB_6 plate, 8.1 mm (0.320 in) thick and 99.89% pure (by spark-source mass spectrometry) were slow and unsatisfactory. In the Y-12 Glass Shop it was possible to satisfactorily core disks from the LaB_6 plate up to 102 mm (4 in) in diameter. Although the process was slow, the coring was done with a brass cylinder using water with carborundum (SiC) as an abrasive. Drilling the 36 1.0-mm (40-mil)-diameter holes, however, was not successful. Diamond-plated mandrels (turned in a high-speed rotary grinding head) were used for this operation. The mandrels or drills wore out or broke, and the job was not completed. One factor which added to the difficulties was the presence of hard inclusions in the LaB_6. The plate was fully dense at 4.59 g/cm^3—implying 5% free boron, probably inclusions.

An attempt to part a 1-in-diameter LaB_6 cylinder down the middle with a plated diamond parting wheel took 8 hours. The use of EDM to part a 1-in-diameter cylinder also took 8 hours; a copper and tungsten electrode was utilized in this instance.

To investigate alternative machining techniques, personnel from a Y-12 Plant machine shop and the Y-12 Development Division visited a company(m) which reportedly had good capabilities for drilling hard materials with ultrasonic-assisted diamond-loaded tools. These techniques were convincingly demonstrated. In fact, the 20 or so remaining holes to be drilled in the LaB_6 plate were completed by them in approximately 2-1/2 hours.

Attempts were made at the Y-12 Plant to reduce the thickness of a dense, hot-pressed LaB_6 plate to facilitate drilling through the thinner section. To accomplish this, ECG techniques were used. Under nonoptimum conditions, in a period of 16 hours, an area of 89 mm (3.5 in) by 152 mm (6 in) was ground down to 5.3 mm (0.210 in) from an original thickness of 8.1 mm (0.320 in).

Other Borides - One of the first borides tested, Boride V (Appendix B), which is a boron-silicon-carbon composite, reacted rapidly and corroded extensively in the HF flame

(m) Bullen Ultrasonics, Inc., Eaton, Ohio.

(Run HF-82). Since the material formed only volatile fluorides, there was no possibility that a protective film would form.

Thermal analyses revealed a solid solution of strontium fluoride ($2SrF_2$) and 1 LaF_3 with a high melting point; and it has been reported[21] that a continuous solid solution of the borides, LaB_6 and strontium hexaboride (SrB_6), exists. Thus, the composite $La_{0.33}Sr_{0.67}B_6$ was prepared by reactive hot-pressing the mixture $La_2O_3 + 4SrO + 80B$. About 25 wt % excess boron above the stoichiometric amount was used. Pressing at 2450 K for 3 hours, under a pressure of 67.5 to 42.0 MPa (9.8 to 6.1 ksi), a specimen with a bulk density of 2.82 g/cm^3 and 87% of the theoretical density was obtained. The material was tested (Run HF-161) and did experience some corrosion (6.2% weight loss), and some formation of liquid on the surface was observed after having reached a maximum temperature of 1802 K. Internal fluoriding had occurred, and the fluoride coating was not very dense or adherent. Further testing of a dense specimen would be necessary to adequately compare the behavior of this hexaboride solid solution to LaB_6.

In an initial run, HF-87, with CaB_6, which had a porosity of approximately 21%, the specimen fragmented almost immediately upon exposure to the HF flame. Additional specimens, having essentially 100% theoretical density were procured which had a bulk density of 2.43 g/cm^3 and zero open porosity. With a dense specimen, a protective CaF_2 film formed during a test (Run HF-169); however, a weight loss of 4.5% occurred during an exposure period of approximately 3 min at a surface temperature of about 1500 K. Additionally, CaB_6 was found not to be as resistant to thermal shock as LaB_6 (since CaB_6 specimens required programmed flame temperature increases) in $\leq$ 200 K increments above 1700 K.

Another experiment was conducted with a dense CaB_6 specimen in an effort to determine the breakpoint of the CaF_2 film. Apparently, the CaF_2 film affords some protection even above its melting point, up to the temperature where its viscosity becomes low enough to allow little substrate protection. As visually observed in Run HF-167, the film was blown to the edge of the test cylinder which allowed rapid corrosion. A photograph of the specimen tested in Run HF-167 appears in Figure 49. Here the CaF_2 is seen as globules around the edge of the specimen and as a crescent-shaped layer (facing upward) on the top surface. The time-versus-temperature curve for Run HF-167 is presented in Figure 50. As

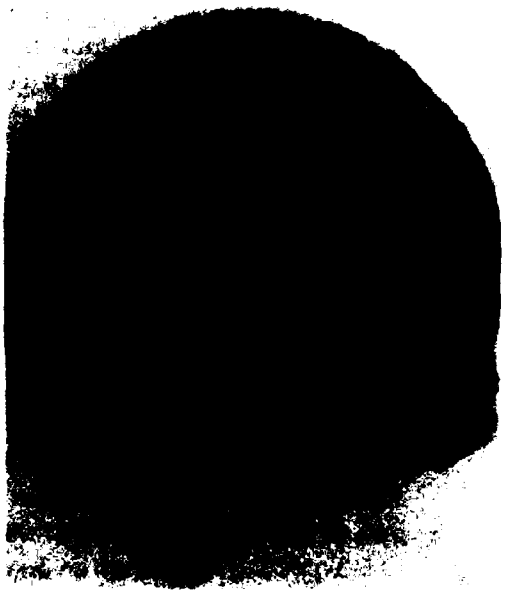

181203

Figure 49. CALCIUM HEXABORIDE SPECIMEN EXPOSED TO A HYDROGEN FLUORIDE FLAME (TEMPERATURE EXCEEDING THE MAXIMUM SURFACE TEMPERATURE FOR NEAR ZERO CORROSION). (Run HF-167.)

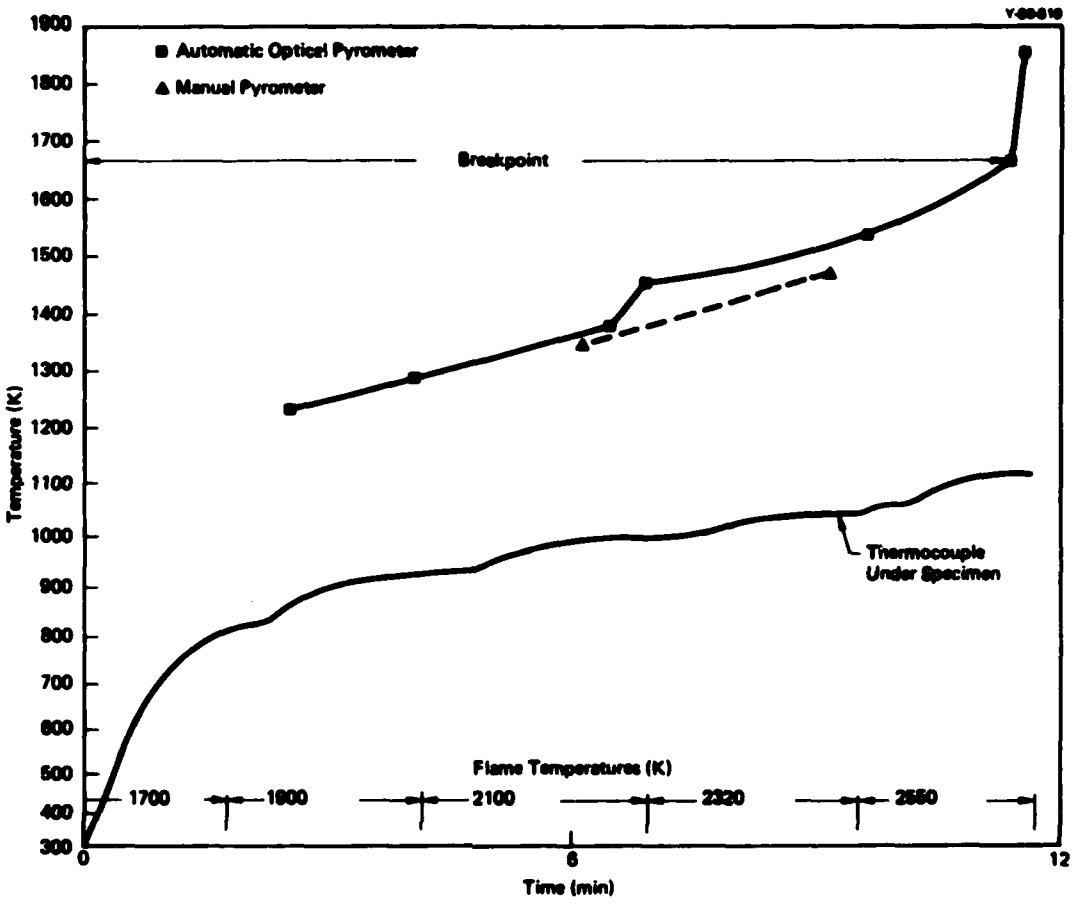

Figure 50. TEMPERATURE-VERSUS-TIME CURVE FOR CALCIUM HEXABORIDE EXPOSED TO HYDROGEN FLUORIDE FLAME. (Run HF-167.)

indicated by the pyrometer readings, a breakpoint occurs at 1661 K (1785 K with assumed emissivity correction); and there is a subsequent temperature rise to a maximum of 1924 K.

General Discussion of Test Results

The surface temperatures achieved for a particular material in the HF torch environment depend upon the balance of the heat input from the impinging flame, the heat input of the fluoriding reaction(s) involved, the heat removal by conduction to the sample support, and by radiation losses to the chamber and gases. The presence of a protective fluoride film significantly reduces the heat input from fluoriding. The degree of protection afforded by the fluoride film depends upon the porosity, adherence, and mechanical integrity of the fluoride film. Causes of film failure include melting, vaporization, microcracking, or spallation. With melting, the remaining protection depends upon the viscosity and vaporization characteristics of the molten fluoride. After film failure, the rapid rise in surface temperature results from the uninhibited exothermic fluoriding reaction; typically, the ΔH of this fluorination reaction would become the dominant heat source—supplying over 4000 times the heat supplied by the torch.

The performance of different materials in the $2F_2$ and H_2 flame was divided into three categories: (1) those with no region of near zero(n) (insignificant) weight loss above 1050 K (lower limit of pyrometry used) as shown in Table 4; (2) those which failed by fragmentation as shown in Table 5; and (3) those with a measured region of near-zero(n) weight loss above 1050 K as shown in Table 6.

Table 5

FLUORIDE FILM FORMERS WHICH FAILED BY FRAGMENTATION

Material	Run	Anticipated Reaction-Product Fluoride(1)
Sc_2O_3	HF-93	ScF_3 (mp = 1788 K; bp = 2025 K); OF_2
$CaZrO_3$	HF-81	CaF_2; ZrF_4; OF_2
YN	HF-49	YF_3 (mp = 1421 K; bp = 2205 K); NF_3

(1) Assuming highest valence fluoride forms, the mp (melting point), bp (boiling point), and/or subl (sublimation point) are shown when a particular fluoride is first listed in Table 4, 5, or 6. Obtained from References 10, 14, and 15.

None of the materials in Table 4 were protected significantly by a fluoride film to prevent rapid reaction. The rapid reaction of the two cerium compounds (CeO_2 and CeS) is attributed to the low-melting CeF_4 which is favored by the excess fluorine. Similarly, the low-melting fluoride eutectic, CaF_2-AlF_3, results in the low fluorine stability of $CaAl_4O_7$. Fluorides of other materials in Table 4 were volatile above 1050 K in agreement with available data[2,10,22,23] affording no protection for the substrate.

Materials in Table 5 failed shortly after torch ignition. Failure was attributed either solely to thermal shock ($CaZrO_3$) or to a combination of thermal shock and vapor pressure buildup of entrapped fluorides (possibly for Sc_2O_3 or YN). Two materials of high porosity (> 20%) that fragmented were Y_2O_3 and CaB_6, yet higher density specimens of these materials did not fragment and are included in Table 6. Calcium, strontium, and barium oxides cracked during tests but did not disintegrate and are included in Table 6.

Table 6 identifies the materials which formed a fluoride film that offers significant protection above 1050 K. Breakpoint temperatures were adjusted for assumed emissivity corrections of 0.4 for ceramic and 0.5 for metallics. The adjusted breakpoint temperatures, T_f, represent the fluoride film failure point—a temperature below which some significant protection is afforded. From the run data in the appendices and from observations during testing, it was observed that, if the surface temperature is approximately 95% of T_f, negligible corrosion occurs; this estimated upper use temperature is also given in Table 6.

The fluoride film-forming materials of Table 6 may be separated into two types: (1) vaporizing fluoride formers and (2) melting fluoride formers. Only carbon and Al_2O_3 were exclusively vaporizing fluoride formers since their fluorides ($CF_{x\approx1}$ and AlF_3, respectively) sublime. For graphite, when 1140 K surface temperature is exceeded, the CF_x appears to sublime followed by evolution of either CF_x or CF_4; thus, in an excess fluorine, controlled-atmosphere environment, the CF_x film is stable approximately 400 K above the value given by Ebner[24] (725 K). For Al_2O_3, above 1245 K (1180 K excluding emissivity correction), extensive corrosion occurs although (as for graphite) configuration is

(n) Less than 0.5% weight loss.

Table 6

MATERIALS WITH A REGION OF NEAR ZERO WEIGHT LOSS ABOVE 1050 K

Material	Breakpoint Determination Run	Breakpoint Temperature Excluding Emissivities[1] (K)	Protective Fluoride Film[2]	Average Breakpoint Temperature or Fluoride Film Failure Point, T_f (K), Including Assumed Emissivity Correction[1,3]	Estimated Upper Use Temperature 0.95 T_f[4] (K)
LaB_6	HF-171	1740	LaF_3 (mp = 1763 K; bp = 2445 K); [BF_3]	1875	1800
CaB_6	HF-167	1680	CaF_2; [BF_3]	1785	1700
La_2O_3·Si_3N_4	HF-125	1495	LaF_3; [SiF_4; NF_3; OF_2]	1595	1500
Sc	HF-119	1400	ScF_3	1465	1400
Ni-270	HF-110 HF-140	1390 1420	NiF_2 (mp = 1430 K; bp = 2150 K)	1465	1400
SrO	HF-14	1375	SrF_2 (mp = 1736 K; bp = 2573 K); [OF_2]	1460	1400
$LaCrO_3$	HF-122	1365	LaF_3; [OF_2; CrF_3 (subl = 1370 K); CrF_4 (mp = 550; bp = 570 K)]	1450	1400
Y	HF-111	1365	YF_3 (mp = 1421 K; bp = 2205 K)	1425	1350
Y_2O_3	HF-163	1340	YF_3; [OF_2]	1420	1350
NiAl	HF-109 HF-149	1320 1280	NiF_2; AlF_3	1355	1300
Ni (Y_2O_3 doped)	HF-202	1290	NiF_2; YF_3; [OF_2]	1345	1300
MgO	HF-74 HF-137 HF-147 HF-155	1260 1240 1280 1245	MgF_2 [OF_2]	1325	1250
Al_2O_3	HF-132 HF-135	1180 1185	AlF_3; [OF_2]	1245	1200
TiAl	HF-124	1165	AlF_3; [TiF_4 (subl = 547 K)]	1205	1150
BeO	HF-133 HF-134	1095 1160	BeF_2 (mp ~ 825 - 1025 K; bp = 1460 K); [OF_2]	1185	1150
Graphite	HF-144	1140	$CF_{x\sim1}$ (est. subl = 1140 K)	1140	1100
CaO	HF-48	ND	CaF_2; [OF_2]	> 1160 (cracked)	
BeO	HF-48	ND	BeF_2 (mp = 1027 K; bp = 2475 K)	> 1110 (cracked)	

(1) Temperatures rounded to nearest 5 K; ND = not determined.

(2) Assuming highest valence fluoride forms, the mp (melting point), bp (boiling point), and/or subl (sublimation point) are shown when a particular fluoride is first listed in Tables 4, 5, or 6. Obtained from References 6, 7, 10, 14, 15, and 22. Volatile fluorides in brackets.

(3) With values of 0.4 for ceramic and 0.6 for metallic specimen emissivities assumed; emissivity corrections from Bureau of Standards Monograph 30; no correction for graphite as measurement is from embedded thermocouple.

(4) Temperatures rounded to nearest 50 K; since these values are a multiple of T_f, emissivities are also included.

maintained because of the uniform vaporization of the fluorides. Both carbon and Al_2O_3 had corrosion rates that increased uniformly with increasing temperatures above the film failure points. After film failure, these two materials had relatively low corrosion rates when tested beyond their breakpoints. For instance, after exceeding T_f with a 1500 K specimen surface temperature, carbon experienced a 6.7% weight loss per minute, and Al_2O_3 had a 12.3% weight loss per minute.

Most film-forming ceramic samples failed below the reported fluoride or fluoride and substrate eutectic melting points, probably from vaporization or cracking of the film followed by rapid exothermic reaction of the exposed substrate elevating the surface temperature above the fluoride melting point. Comparing MgO and Al_2O_3 polycrystalline and single crystal specimens, it appears that there is little effect of grain boundaries on the upper use temperature.

The film-forming metallic specimens appear to fail close to the reported fluoride melting points (or in between the melting points for intermetallics) with the resultant exothermic rise in temperature causing melting of the substrate metal. Scandium metal, however, exhibited film failure approximately 300 K below its reported fluoride melting point, since failure was probably from fluoride vaporization. The utility of metallic specimens above 1400 K is limited because of their low strengths and low creep resistance above 75 to 85% of their melting temperature.

Three materials could withstand surface temperatures of approximately 100 K above their reported fluoride melting points before film failure occurred: BeO, CaB_6, and LaB_6. With BeO, a high-viscosity glass-forming fluoride protects the substrate until rapid vaporization causes failure.

With the borides, CaB_6 and LaB_6, the initial formation of fluorides is quite rapid, as anticipated. However, the films have good adherence and are very protective with CaB_6 having greater weight loss above 1500 K surface temperature than LaB_6. The CaB_6 still exhibits a relatively low corrosion rate, however, of approximately 4.5% weight loss for approximately 180 s at a surface temperature of approximately 1500 K. For CaB_6, the molten fluoride film viscosity decreases rapidly and allows corrosion before complete film failure. For LaB_6, the fluoride film exhibits some flow above 1755 K (1635 K excluding emissivity correction); but the LaF_3 has a high viscosity; its film failure point of 1875 K (1740 K excluding emissivity correction) represents the point at which both rapid vaporization of the LaF_3 occurs and the viscosity of the LaF_3 decreases to allow rapid flow.

Other materials protected by a LaF_3 film were $La_2O_3 \cdot Si_3N_4$ and $LaCrO_3$. The oxynitride has film failure approximately 300 K below LaB_6, probably from extensive cracking or lack of adherence of the LaF_3. Lanthanum chromite forms a thick, poorly adherent film which melts more than 400 K below the LaF_3 coating failure on LaB_6. Therefore, the nature (and protectability) of the fluoride film which forms is dependent on the substrate precursor.

The performance of materials in Table 6 may be ranked by the estimated upper use temperature (95% of T_f, rounded to the nearest 50 K) yielding: LaB_6 (1800 K) > CaB_6 (1700 K) > $La_2O_3 \cdot Si_3N_4$ (1500 K) > [scandium, nickel, SrO, $LaCrO_3$] (1400 K) > [yttrium, Y_2O_3] (1350 K) > [NiAl, Y_2O_3 doped nickel] (1300 K) > MgO (1250 K) > Al_2O_3 (1200 K) > [TiAl, BeO] (1150 K) > carbon (1100 K).

In addition to the stability of the protective fluoride film on a substrate, the density of the substrate was shown to have a significant effect on performance (besides its effect on fragmentation mentioned for Y_2O_3 and CaB_6). For instance, the relatively porous $La_{0.33}Sr_{0.67}B_6$ test specimens (87% dense, HF-161) and porous PS LaB_6 test plates (81% dense, HF-173 and 175) exhibited more corrosion than dense (≥ 95% dense, HF-69, 75, 76, 78, 96 to 103, 141 to 143, and 171) LaB_6 specimens.

Considering test plate performance, it appears that the material behavior (with respect to fluoride film characteristics) directly correlates with data for test cylinders. The thermal shock conditions for test plates in the configuration test chamber are much worse than for cylindrical specimens, since MgO, Al_2O_3, and LaB_6 test plates cracked and only nickel and graphite test plates survived the thermal shock conditions without cracking. With design changes to reduce thermal stresses and by annealing test plates prior to use, it is expected that LaB_6 can withstand these conditions, especially if pure LaB_6 (ie, no free boron) is used. By comparing slots (with sharp edges) with holes in the graphite test plates, it was determined that the presence of the sharp edges initiated corrosion.

The graphite configuration test chamber was shown to be protected by either a PS insertable LaB_6 liner or a direct PS LaB_6 coating. Thus, chamber surface temperatures well above the 1140 K limit for unprotected graphite are possible.

There has been only one related study utilizing a torch test. In that study,[24] Ebner included air, limited testing to six refractories, and used surface temperatures well above all reported fluoride melting points. Thus, no fluoride film protection could result, and direct comparison with the current work was difficult. However, when limiting comparison with graphite and Al_2O_3 (evaluated after film failure), the present study produced uniform, relatively low corrosion rates in keeping with Ebner's findings that graphite had the lowest corrosion rates. Ebner did not investigate LaB_6.

Above the temperature at which an adherent protective fluoride film might form (or generally above the fluoride melting point), a simple theoretical analysis of material behavior is possible. The very high surface temperatures required for nil film protection occur when specimens are thermally insulated so that most of the heat from the flame is absorbed by the specimen. Such high temperatures were used by Ebner.[24] The kinetics of a fluorine reaction with the surface of a material would then depend only on: (1) the number of atoms required to be attached to the surface in order to form the most stable fluorine rich fluoride (assuming a fluorine rich flame) and (2) the atomic density of the material (number of atoms per cubic centimeter). The difficulty of attaching a certain number of fluorine atoms will vary directly with the number required for fluorine formation, and the

resultant vacancy in the lattice of the surface will depend on the atomic (or ionic, covalent, or metallic) radii of the element evolved. The simplest method of calculating the kinetics under these assumptions is as follows:

$$V = \frac{m}{A} = \frac{mM}{\rho Nf},$$

where:

V is the volume loss (in cubic centimeters) on the material surface that is created when 10 fluoride atoms caused removal of volatile fluorides;

m is the number of atoms removed from the material surface when 10 fluorine atoms are appropriately attached to the surface;

A is the atomic density of the material in atom per cubic centimeters and is equal to (ρNf)/M;

ρ is the bulk density of the material in gram per cubic centimeter;

N is Avogadro's number, 6.0236×10^{23} atoms per mole;

f is the number of moles per formula weight;

M is the mass (in grams) per formula weight.

Thus, a minimum value of V signifies the best corrosion resistance in a high-temperature fluorine environment when surface temperatures exceed the film failure temperatures. Therefore, for materials listed in Table 4 (with volatile fluorides) or for fluoride film formers above the film failure point (as Ebner's study),[24] the relative performance ranking can be calculated. This rather simple approach was used to some extent in selecting materials which were film formers but had low values of V.

In reviewing the outcome of thermocouple experiments conducted with several of the candidate materials, it was established that the use of thermocouples gave a good representation of the behavior of the specimens during test. Comparison of the automatic pyrometer measurements (read at the top center of the specimens) with the readings recorded by the top center thermocouple (located below the position of flame heat impingement) showed good agreement up to the breakpoint temperatures. In the case of MgO and LaB_6, the ΔTs between the thermocouple and pyrometer readings were higher than for the other materials tested. These larger temperature differences were probably due to the low heat conduction characteristics of the fluoride layers. Breakpoint temperatures were readily recognized because of the sharp rise in the pyrometer recorded curve that shows the onset of exothermic reaction. At this point, the ΔTs between the pyrometer and

thermocouple readings tended to diverge. Errors in pyrometer measurements can be introduced after breakpoint temperatures are reached because of the presence of fluoride vapors and changes in emissivity characteristics of the test specimen.

FURTHER MATERIALS CONSIDERATIONS

Impregnation or Coating of Carbon with Fluoride

As a result of initial tests indicating that graphite had potential for application in the HF torch environment, the possibility of impregnating or coating porous graphite with high-melting fluorides was considered. It was felt the fluoride could provide a protective layer allowing little or no corrosion of the graphite. Problems forseen with such a system were the possible interactions of fluorides with carbon or with carbon fluorides (CF_x or CF_4).

Thermogravimetric analyses (TGA) of carbon mixed with CaF_2 in graphite or tungsten crucibles were almost identical up to 1900 K. There was no evidence of reaction between CaF_2 and graphite—only volatilization of CaF_2 occurred. Since there was no reaction of CaF_2 and graphite, the wetting behavior of CaF_2 with graphite was qualitatively determined by (1) painting porous (approximately 15%) graphite with an aqueous slurry of CaF_2 and (2) rapidly heating (approximately 100 K/min) to a temperature approximately 100 K above the fluoride melting point in argon, holding for 15 min, and furnace cooling. This revealed the fluoride to be nonwetting, as CaF_2 beads had formed on the graphite surface. A similar test with LaF_3 showed the same nonwetting behavior.

To form a uniform fluoride layer on graphite, physical vapor deposition in a vacuum of CaF_2 onto graphite was used. A thin (approximately 1 μm), adherent film of CaF_2 was formed on the graphite. On exposure to the HF torch, however, in Run HF-37, corrosion was equal to that of uncoated graphite.

Although the nonwetting behavior of fluorides on graphite presents problems with loading carbon with fluorides, several approaches are being investigated,[i] including hot isostatic-pressure impregnation; sintered or hot-pressed carbon-fluoride composites; and sintered or hot-pressed carbon- or graphite-LaB_6 composites.

Thermal Analyses of Fluorides

In order to better understand the relative protection afforded by fluoride films, the behavior of selected pure fluorides was studied by TGA and differential thermal analyses (DTA). The former technique yields information on the fluoride volatilizable characteristics in vacuum ($<1.3 \times 10^{-3}$ Pa); whereas, the latter accurately defines melting points from heating and cooling curves. The data obtained are given in Table 7. Temperatures, T_i, represent weight loss initiation; T_e or $T_{3\%}$ represents the point at which rapid weight loss occurs and indicates the upper use temperatures of the pure fluorides in vacuum. The values shown are

considerably lower than the breakpoints or fluoride film failure points (see Table 6) determined for materials which form these fluorides. It is suspected that the excess fluorine ($2F_2$ and H_2) may suppress to some extent the fluoride volatilization in the torch environment; also, HF torch tests are at 1-atm pressure, and Table 7 weight loss behavior is for vacuum.

Table 7

FLUORIDE CHARACTERIZATION BY THERMAL ANALYSES

Materials[2]	Characteristic Weight Change Temperatures[1]			Melting Point (K)[6]
	T_i[3]	T_e[4]	$T_{3\%}$[5]	
AlF_3	900	995	980	-
CaF_2	1385	1590	1565	-
SrF_2	1455	1620	1605	1740
LaF_3	1360	1640	1600	1765
$2SrF_2$-$1LaF_3$ Solid Solution	1435	1580	1575	1835

(1) Determined from TGA data using a thermoanalyzer, Model TA-1 from Mettler Instrument Company, Princeton, New Jersey, with ultrahigh temperature (2773 K) furnace using a vacuum $< 1.33 \times 10^{-3}$ Pa ($< 10^{-5}$ torr), a heating rate of 10 K/min, and a tungsten-tungsten, 26 wt % rhenium thermocouple, and with tungsten crucibles (no lids); temperatures rounded to nearest 5 K.

(2) Greater than 99.6 wt % pure by spark-source mass spectrographic analyses.

(3) Initiation temperature as indicated by the initial change in slope of the weight loss curve.

(4) Extrapolated temperature of rapid weight loss as determined by the intersection of tangent lines—one to the base curve and one to the point on the curve where 10% weight loss (based on initial weight) after 1273 K occurred (or after 773 K for AlF_3).

(5) Temperature at which 3% weight loss (based on initial weight) after 1273 K occurred (or after 773 K for AlF_3).

(6) Determined from DTA data using a thermoanalyzer, Mettler Model TA-1, with high-temperature (1873 K) furnace, a flowing (5.1 L/h) helium atmosphere, a heating and cooling rate of 8 K/min, a platinum-platinum, 10 wt % rhodium thermocouple, and molybdenum (Grade TZM) crucibles and lids; average of three peaks from cooling curves.

Since there was a citation to an anomalous solid solution[23] at the $2SrF_2$-$1LaF_3$ composition, this mixture and the end-members were examined by DTA. The SrF_2 and LaF_3 end-members melted within 5 K of reported[10] values. The $2SrF_2$-LaF_3 mixture melted 65 K higher than LaF_3 and 95 K higher than SrF_2. Subsequent X-ray diffraction analyses revealed only the SrF_2 with a slightly shifted diffraction pattern indicative of the solid solution $2SrF_2$-$1LaF_3$ (since no free LaF_3 was detected). This complete phase diagram is being determined,[(i)] and the solid solution region extends to 57 mol % LaF_3 in SrF_2 with maximum melting points in the region 25 to 33 mol % LaF_3 or the $2SrF_2$-$1LaF_3$ composition.

Summarizing Table 7, it appears (from T_e or $T_{3\%}$ datum) that, in a vacuum environment, the maximum fluoride use temperatures would be expected to be around 1600 K for minimal weight losses or change in dimensions of a material protected by these fluorides.

Tetrafluoromethane Addition Experiments

Two runs were conducted to determine the effect of the addition of CF_4 to the HF flame on the corrosion behavior of ATJ graphite. The possibility was surmised, from preliminary studies, of a significant reduction in the reaction of graphite with fluorine by the addition of low-level CF_4 (<1 mol %). The two runs (HF-172 and HF-176) were conducted with the graphite configuration test chamber; each ATJ graphite test plate was 3.81 mm (0.150 in)

thick and was provided with 36 1.0-mm (0.040 in)-diameter drilled holes. The CF_4 was introduced into the flame nozzle through the hydrogen feed line.

In Run HF-172, the CF_4 flow rate was 800 cm^3/min so that it constituted 4.16 wt % and 0.53 mol % of the total inlet gas flow to the nozzle. In Run HF-176, the CF_4 flow was 7.89 wt % and 1.04 mol % of the total flow. Detailed data for these runs may be found in Appendices B and C. The areas around the centers of the tested plates showed signs of corrosion. This is readily seen in photographs taken of Plate HF-176, Figures 51 and 52. The

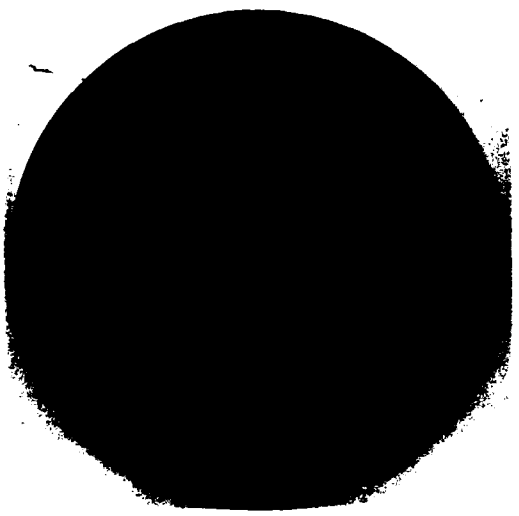

183327

Figure 51. TETRAFLUOROMETHANE ADDITION EXPERIMENT WITH GRAPHITE TEST PLATE EXPOSED FACE TO HYDROGEN FLUORIDE FLAME.

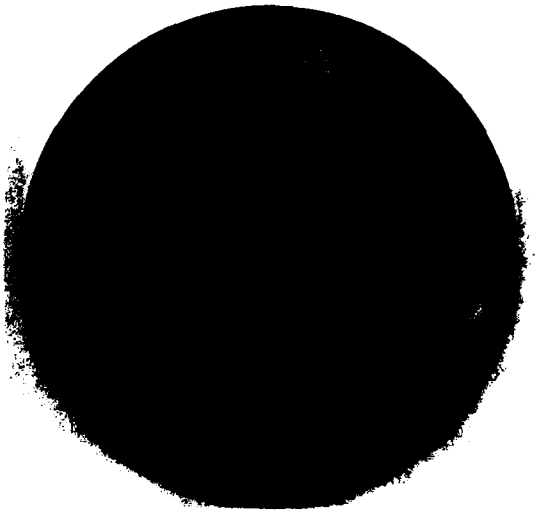

183328

Figure 52. TETRAFLUOROMETHANE ADDITION EXPERIMENT WITH GRAPHITE TEST PLATE EXPOSED BACK FACE TO HYDROGEN FLUORIDE FLAME.

hole diameters in Plate HF-172 had increased in diameter from 1.0 to 1.8 mm (0.040 to 0.070 in); in Plate HF-176 the increase was from 1.0 to 1.2 mm (0.040 to 0.046 in). Furthermore, in Run HF-176, the test chamber had cracked and showed signs by its sooty appearance of having reacted with the flame gases. A photograph of the chamber, which cracked during the run, may be seen in Figure 53. In addition, the sapphire sight glass in the chamber was etched, and this was an unusual occurrence. During the runs, it was noted that the flame did not have its characteristic bluish color but, instead, was green to greenish blue.

Comparison of the above two runs with Run HF-146, in which no CF_4 was added to the flame, indicates the graphite corrosion rate in Run HF-176 was less than in Run HF-146, 0.709 g/min weight loss versus 0.969 g/min. Based on the work conducted thus far, the addition of CF_4 does not significantly improve the corrosion resistance of graphite to the HF flame. The failure of the graphite chamber in Run HF-176 indicates CF_4 addition can introduce significant problems.

Fluorine to Hydrogen Ratio Change

Consideration had been given in this evaluation program to the use of gas compositions wherein the 2:1 F_2:H_2 ratios would be altered. Accordingly, two runs (HF-178 and HF-180) were conducted with a 1:1 F_2:H_2 ratio and one run (HF-179) with a 3:1 F_2:H_2 ratio. Dense LaB_6 cylindrical specimens were employed as the test material.

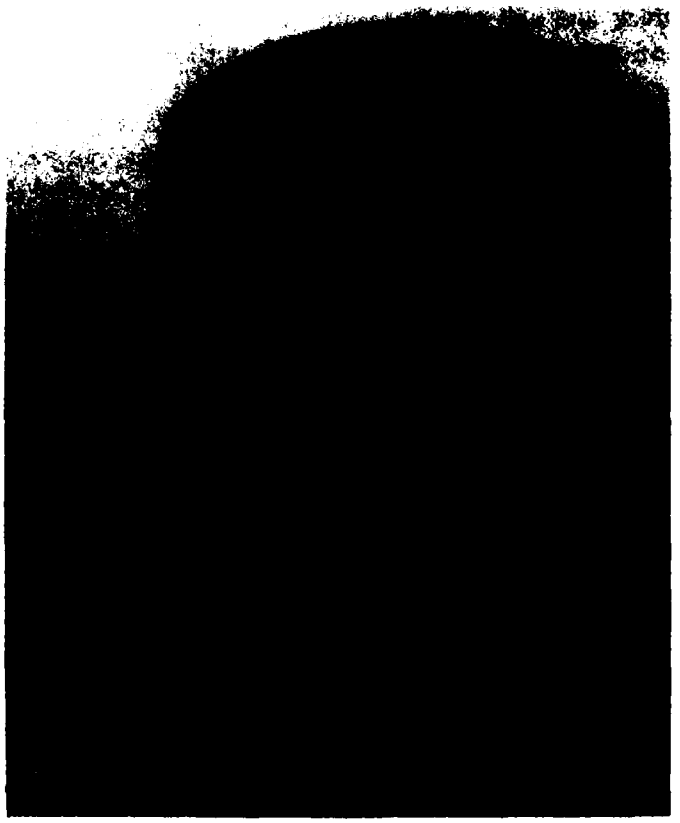

184545

Figure 53. CONFIGURATION TEST CHAMBER AFTER TETRAFLUOROMETHANE ADDITION EXPERIMENT. (Run HF-176.)

Specimen surface temperatures attained with the 1:1 F_2:H_2 ratio gas compositions were 1416 and 1493 K. The maximum surface temperature attainable with the 3:1 F_2:H_2 ratio flame was only 1103 K. Evidently the excess fluorine acts as a diluent and, combined with its high heat of dissociation, results in lower flame temperatures. In each instance, dimensional changes in the tested specimens were low. One difference occurring in the samples of the two experiments could be seen in the appearance of the resultant LaF_3 layers. With a 1:1 F_2:H_2 ratio, the fluoride layer appeared to be thin and light gray in color. In the other case, the fluoride layer was white.

The differences in morphology of LaB_6 specimens exposed to a 1:1 F_2:H_2 or a 3:1 F_2:H_2 flame is illustrated in Figures 54 to 57. Figure 54 (top views of the LaF_3 coatings) shows that the top surface is microcracked and that there is approximately a factor of three grain size difference in the fluoride films (since the 1000X and 3000X photos of 1:1 F2:H_2 exposed materials correspond to the 3000X and 10,000X photos of 3:1 F_2:H_2 exposed materials). Microcracking and grain size of this top surface for the 1:1 F_2:H_2 exposed LaB_6 correspond to the 2:1 F_2:H_2 exposed LaB_6 specimens examined (specimen after Run HF-78 and specimen after Run HF-141).

Figure 55 illustrates the edge views of the LaF_3 coatings. The 1:1 F_2:H_2 exposed LaB_6 forms a LaF_3 coating with an apparent transition layer (sine wavelike band, 20 to 30 μm below the exposed surface, of coarse grained material. The 3:1 F_2:H_2 exposed LaB_6 forms

LANTHANUM HEXABORIDE SPECIMEN EXPOSED TO 1:1 F_2:H_2

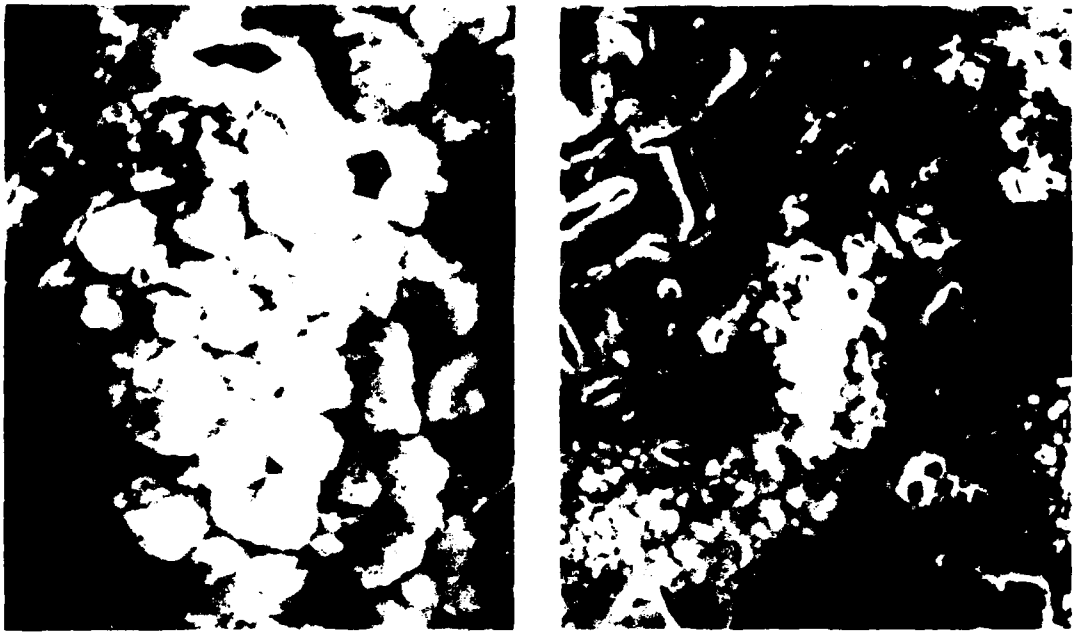

(a) 3000X. SM-69533 (b) 1000X. SM-69534

LANTHANUM HEXABORIDE SPECIMEN EXPOSED TO 3:1 F_2:H_2

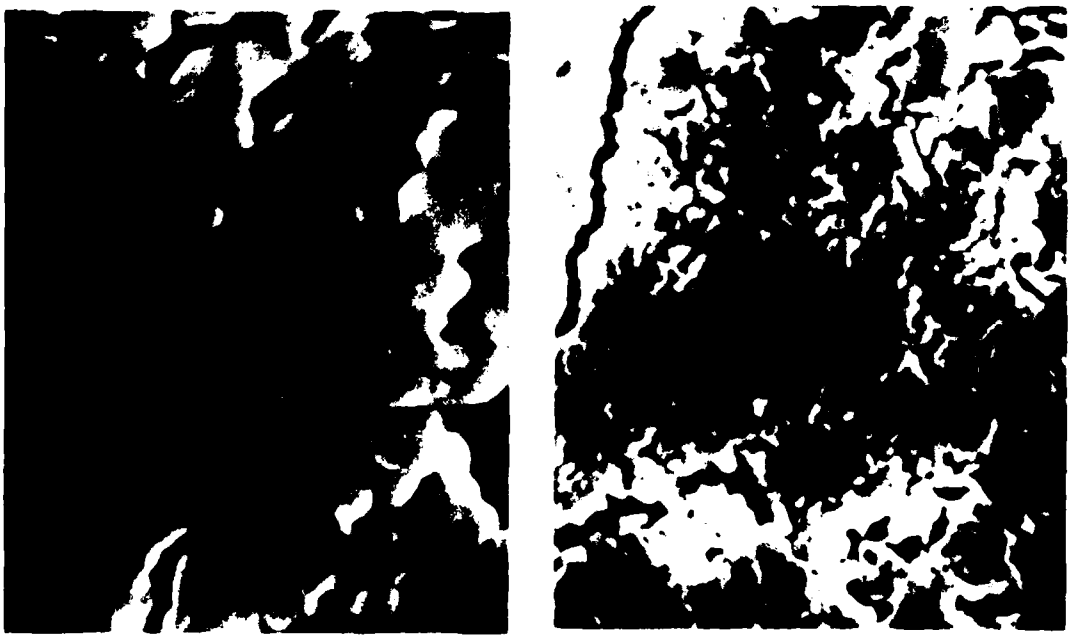

(c) 10,000X. SM-69537 (d) 3000X. SM-69538

Figure 54. SCANNING ELECTRON MICROSCOPE PHOTOGRAPH OF LANTHANUM FLUORIDE COATINGS ON LANTHANUM HEXABORIDE. (Top views of cylinders.)

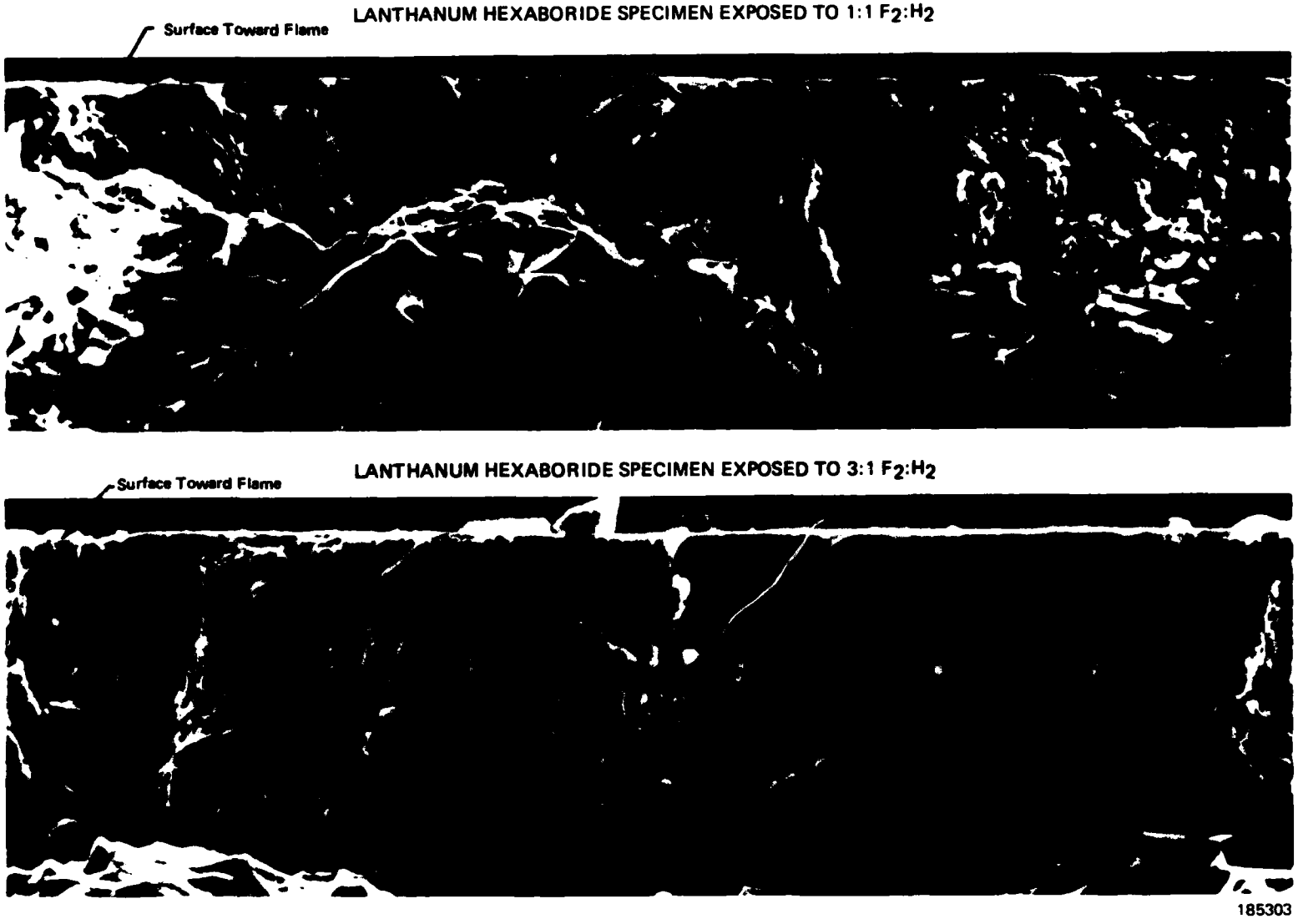

Figure 55. SCANNING ELECTRON MICROSCOPE PHOTOGRAPH OF LANTHANUM FLUORIDE COATINGS ON LANTHANUM HEXABORIDE. (Edge views of top coatings on cylinders; 1000X.)

185301

Figure 56. SCANNING ELECTRON MICROSCOPE PHOTOGRAPH OF LANTHANUM FLUORIDE COATING ON LANTHANUM HEXABORIDE AFTER 1:1 F_2:H_2 EXPOSURE. (Edge view of top coating on cylinder; 3000X.)

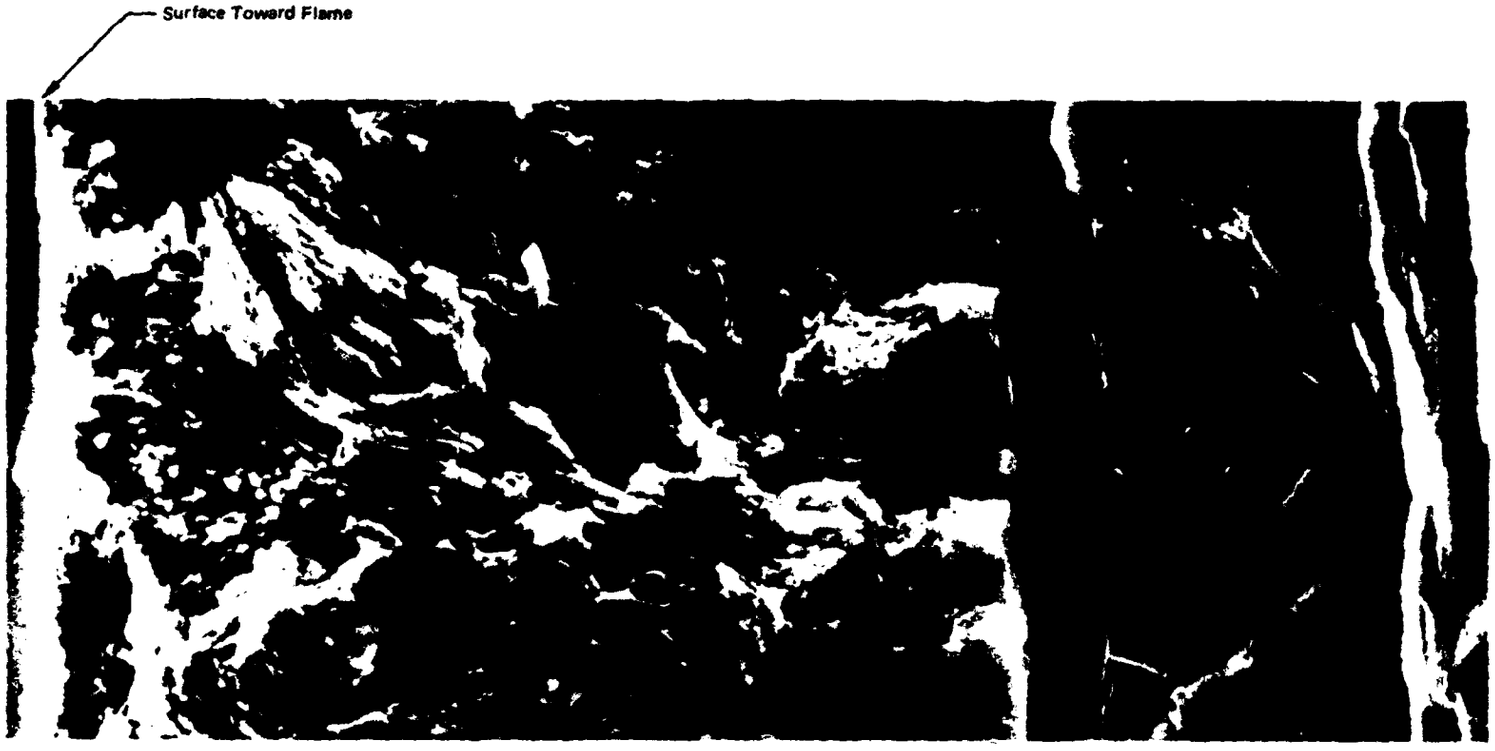

185302

Figure 57. SCANNING ELECTRON MICROSCOPE PHOTOGRAPH OF LANTHANUM FLUORIDE COATING ON LANTHANUM HEXABORIDE AFTER 3 * F_2 H_2 EXPOSURE. (Edge view of top coating on cylinder; 3000X.)

columnar-shaped (elongated) grains with a microcracked region where transition from LaF_3 to LaB_6 occurs. The 1:1 F_2:H_2 exposed LaB_6 had a 35- to 90-μ (approximately 60-μm average) LaF_3 layer; the 3:1 F_2:H_2 exposed LaB_6 had a 35- to 50-μm average) LaF_3 layer. The morphology differences are further illustrated in Figure 56 and 57. Both LaF_3 coatings are adherent and protective overall with minimal weight and dimensional changes resulting (Runs HF-178 to 180).

CONCLUSIONS

Resistance of materials to the HF flame depends on the formation of a protective fluoride film with the following characteristics of the film being beneficial:

1. An adherent, relatively dense, continuous film.

2. High melting point.

3. Sufficiently low vapor pressure.

4. No eutectic between fluoride film and substrate or else a high-melting-point eutectic.

Substrate protection deteriorates when the fluoride film melts, vaporizes, microcracks, or spalls.

When the fluoride film fails to limit substrate exposure and to kinetically inhibit the fluoriding reaction, the surface temperatures of the substrate surge from the rapid exothermic reaction.

After fluoride film failure, materials whose fluorides fail by vaporization (carbon, Al_2O_3, BeO, LaB_6) have good configurational stability and, except for BeO, have relatively low rates of corrosion.

Melting point of the substrate is relatively unimportant (if it is above required use temperatures) since performance depends primarily on the fluoride film characteristics.

Thermal-shock-sensitive materials can perform in the HF flame provided programmed heat-up and cool-down cycles are employed.

A ranking of fluoride film formers with maximum use temperatures in the range 1800 to 1400 K is: $LaB_6 > CaB_6 > La_2O_3 \cdot Si_3N_4 >$ (Sc, Ni, SrO, $LaCrO_3$).

Plasma-sprayed LaB_6 shows promise of protecting substrate materials in an HF flame environment. The concept of adding an intermediate layer between the substrate and the LaB_6 layer, to accommodate CTE mismatches, should be investigated.

Under test conditions existing in the configuration test chamber, dense LaB_6 test plates were found to be thermally shock sensitive (possibly affected by free boron). Improvement of its shock sensitivity, by forming composites with carbon, should be further investigated.[i] Also, test plate design might be modified to minimize thermal shock conditions.

Further investigation is required to find materials containing lanthanum that are capable of survival in the HF flame and that have readily machinable characteristics.[i]

REFERENCES

1. Patton, F. S., Googin, J. M., and Griffith, W. L.; ***Enriched Uranium Processing***, p 34; The MacMillan Company, New York (1963).

2. Glassner, A.; ***The Thermochemical Properties of the Oxides, Fluorides, and Chlorides to 2500 K***, Report ANL-5750; Argonne National Laboratory, Argonne, Illinois (1957).

3. Palin, D. E. and Wadsworth, K. D.; "Structure of Carbon Monofluoride," ***Nature***, 162, pp 925 - 926 (1948).

4. "System MgF_2-MgO," ***Phase Diagrams for Ceramists***, 1969 Supplement, p 447, Figure 3692, E. M. Levin, C. R. Robbins, H. F. McMurdie, and M. K. Reser, Editors, The American Ceramic Society, Columbus, Ohio (1969).

5. Sahagian, C. S. and Pitha, C. A.; ***Compendium on High Power Infrared Laser Window Materials***, AFCRL-72-0170, Special Report 135; Air Force Cambridge Research Laboratories, Bedford, Massachusetts (1972).

6. ***JANAF Thermochemical Tables***, 2nd Edition, D. R. Stull and H. Prophet, Project Directors; National Bureau of Standards, Washington, DC (1971).

7. Illig, K., Hosenfeld, M., and Fischer, H.; ***In Beryllium, Its Production and Application***, pp 39 - 51, R. Rimbach and A. J. Michel, Translators; The Chemical Catalog Company, Inc, New York (1932).

8. Bamberger, Carlos E.; ***Personal Communication***, 1968 Data; Oak Ridge National Laboratory, Oak Ridge, Tennessee (1977).

9. ***High-Flux Reactor Materials Gaseous Fuels Research***, GEMP-334B, pp 161 - 184; General Electric Company, Schenectady, New York (1965).

10. Porter, B. and Brown, E. A.; "Melting Points of Inorganic Fluorides," ***Journal of the American Ceramic Society***, 45 (1), p 49 (1962).

11. "System NaF-CaF_2-AlF_3," ***Phase Diagrams for Ceramists***, p 445, Figure 1566, E. M. Levin, C. R. Robbins, H. F. McMurdie, and M. K. Reser, Editors; The American Ceramic Society, Columbus, Ohio (1964).

12. Shaffer, P. T. B.; ***High-Temperature Materials, No 1, Materials Index***, Plenum Press, New York (1964).

13. Wills, R. R., Stewart, R. W., Cunningham, J. A., and Wimmer, J. M.; "The Silicon Lanthanide Oxynitrides," ***Journal of Materials Science***, 11, pp 749 - 759 (1976).

14. Wallace, T. C., Feber, R. C., and Hauth, W. E.; ***Study of Materials Compatibility with HF, F, and F_2 for Combustion Laser Application***, LA-6780-MS; Los Alamos Scientific Laboratory, Los Alamos, New Mexico (1977).

15. Kent, R. A., Zmbov, K. F., Kanaán, A. S., Besenbruch, G., McDonald, J. D., and Margrave, J. L.; "Mass Spectrometric Studies at High Temperature-X, The Sublimation Pressures of Scandium (III), Yttrium (III), and Lanthanum (III) Trifluorides," ***Journal of Inorganic and Nuclear Chemistry***, 28, pp 1419 - 1427 (1966).

16. Van Uitert, L. G., O'Bryan, H. M., Guggenheim, H. J., Barns, R. L., and Zydzik, G.; "Correlation of the Thermal Expansion Coefficients of Rare Earth and Transition Metal Oxides and Fluorides." ***Materials Research Bulletin***, 12, pp 307 - 314 (1977).

17. Dutchak, Ya. I., Fedyshin, Ya. I., and Paderno, Yu. B.; "Thermal Properties of Metallic Hexaborides," ***Inorganic Materials*** (Russian translation), 8, (12) pp 1877 - 1880 (1972).

18. Tanaka, T.; "The Thermal and Electrical Conductivities of LaB_6 at High Temperatures," ***Journal of Physics***, 7, L177-80 (1974).

19. Kingery, W. D., Francl, J., Coble, R. L., and Vasilos, T.; "Thermal Conductivity: X, Data for Several Pure Oxide Materials Corrected to Zero Porosity," ***Journal of the American Ceramic Society***, 37, pp 107 - 110 (1954).

20. Binder, F.; "Contribution to the Knowledge of Cubic Hexaborides," ***Radex-Rundschau***, 1, pp 52 - 71 (1977).

21. Blitznakov, G., Isolovski, L., and Pescher, P.; "Investigation on Cathode Materials Prepared from Mixed Metal Hexaborides," ***Revue International Hautes Temperature Refractories***, 6, pp 159 - 164 (1969).

22. Wicks, C. E. and Block, F. E.; ***Thermodynamic Properties of 65 Elements - Their Oxides, Halides, Carbides, and Nitrides***, Bulletin 605; Bureau of Mines, Washington, DC (1963).

23. ***Fluorine Chemistry***, 1, J. H. Simons, Editor; Academic Press, Inc, New York (1950).

24. Ebner, M.; "Stability of Refractories in Hydrogen-Fluorine Flames," ***Journal of the American Ceramic Society***, 44 (1), pp 7 - 12 (1961).

ACKNOWLEDGMENTS

The authors extend their appreciation to the Air Force Weapons Laboratory and to the Defense Advanced Research Projects Agency for their sponsorship of this work (AFWL Project Orders, 76-182, 77-054, and 78-002) from June 1, 1976, to December 31, 1978.

We especially thank G. W. Weber (formerly at the Oak Ridge Y-12 Plant and Oak Ridge National Laboratory, presently with the High Performance Silicon Carbide Division of Carborundum Company, Niagara Falls, New York) for his assistance and direction while project manager for the major portion of this contract work.

The work was performed with Capt. P. H. Flynn and Capt. N. Pchelkin of Air Force Weapons Laboratory at Kirtland Air Force Base, New Mexico, as technical monitors for the program.

APPENDIX

FACILITY DRAWINGS AND PHOTOS

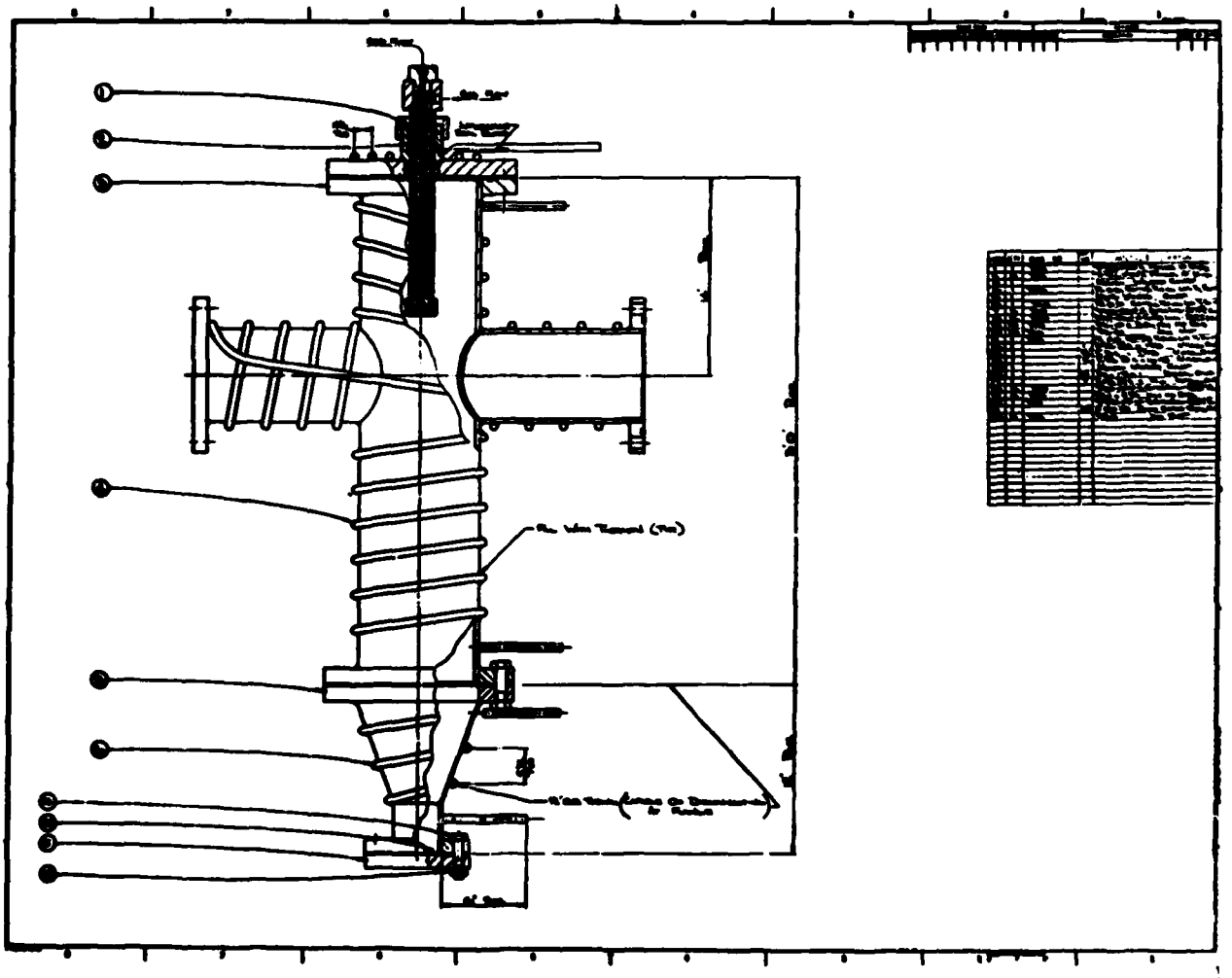

Figure A-1. NOZZLE AND REACTOR ASSEMBLY.

APPENDIX A

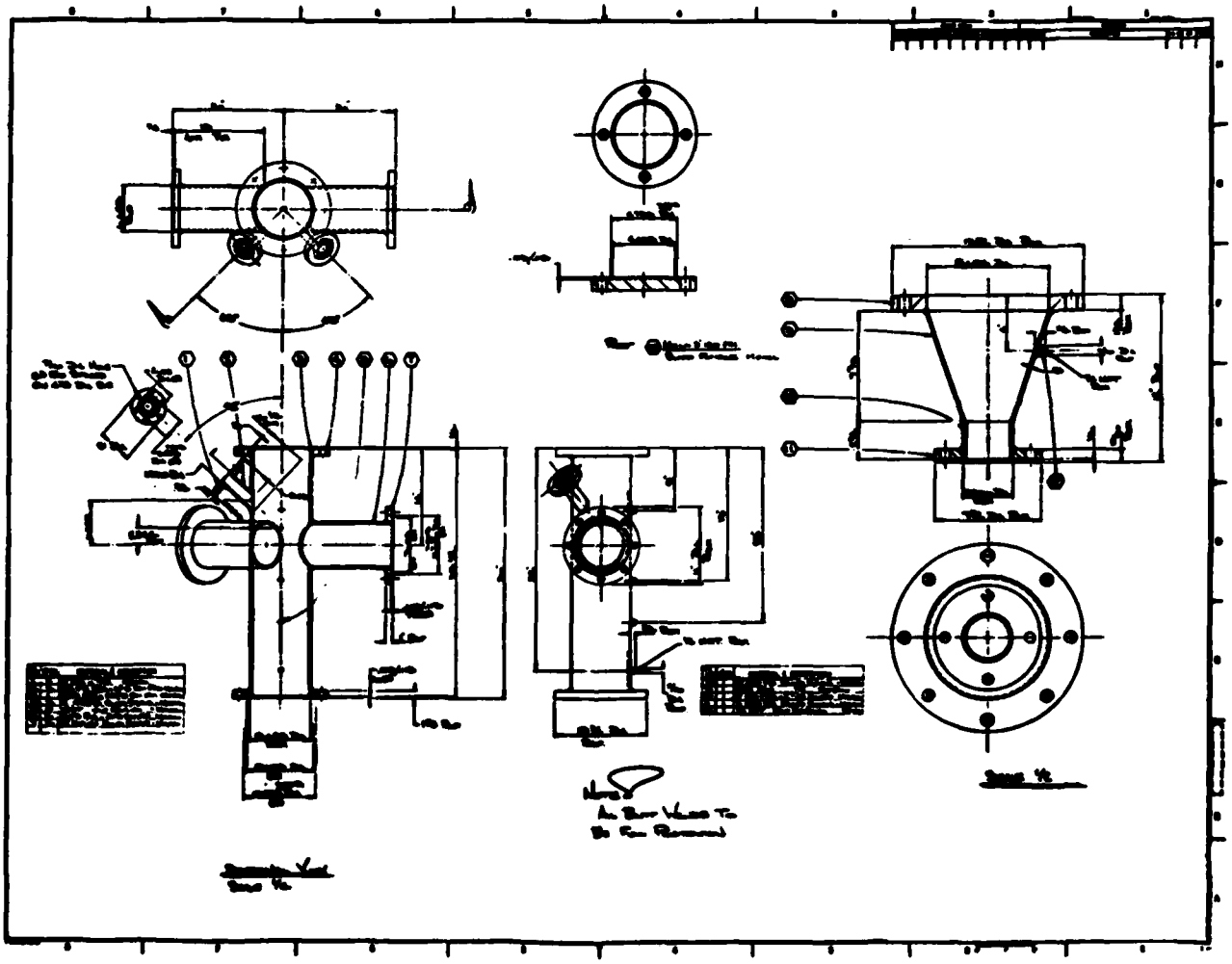

Figure A-2. REACTOR DETAILS.

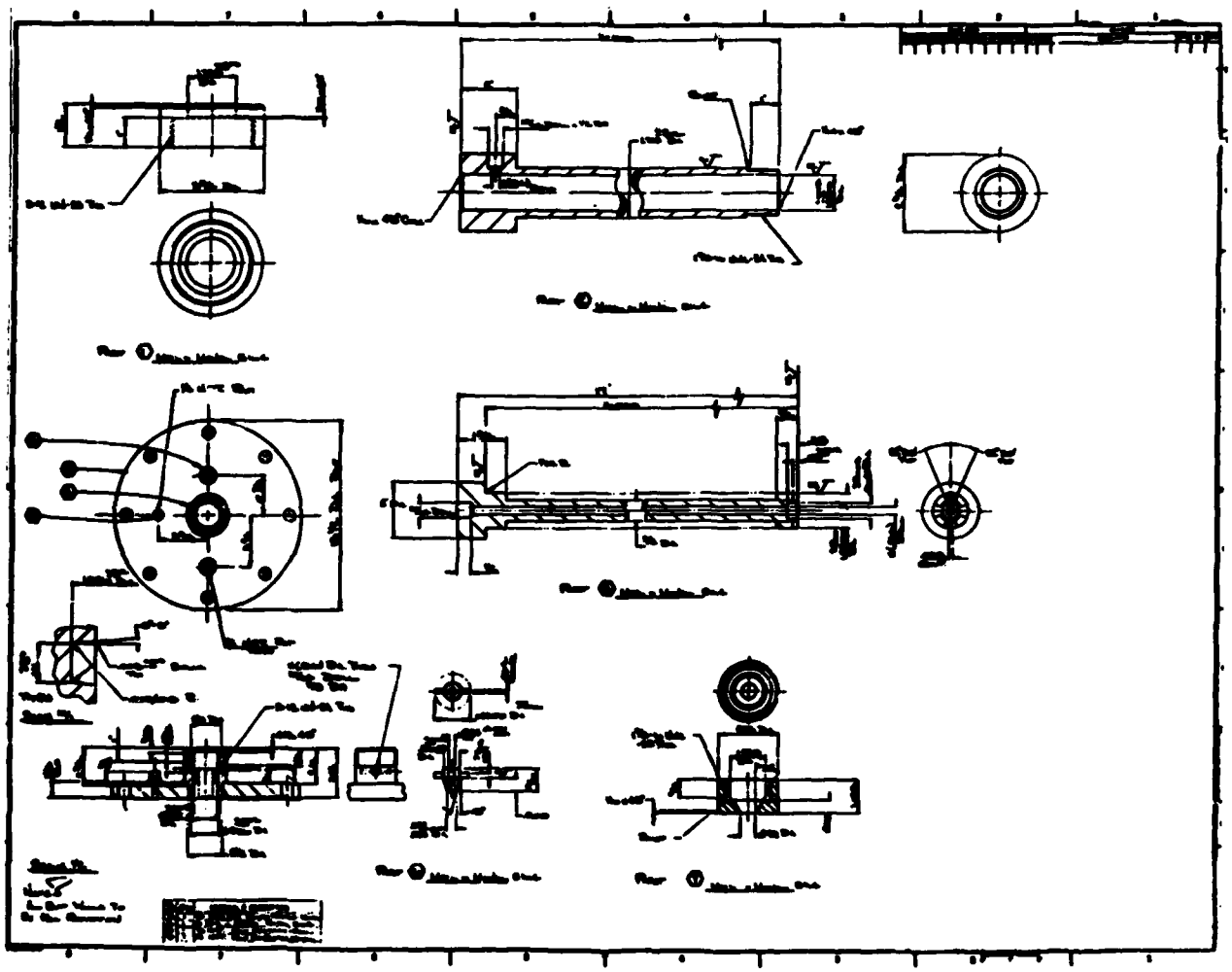

Figure A-3. NOZZLE DETAILS.

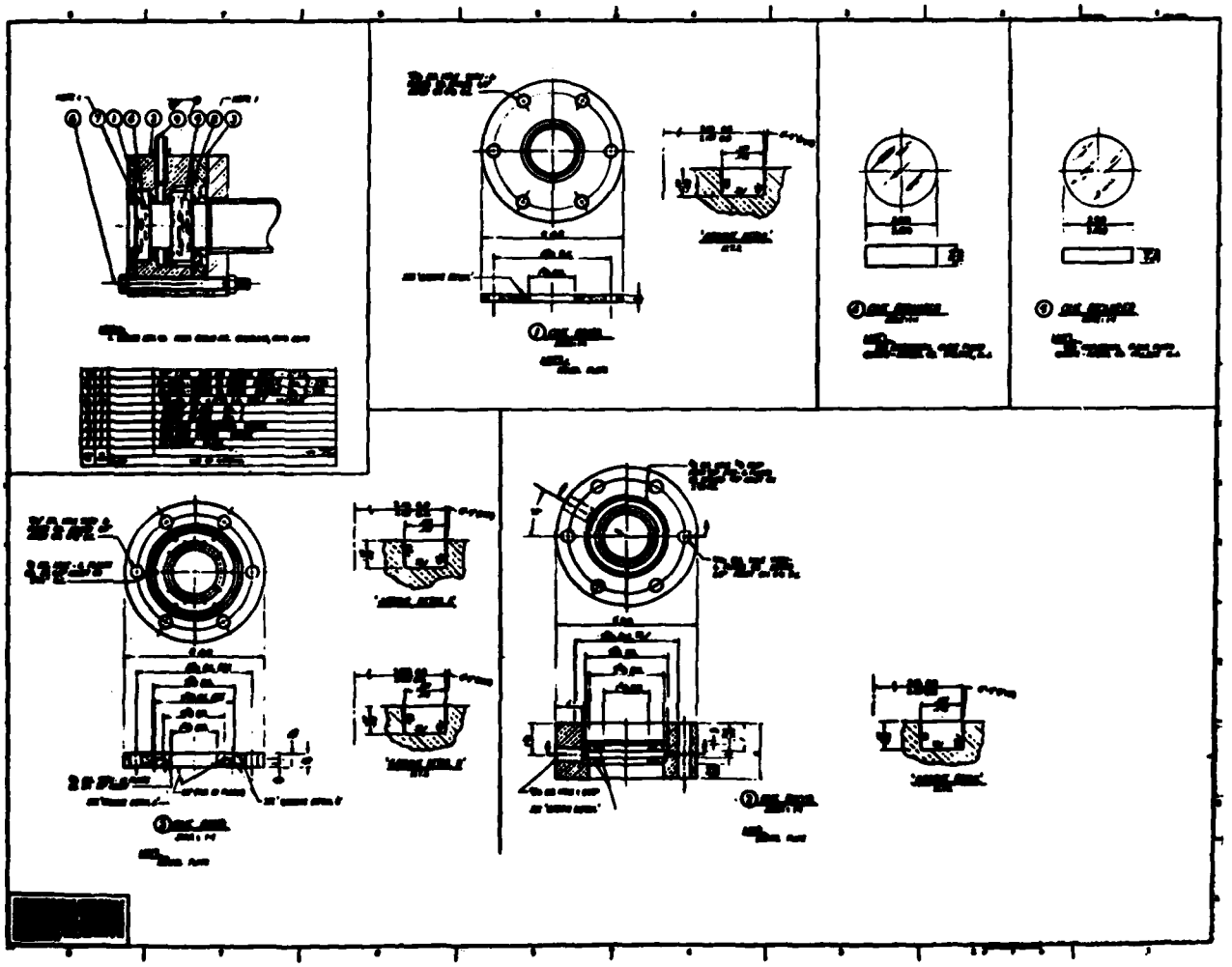

Figure A-4. SIGHT PORT DETAILS.

172921

Figure A-5. GAS CYLINDER STORAGE SHED.

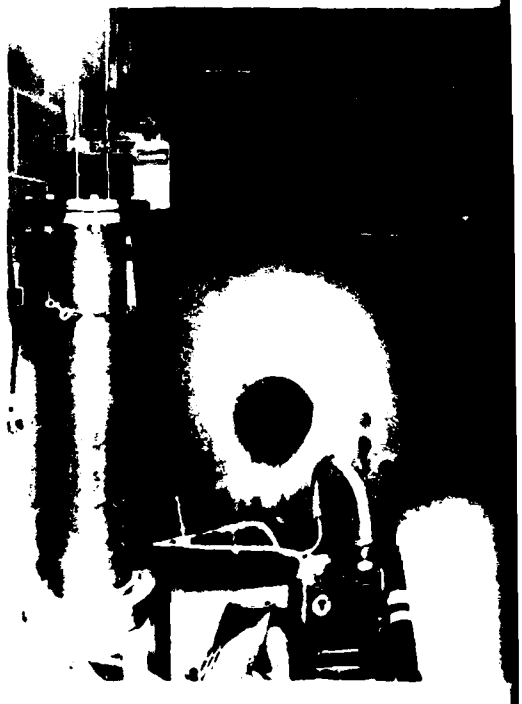

Figure A-6. FLUORINE "PIG" AN

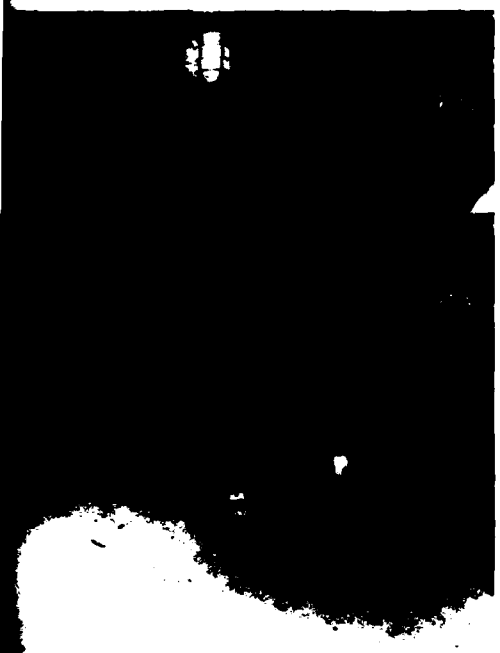

172918

"PIG" AND CHEMICAL TRAP.

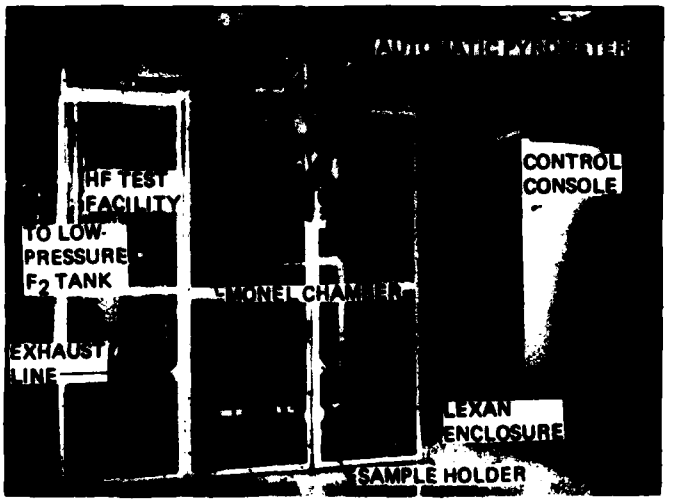

180247

Figure A-7. HYDROGEN FLUORIDE TEST FACILITY.

Figure
TEST

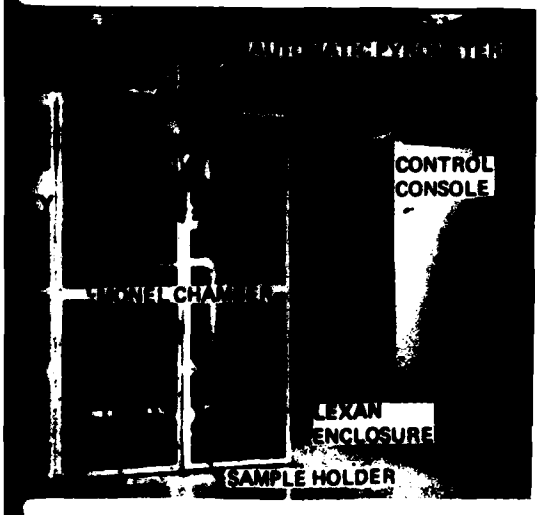

180247

7. HYDROGEN FLUORIDE TEST FACILITY.

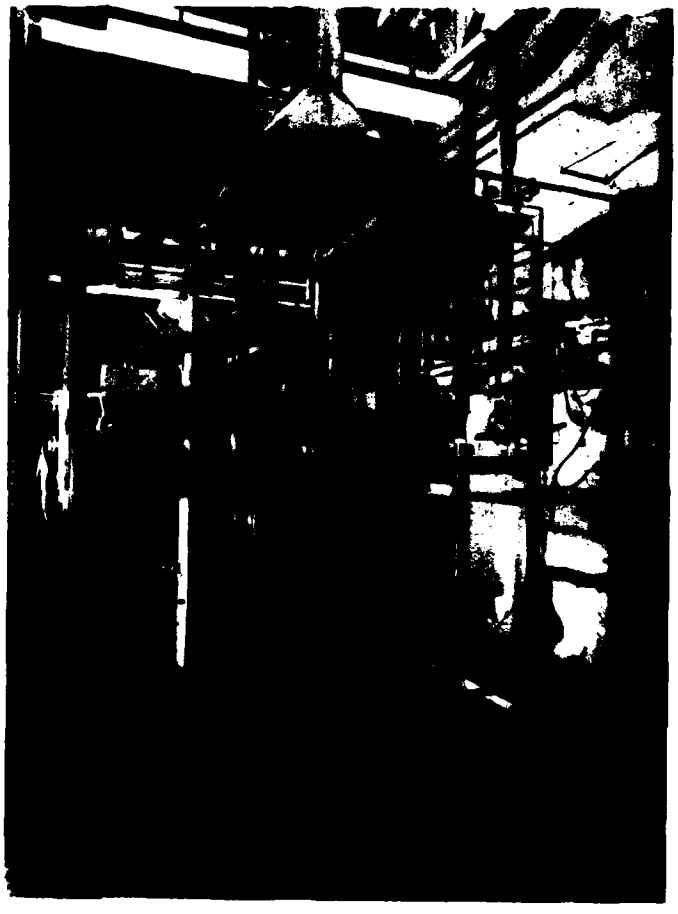

172919

Figure A-8. CONTROL VALVE STATION IN HYDROGEN FLUORIDE TEST FACILITY.

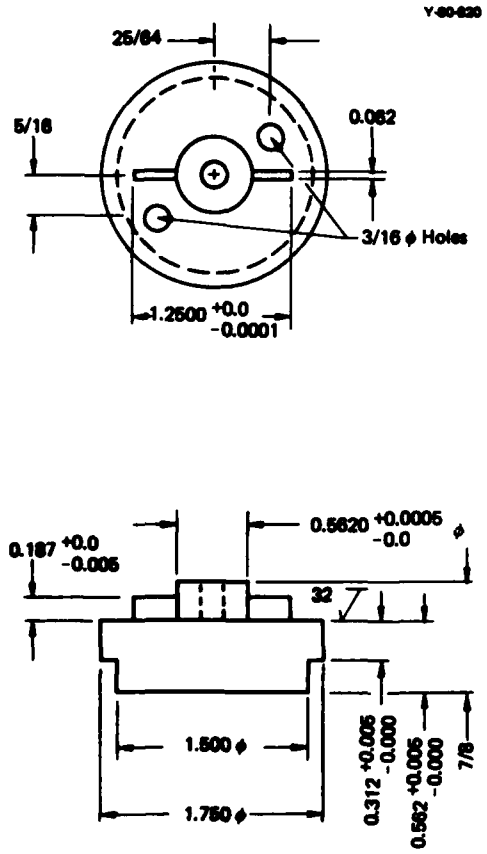

Figure A-9. REVISED NOZZLE TIP FABRICATED OF MONEL OR NICKEL. (Dimensions shown in inches.)

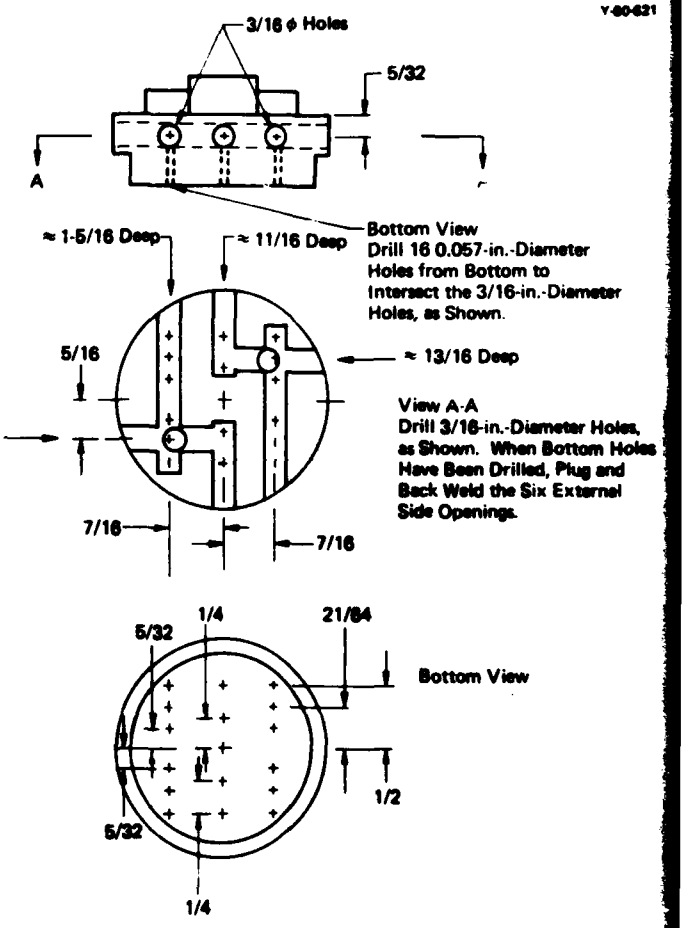

Figure A-10. REVISED NOZZLE TIP SHOWING LOCATION OF HOLES FOR FLUORINE AND HELIUM INLET AND DISCHARGE OPENINGS. (Dimensions shown in inches.)

Y-60-621

Y-60-622

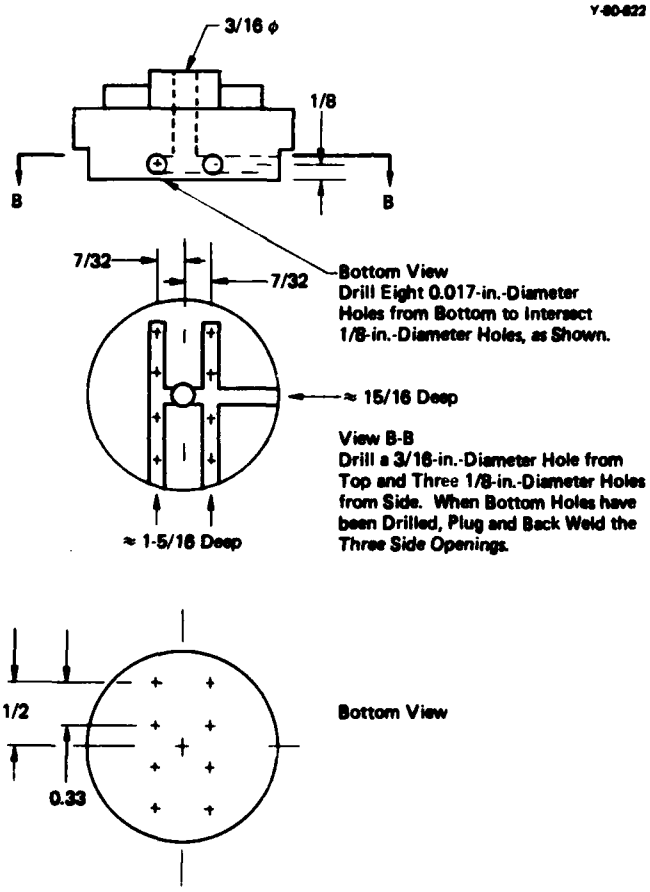

Figure A-11. REVISED NOZZLE TIP SHOWING LOCATION OF HOLES FOR HYDROGEN INLET AND DISCHARGE OPENINGS. (Dimensions shown in inches.)

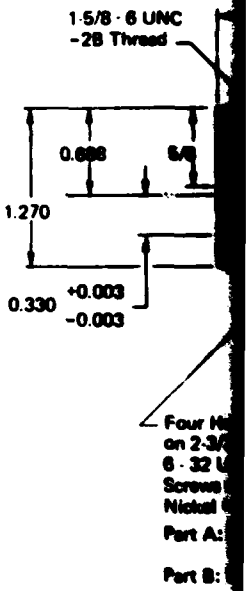

Figure A-12. NOZZLE
(Dimensions shown in in

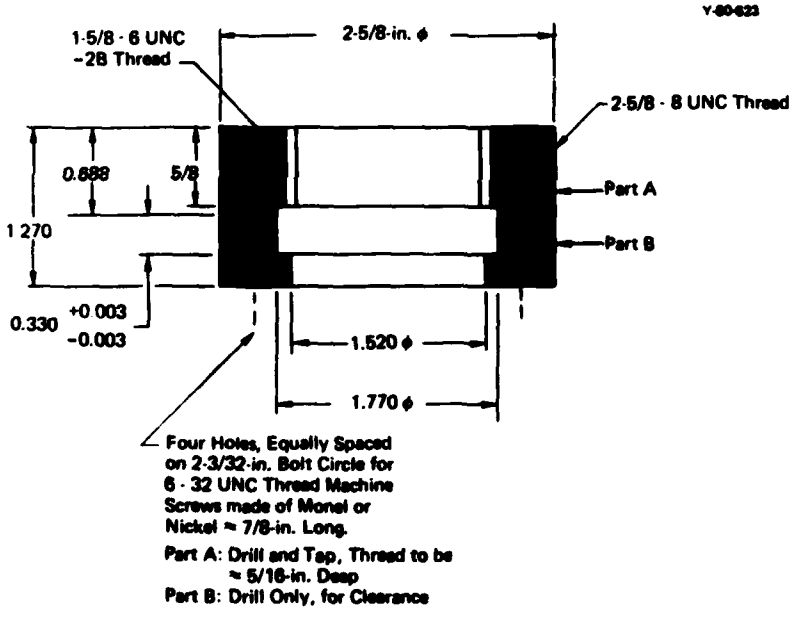

Figure A-12. NOZZLE TIP FOLLOWER FABRICATED OF MONEL OR NICKEL. (Dimensions shown in inches.)

APPENDIX B

SUMMARY OF TEST CONDITIONS DURING THE EXPOSURE OF SPECIMENS TO A HYDROGEN FLUORINE FLAME

Table B-1

SUMMARY OF TEST CONDITIONS DURING THE EXPOSURE OF SPECIMENS TO A HYDROGEN FLUORINE FLAME[1]

Run	P-14[2]	P-19[3]	P-20[4]		P-23				P-24				P-25
Specimen Identification	CeO_2	Y_2O_3	WC: HfC 65:35		Al_2O_3				Al_2O_3				Natural Flake Graphite
Source	Cerac	Cerac H 600-A-1	Cerac H 6131-A-1-1		Coors, AF-5				Coors, AF-5				Y-12, CL-8A[5]
Nozzle Flows													
Helium (ft^3/min)	2.7	3.0	3.6	3.3	3.6	3.5	3.4	3.3	3.6	3.3	3.3	3.0	3.0
Fluorine	1.1	1.4	1.2	1.2	0.8	1.0	1.2	1.2	0.8	1.0	1.3	1.4	1.4
Hydrogen	0.95	0.8	0.6	0.65	0.4	0.5	0.6	0.6	0.4	0.5	0.65	0.7	0.7
	4.75	5.2	5.4	5.15	4.8	5.0	5.2	5.1	4.8	4.8	5.25	5.1	5.1
Theoretical Flame Temperature (K)	~ 2400	2250	2000	~ 2100	1650	1850	2035	2080	1650	1915	2150	2280	2280
Duration of Run (min)	3	1.25	1.75	2	1	0.5	0.5	2	1.5	1	0.75	2	2
Chamber Temperature Profile (°C)													
Thermocouple 1	408	317	190	280	-	-	-	205	-	-	-	230	230
2	645	228	318	365	-	-	-	428	-	-	-	500	485
3	513	203	265	295	-	-	-	320	-	-	-	350	360
4	343	157	212	220	-	-	-	232	-	-	-	263	250
Optical Pyrometer (°C)[6]	1950 Manual	850 Visual	1200	1380		< 850			-	-	-	1410	1470
Thermocouple Reading under the Specimen (°C)	Thermocouple Burned Out	570	800	875	-	-	-	620	-	-	-	810	883

Table B-1 (continued)

Run	P-27	P-29	P-30	P-31				P-33	P-34	P-35			
Specimen Identification	Fibrous Carbon-Carbon Composite	CoS	W	Calcium Aluminate Cement				Carbon-Carbon Composite	Carbon-Carbon Composite	CeO_2			
Source	Y-12, IPT-76[5]	Cerac H 6000 C-1	Y-12, AF-8	Y-12, AF-7				Marquardt[7] A AF-9	Marquardt B	Cerac Lot H 6000 B-2			
Nozzle Flows													
Helium (ft^3/min)	3.0	3.0	3.0	3.6	3.3	3.3	3.0	3.0	3.0	3.6	3.3	3.3	3.0
Fluorine	1.4	1.4	1.4	0.8	1.0	1.3	1.4	1.4	1.4	0.8	1.0	1.3	1.4
Hydrogen	0.7	0.7	0.7	0.4	0.5	0.65	0.7	0.7	0.7	0.4	0.5	0.65	0.7
	5.1	5.1	5.1	4.8	4.8	5.25	5.1	5.1	5.1	4.8	4.8	5.25	5.1
Theoretical Flame Temperature (K)	2280	2280	2280	1650	1915	2150	2280	2280	2280	1650	1915	2150	2280
Duration of Run (min)	2.5	< 1.0	< 1.0	1.2	0.5	0.7	2.3	2.0	2.0	1.0	0.58	0.75	2.17
Chamber Temperature Profile (°C)													
Thermocouple 1	230	316	234	-	-	-	347	218	255	-	-	-	229
2	480	373	527				358	487	540				530
3	373	270	345				215	375	400				363
4	260	208	202				142	238	255				239
Optical Pyrometer (°C)	1460	1670	Did Not Record	-	-	-	1375	1550	1625	-	-	-	1300
Thermocouple Reading under the Specimen (°C)	886	820	Thermocouple Failed Temperature Had Gone to ≈ 1400°C	-	-	-	696	804	788	-	-	-	707

Table B-1 (continued)

Run	P-36	P-37		P-38	HF-1	HF-2	HF-3	HF-4	HF-5			
Specimen Identification	Y_2O_3	Fibrous Carbon-Carbon		Natural Flake Graphite	PyG and SiC on Carbon-Carbon	BaO	ATJ Graphite	Poco Graphite	Al_2O_3			
Source	Cerac H 6000 A-3	Y-12, IPT-76[5]		Y-12, CL-8A[5]	Atlantic[8] Research	Cerac, AF-10	Y-12[5]	Y-12, AFX-5Q-1[5]	Coors, AF-5			
Nozzle Flows												
Helium (ft^3/min)	3.6	3.0	3.0	3.0	3.0	3.6	3.0	3.0	3.6	3.3	3.3	3.0
Fluorine	0.8	1.4	1.4	1.4	1.4	0.9	1.4	1.4	0.8	1.9	1.3	1.4
Hydrogen	0.4	0.7	0.7	0.7	0.7	0.4	0.7	0.7	0.4	0.5	0.65	0.7
	4.8	5.1	5.1	5.1	5.1	4.8	5.1	5.1	4.8	4.8	5.25	5.1
Theoretical Flame Temperature (K)	1650	2280	2280	2280	2280	1650	2280	2280	1650	1915	2150	2280
Duration of Run (min)	0.25	2.0	2.0	2.0	2.0	0.25	2.0	2.0	1.0	0.6	0.6	2.0
Chamber Temperature Profile (°C)												
Thermocouple 1	-	253	244	232	362		230	219	-	-	-	230
2		503	501	498	344		500	504				523
3		394	389	399	205		351	370				375
4		238	244	263	143		230	236				240
Optical Pyrometer (°C)	-	1430	1450	1460	1565	1315	1400	1435	-	-	-	1350
Thermocouple Reading under the Specimen (°C)	-	793	778	770	510	980	Thermocouple Failed	833	-	-	-	777

Table B-1 (continued)

Run	HF-6				HF-7				HF-8	HF-9			
Specimen Identification	WC: HfC(65:35)				MgO				Isotropic Carbon	MgO			
Source	Cerac H 6131-A-1-2				Y-12, S-1, S-2				Y-12, HMC-7BA-1[5]	Y-12, S-4, S-3			
Nozzle Flows													
Helium (ft^3/min)	3.6	3.3	3.3	3.0	3.6	3.3	3.0	3.0	3.0	3.6	3.3	3.0	3.0
Fluorine	0.8	1.0	1.3	1.4	0.8	1.0	1.2	1.4	1.4	0.8	1.0	1.2	1.4
Hydrogen	0.4	0.5	0.65	0.7	0.4	0.5	0.6	0.7	0.7	0.4	0.5	0.6	0.7
	4.8	4.8	5.25	5.1	4.8	4.8	4.8	5.1	5.1	4.8	4.8	4.8	5.1
Theoretical Flame Temperature (K)	1650	1915	2150	2280	1650	1950	2160	2280	2280	1650	1950	2160	2280
Duration of Run (min)	1.0	0.58	0.5	2.17	1.0	0.67	0.67	2.42	2.0	1.0	0.58	0.67	1.0
Chamber Temperature Profile (°C)													
Thermocouple 1	-	-	-	248	-	-	-	229	238	-	-	-	362
2				518				530	498				490
3				400				407	361				322
4				260				269	231				223
Optical Pyrometer (°C)	-	-	-	1585	-	-	-	940	1555	-	-	-	1725
Thermocouple Reading under the Specimen (°C)	-	-	-	891	-	-	-	705	840	-	-	-	950

Table B-1 (continued)

Run	HF-10	HF-11		HF-12				HF-13	HF-14			
Specimen Identification	Anisotropic Carbon	ATJS Graphite		BN				Glassy Carbon	SrO			
Source	Y-12, SB-15-1	Y-12		Union Carbide				Y-12, AF-14	Cerac H-6000 D-1			
Nozzle Flows												
Helium (ft^3/min)	3.0	3.0	3.0	3.6	3.3	3.0	3.0	3.0	3.6	3.3	3.0	3.0
Fluorine	1.4	1.4	1.4	0.8	1.0	1.2	1.4	1.4	0.8	1.0	1.2	1.4
Hydrogen	0.7	0.7	0.7	0.4	0.5	0.6	0.7	0.7	0.4	0.5	0.6	0.7
	5.1	5.1	5.1	4.8	4.8	4.8	5.1	5.1	4.8	4.8	4.8	5.1
Theoretical Flame Temperature (K)	2280	2280	2280	1650	1950	2160	2280	2280	1650	1950	2160	2280
Duration of Run (min)	2.0	2.0	2.0	1.0	0.92	0.92	2.17	2.0	1.0	0.75	0.75	2.0
Chamber Temperature Profile (°C)												
Thermocouple 1	235	240	213	-	-	-	267	255	-	-	-	305
2	495	492	477				490	495				372
3	388	392	377				360	290				329
4	235	253	250				291	200				273
Optical Pyrometer (°C)	1380	NA	NA	-	-	-	1605	1620	-	-	-	≈ 1340[9]
Thermocouple Reading under the Specimen (°C)	775	820	800	-	-	-	950	878	-	-	-	650

Table B-1 (continued)

Run	HF-15	HF-16	HF-17	HF-18[10]	HF-19	HF-20			HF-21		HF-22		HF-23
Specimen Identification	W	w/CM Mo 500 Coating	ATJ Graphite 2	Mo w/W Coating	TaC HfC (80:20)	TaC HfC			Alumina		Alumina from HF-21		Poco Graphite
Source	Y-12 AF-8	Rocketdyne[11] WC-DI-77-2-20	Y-12	Rocketdyne WBI-77-2-18	Cerac	Cerac H 5670A-2			Coors		Coors		Y-12 AFX-5Q-Z
Nozzle Flows													
Helium (ft^3/min)	3.0	3.0	3.6	3.0	3.0	3.6	3.3	3.0	3.6	3.3	3.9	3.3	3.6
Fluorine	1.4	1.4	0.8	1.2	1.2	0.8	1.0	1.2	0.8	1.0	1.0	1.2	0.9
Hydrogen	0.7	0.7	0.4-0.5	0.6	0.6	0.4	0.5	0.6	0.4	0.5	0.5	0.6	0.5
	5.1	5.1	4.8	4.8	4.8	4.8	4.8	4.8	4.8	4.8	5.4	5.1	5.0
Theoretical Flame Temperature (K)	2280	2280	> 1650	2160	2160	1650	1915	2160	1650	1915	1775	2080	≈ 1775
Duration of Run (min)	2.75	2.0	2.0	2.17	15 - 30	1.0	1.25	2.0	3.25	3.0	2.5	2.25	2.75
Chamber Temperature Profile (°C)													
Thermocouple 1	239	255	150	210	-	-	-	245	170			290	250
2	525	521	334	448				485	320			220	223
3	402	363	218	300				291	220			190	177
4	250	223	173	182				180	140			140	110
Specimen Thermocouple (°C)	1050 Before Failure	1014	650	900	570	-	-	905	540	485		560	506
Optical Pyrometer (°C)	1200[12]	1570	1100	1420	≈ 1330	-	-	1560	No Indication < 850			1280	< 850°C

Table B-1 (continued)

Run	H-24[13]			HF-25		HF-26	HF-27			HF-28	HF-29		HF-30[15]
Specimen Identification	Alumina			Graphite		NiAl	NiAl			ATJ Graphite	NiAl		ATJ Graphite[5]
Source	Coors			MP 11B-1		UTRC[14]	HF-26			Y-12	UTRC		Y-12
Nozzle Flows													
Helium (ft^3/min)	3.9	3.3	3.0	3.9	3.6	3.9	3.7	3.7	3.5	3.9	3.4	3.3	3.6
Fluorine	1.0	1.0	1.3	1.0	1.2	1.0	1.1	1.2	1.2	1.0	1.3	1.3	1.2
Hydrogen	0.5	0.5	0.7	0.5	0.6	0.5	0.55	0.6	0.6	0.5	0.65	0.65	0.6
	5.4	4.8	5.0	5.4	5.4	5.4	5.35	5.5	5.3	5.4	5.35	5.25	5.4
Theoretical Flame Temperature (K)	1775	1900	2200+	1775	2000	≈ 1775	1890	1970	2025	1760	2120	2150	2000
Duration of Run (min)	2.83	3.42	1.75	2.75	2.08	3.25	3.0	3.0	2.0	2.17	2.67	2.0	2.17
Chamber Temperature Profile (°C)													
Thermocouple 1	-	247	-	-	260	305			436	236	-	434	267
2		350			450	262			407	415	-	409	463
3		277			359	166			213	323	-	200	367
4		200			250	90			108	215	-	97	256
Specimen Thermocouple (°C)	500	545	868	550	782	300			470	772	-	460	690
Optical Pyrometer (°C)	Not Used			-	1360	≈ 800 Visual			930	1170	-	915	800 Visual

Table B-1 (continued)

Run	HF-31	HF-32	HF-33	HF-34	HF-35	HF-36	HF-37	HF-38			HF-39		
Specimen Identification	ATJ Graphite[5]	ATJ Graphite[5]	ATJ Graphite[5]	ATJ Graphite[5]	ATJ Graphite[5]	ATJ Graphite[5]	ATJ Graphite with 1 μm CaF_2 coat	Alumina			Alumina		
Source	Y-12	Y-12	Y-12	Y-12	Y-12	Y-12	Y-12	Coors			Coors		
Nozzle Flows													
Helium (ft^3/min)	3.3	3.4	3.4	3.6	3.7	3.7	3.6	3.8	3.6	3.6	3.8	3.6	3.7
Fluorine	1.4	1.3	1.2	1.2	1.1	1.0	1.2	0.9	1.0	1.2	0.9	1.0	1.1
Hydrogen	0.7	0.65	0.6	0.6	0.55	0.5	0.6	0.45	0.5	0.6	0.45	0.5	0.55
	5.4	5.35	5.2	5.4	5.35	5.2	5.4	5.15	5.1	5.4	5.15	5.1	5.35
Theoretical Flame Temperature (K)	2215	2120	2045	2000	1900	1810	2000	1700	1830	2000	1700	1830	1900
Duration of Run (min)	2.5	2.25	2.0	2.37	4.0	5.0	2.37	1.0	1.2	4.0	1.0	1.15	4.0
Chamber Temperature Profile (°C)													
Thermocouple 1	312	290	270	272	268	250	302	-	-	280	-	-	300
2	532	490	480	478	460	433	482			522			464
3	429	378	367	372	352	345	382			403			352
4	293	250	240	248	240	230	252			270			247
Specimen Thermocouple (°C)	890	840	1040	1020	1015	800 Visual	1020	-	-	935	-	-	No Indication < 850
Optical Pyrometer (°C)	1125	1085	813	815	763	643	749	-	-	740	-	-	660

AD-A097 426 UNION CARBIDE CORP OAK RIDGE TENN Y-12 PLANT F/G 11/2
MATERIALS FOR HIGH-TEMPERATURE HYDROGEN FLUORINE ENVIRONMENTS.(U)
MAR 81 C E HOLCOMBE, L KOVACH W-7405-ENG-26
UNCLASSIFIED Y-2201 NL

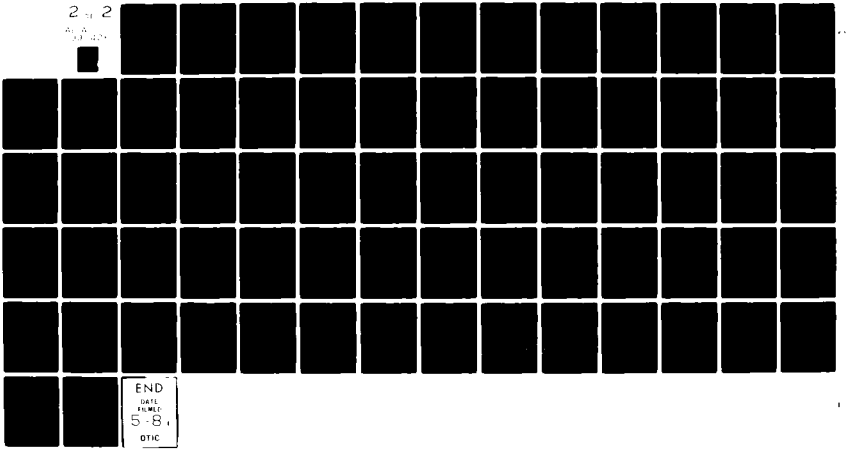

END
DATE FILMED
5-81
DTIC

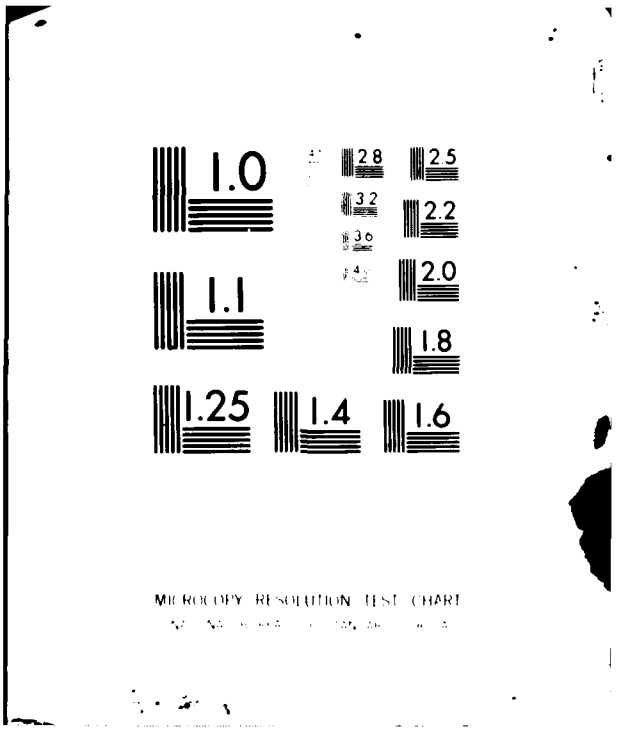
1.0
2.8
2.5
3.2
2.2
3.6
2.0
1.1
1.8
1.25
1.4
1.6
MICROCOPY RESOLUTION TEST CHART

Table B-1 (continued)

Run	HF-40	HF-41	HF-42	HF-43	HF-44	HF-45	HF-46			HF-47		
Specimen Identification	CVD W on Mo	1.2% Y_2O_3 Doped Ni	YD Ni	Ni-270	Ni-270	Ni-200 Foil 5-mil Thick	BaO			SrO		
Source	Rocketdyne	UTRC	UTRC	-	-	-	Cerac			Cerac		
Nozzle Flows												
Helium (ft^3/min)	3.6	3.7	3.6	3.6	3.0	3.0	3.8	3.6	3.6	3.8	3.6	3.6
Fluorine	1.2	1.1	1.2	1.2	1.4	1.4	0.9	1.0	1.2	0.9	1.0	1.2
Hydrogen	0.6	0.55	0.6	0.6	0.7	0.7	0.45	0.5	0.6	0.45	0.5	0.6
	5.4	5.35	5.4	5.4	5.1	5.1	5.15	5.1	5.4	5.15	5.1	5.4
Theoretical Flame Temperature (K)	2000	1900	2000	2000	2280	2280	1700	1830	2000	1700	1830	2000
Duration of Run (min)	2.07	2.37	4.17	4.17	4.03	2.35	1.27	1.35	4.38	1.0	1.0	4.0
Chamber Temperature Profile (°C)												
Thermocouple 1	319	300	340	327	390	340	-	-	279	-	-	280
2	482	435	495	470	576	580			505			490
3	375	320	377	363	440	438			405			415
4	258	238	282	277	320	284			268			280
Optical Pyrometer (°C)	1180	< 850	< 850	< 850	1010	1145			≈ 820			910
Thermocouple Reading under the Specimen (°C)	840	653	700	690	970	815	-	-	697	-	-	698

Table B-1 (continued)

Run	HF-48			HF-49	HF-50	HF-51			HF-52			HF-53		
Specimen Identification	CaO			YN	Y	$CaAl_4O_7$			CeO_2 (AF-3)			Y_2O_3 (AF-2)		
Source	Cerac H 5203-2C			Cerac H6131-C-1-2	Y-12	HP-CA-25			Cerac H6000 B-5			Cerac H6000 A-5		
Nozzle Flows														
Helium (ft^3/min)	3.8	3.6	3.6	3.8	3.0	3.8	3.6	3.6	3.8	3.6	3.6	3.8	3.6	3.6
Fluorine	0.9	1.0	1.2	0.9	1.4	0.9	1.0	1.2	0.9	1.0	1.2	0.9	1.0	1.2
Hydrogen	0.45	0.5	0.6	0.45	0.7	0.45	0.5	0.6	4.5	0.5	0.6	0.45	0.5	0.6
	5.15	5.1	5.4	5.15	5.1	5.15	5.1	5.4	5.15	5.1	5.4	5.15	5.1	5.4
Theoretical Flame Temperature (K)	1700	1830	2000	1700	2280	1700	1830	2000	1700	1830	2000	1700	1830	2000
Duration of Run (min)	1.0	1.0	4.5	0.01	4.0	1.0	1.0	4.0	1.0	1.0	4.0	1.0	1.0	4.0
Chamber Temperature Profile (°C)														
Thermocouple 1	-	-	297	-	378	-	-	268	-	-	295	-	-	332[16]
2			486		540			509			507			290
3			395		415			405			400			155
4			270		306			285			270			83
Optical Pyrometer (°C)	-	-	870	-	860	-	-	1060	-	-	1040			< 850
Thermocouple Reading under the Specimen (°C)	-	-	Failed	190	750	-	-	730	-	-	760	-	-	610

Table B-1 (continued)

Run	HF-54	HF-55			HF-58					HF-59						HF-60	HF-61
Specimen Identification	Y_2O_3 (AF-2)	CeS			Alumina					Alumina						Ta	CeO_2 (AF-3)
Source	Cerac H6000 A-5	Cerac			Coors					Coors						Y-12	Cerac H6000 B-1
Nozzle Flows																	
Helium (ft^3/min)	3.8	3.8	3.6	3.6	3.8	3.6	3.6	3.6	3.8	3.8	3.6	3.6	3.4	3.6	3.8	3.6	3.8
Fluorine	0.9	0.9	1.0	1.2	0.9	1.0	1.2	1.0	0.9	0.9	1.0	1.2	1.28	1.0	0.9	1.2	0.9
Hydrogen	0.45	0.45	0.5	0.6	0.45	0.5	0.6	0.5	0.45	0.45	0.5	0.6	0.64	0.5	0.45	0.6	0.45
	5.15	5.15	5.1	5.4	5.15	5.1	5.4	5.1	5.15	5.15	5.1	5.4	5.32	5.1	5.15	5.4	5.15
Theoretical Flame Temperature (K)	1700	1700	1830	2000	1700	1830	2000	1830	1700	1700	1830	2000	2110	1830	1700	2000	1700
Duration of Run (min)	0.004	1.0	1.0	1.5	1.0	1.0	5.0	1.0	≈ 1.0	1.0	1.0	2.5	3.0	1.0	1.17	4.0	4.0
Chamber Temperature Profile (°C)																	
Thermocouple 1	-	-	-	233	-	-	310	-		-	-	-	315	-	-	325	255
2	-			510			493						550			497	410
3	-			383			390						435			390	308
4	-			262			268						290			270	200
Optical Pyrometer (°C)	-			1270			No Indication < 850						1145			1300	955
Thermocouple Reading under the Specimen (°C)	-	-	-	830	-	-	700	-	-	-	-	-	773	-	-	970	600

Table B-1 (continued)

Run	HF-62	HF-63			HF-67					HF-68				
Specimen Identification	BaO	SrO			Hot-Pressed MgO					Hot-Pressed SiC				
Source	H 6018	Cerac			Research Chemicals (Haselden)					Research Chemicals (Haselden)				
Nozzle Flows														
Helium (ft^3/min)	3.8	3.8	3.6	3.8	3.8	3.6	3.6	3.6	3.8	3.8	3.6	3.6	3.6	3.8
Fluorine	0.9	0.9	1.1	0.9	0.9	1.0	1.2	1.0	0.9	0.9	1.0	1.2	1.0	0.9
Hydrogen	0.45	0.45	0.55	0.45	0.45	0.5	0.6	0.5	0.45	0.45	0.5	0.6	0.5	0.45
	5.15	5.15	5.25	5.15	5.15	5.1	5.4	5.1	5.15	5.15	5.1	5.4	5.1	5.15
Theoretical Flame Temperature (K)	1700	1700	1910	1700	1700	1830	2000	1830	1700	1700	1830	2000	1830	1700
Duration of Run (min)	4.0	1.0	4.0	1.0	1.0	1.0	4.5	1.0	1.0	1.0	1.0	4.5	1.0	1.0
Chamber Temperature Profile (°C)														
Thermocouple 1	270	-	273	-			325			-	-	315	-	-
2	405		480				520					525		
3	310		370				400					410		
4	200		236				265					270		
Optical Pyrometer (°C)	No Indication < 850		855				No Indication[17] < 850					1255		
Thermocouple Reading Under the Specimen (°C)	605	-	700	-			710			-	-	815	-	-

Table B-1 (continued)

Run	HF-69					HF-70			HF-71					HF-72				
Specimen Identification	Hot-Pressed LaB_6					ATJ Graphite			Al_2O_3					MgO				
Source	Research Chemicals (Haselden)					Y-12			Coors					From Run HF-67[18]				
Nozzle Flows																		
Helium (ft^3/min)	3.8	3.6	3.6	3.6	3.8	3.6	3.8	3.6	3.8	3.6	3.4	3.6	3.8	3.8	3.6	3.4	3.6	3.8
Fluorine	0.9	1.0	1.2	1.0	0.9	1.2	0.9	1.0	0.9	1.0	1.3	1.0	0.9	0.9	1.0	1.3	1.0	0.9
Hydrogen	0.45	0.5	0.6	0.5	0.45	0.6	0.45	0.5	0.45	0.5	0.65	0.5	0.45	0.45	0.5	0.65	0.5	0.45
	5.15	5.1	5.4	5.1	5.15	5.4	5.15	5.1	5.15	5.1	5.35	5.1	5.15	5.15	5.1	5.35	5.1	5.15
Theoretical Flame Temperature (K)	1700	1830	2000	1830	1700	2000	1700	1830	1700	1830	2120	1830	1700	1700	1830	2120	1830	1700
Duration of Run (min)	1.0	1.0	4.5	1.0	1.0	6.0	3.83	2.78	1.0	1.0	4.0	1.0	1.0	1.0	1.0	4.5	1.0	1.0
Chamber Temperature Profile (°C)																		
Thermocouple 1	-	-	307	-	-	300	-	265	-	-	340	-	-	-	-	330	-	-
2			480			490		440			550					515		
3			385			400		345			370					430		
4			260			285		207			230					300		
Optical Pyrometer (°C)			< 850			1175	-	1180			1170					850		
Thermocouple Reading under the Specimen (°C)	-	-	710	-	-	823	630	755	-	-	880	-	-	-	-	750	-	-

Table B-1 (continued)

Run	HF-73					HF-74					HF-75					HF-76				
Specimen Identification	MgO					MgO					LaB_6					LaB_6				
Source	From Run HF-72					From Run HF-73					From Run HF-69					From Run HF-75				
Nozzle Flows																				
Helium (ft^3/min)	3.8	3.6	3.3	3.6	3.8	3.8	3.6	3.1	3.6	3.8	3.8	3.6	3.4	3.6	3.8	3.8	3.6	3.3	3.6	3.8
Fluorine	0.9	1.0	1.4	1.0	0.9	0.9	1.0	1.5	1.0	0.9	0.9	1.0	1.3	1.0	0.9	0.9	1.0	1.4	1.0	0.9
Hydrogen	0.45	0.5	0.7	0.5	0.45	0.45	0.5	0.75	0.5	0.45	0.45	0.5	0.65	0.5	0.45	0.45	0.5	0.7	0.5	0.45
	5.15	5.1	5.4	5.1	5.15	5.15	5.1	5.35	5.1	5.15	5.15	5.1	5.35	5.1	5.15	5.15	5.1	5.4	5.1	5.15
Theoretical Flame Temperature (K)	1700	1830	2215	1830	1700	1700	1830	2320	1830	1700	1700	1830	2120	1830	1700	1700	1830	2215	1830	1700
Duration of Run (min)	1.0	1.0	4.5	1.0	1.0	1.0	1.0	5.0	1.0	1.0	1.0	1.0	4.5	1.0	1.0	1.0	1.0	4.67	1.0	1.0
Chamber Temperature Profile (°C)																				
Thermocouple 1	-	-	362	-	-	-	-	413	-	-	-	-	317	-	-	-	-	340	-	-
2			545					630					530					550		
3			460					490					445					453		
4			330					345					317					340		
Optical Pyrometer (°C)			870			-	-	975[19]	-	-	-	-	970	-	-	-	-	950	-	-
Thermocouple Reading under the Specimen (°C)	-	-	770	-	-	-	-	970	-	-	-	-	810	-	-	-	-	818	-	-

Table B-1 (continued)

Run	HF-77	HF-78					HF-79					HF-80			
Specimen Identification	ATJ Graphite	LaB_6					Al_2O_3					Al_2O_3			
Source	Y-12	From Run HF-76					Coors					TRW[20] - A10201			
Nozzle Flows															
Helium (ft^3/min)	3.0	3.8	3.6	3.1	3.6	3.8	3.8	3.6	3.0	3.6	3.8	3.8	3.6	3.6	3.6
Fluorine	1.4	0.9	1.0	1.5	1.0	0.9	0.9	1.0	1.4	1.0	0.9	0.9	1.0	1.2	1.0
Hydrogen	0.7	0.45	0.5	0.75	0.5	0.45	0.45	0.5	0.7	0.5	0.45	0.45	0.5	0.6	0.5
	5.1	5.15	5.1	5.35	5.1	5.15	5.15	5.1	5.1	5.1	5.15	5.15	5.1	5.4	5.1
Theoretical Flame Temperature (K)	2280	1700	1830	2320	1830	1700	1700	1830	2280	1830	1700	1700	1830	2000	1830
Duration of Run (min)	4.0	1.0	1.0	4.5	1.0	1.0	1.0	1.0	4.5	1.0	1.0	1.0	1.0	4.25	0.58
Chamber Temperature Profile (°C)															
Thermocouple 1	360			360					370			-	-	395	-
2	503			555					603					323	
3	450			465					450					160	
4	323			360					310					85	
Optical Pyrometer (°C)	1270			1060					1350					No Indication < 850	
Thermocouple Reading under the Specimen (°C)	920			835					900				-	440	-

Table B-1 (continued)

Run	HF-81					HF-82					HF-83				
Specimen Identification	$CaZrO_3$					Boride V					Al_2O_3				
Source	Research Chemicals (Haselden)					Manlabs, Inc[21]					TRW - A10203				
Nozzle Flows															
Helium (ft^3/min)	3.8	3.6	3.6	3.6	3.8	3.8	3.6	3.6	3.6	3.8	3.8	3.6	3.6	3.6	3.8
Fluorine	0.9	1.0	1.2	1.0	0.9	0.9	1.0	1.2	1.0	0.9	0.9	1.0	1.2	1.0	0.9
Hydrogen	0.45	0.5	0.6	0.5	0.45	0.45	0.5	0.6	0.5	0.45	0.45	0.5	0.6	0.5	0.45
	5.15	5.1	5.4	5.1	5.15	5.15	5.1	5.4	5.1	5.15	5.15	5.1	5.4	5.1	5.15
Theoretical Flame Temperature (K)	1700	1830	2000	1830	1700	1700	1830	2000	1830	1700	1700	1830	2000	1830	1700
Duration of Run (min)	1.0	1.0	4.42	1.0	1.0	1.0	1.0	4.33	1.0	1.0	1.0	1.0	4.33	1.0	1.0
Chamber Temperature Profile (°C)															
Thermocouple 1	-	-	310	-	-	-	-	322	-	-	-	-	242	-	-
2			390					525					320		
3			300					300					267		
4			210					≈ 170					220		
Optical Pyrometer (°C)			No Indication < 850					1150					Visual < 600 - 700		
Thermocouple Reading under the Specimen (°C)	-	-	690	-	-	-	-	1005	-	-			640		

Table B-1 (continued)

Run	HF-84					HF-85					HF-86				
Specimen Identification	Al_2O_3					Al_2O_3					Vitreous Carbon				
Source	TRW - A10206					TRW - A10207					TRW - G01210				
Nozzle Flows															
Helium (ft^3/min)	3.8	3.6	3.6	3.6	3.8	3.8	3.6	3.6	3.6	3.8	3.8	3.6	3.6	3.6	3.8
Fluorine	0.9	1.0	1.2	1.0	0.9	0.9	1.0	1.2	1.0	0.9	0.9	1.0	1.2	1.0	0.9
Hydrogen	0.45	0.5	0.6	0.5	0.45	0.45	0.5	0.6	0.5	0.45	0.45	0.5	0.6	0.5	0.45
	5.15	5.1	5.4	5.1	5.15	5.15	5.1	5.4	5.1	5.15	5.15	5.1	5.4	5.1	5.15
Theoretical Flame Temperature (K)	1700	1830	2000	1830	1700	1700	1830	2000	1830	1700	1700	1830	2000	1830	1700
Duration of Run (min)	1.0	1.0	4.33	1.0	1.0	1.0	1.0	4.5	1.0	0.97	1.0	1.0	4.17	1.0	1.0
Chamber Temperature Profile (°C)															
Thermocouple 1	-	-	247	-	-	-	-	260			-	-	205	-	-
2			290					410					250		
3			290					295					285		
4			265					190					250		
Optical Pyrometer (°C)			No Indication < 600 - 700					No Indication 780 Manual			-	-	No Indication ≈ 750 Manual		-
Thermocouple Reading under the Specimen (°C)			690					630			-	-	560	-	-

Table B-1 (continued)

Run	HF-87	HF-88			HF-90[22]			HF-93			HF-96				
Specimen Identification	CaB_6	SrO			Al_2O_3			Sc_2O_3			LaB_6				
Source	Cerac	Cerac			Coors			Research Chemicals (Haselden)			HF-78				
Nozzle Flows															
Helium (ft^3/min)	3.8	3.8	3.6	3.1	3.8	3.6	3.6	3.8	3.6	3.6	3.8	3.6	3.0	3.6	3.8
Fluorine	0.9	0.9	1.0	1.5	0.9	1.0	1.2	0.9	1.0	1.2	0.9	1.0	1.6	1.0	0.9
Hydrogen	0.45	0.45	0.5	0.75	0.45	0.5	0.6	0.45	0.5	0.6	0.45	0.5	0.8	0.5	0.45
	5.15	5.15	5.1	5.35	5.15	5.1	5.4	5.15	5.1	5.4	5.15	5.1	5.4	5.1	5.15
Theoretical Flame Temperature (K)	1700	1700	1830	2320	1700	1830	2000	1700	1830	2000	1700	1830	2400	1830	1700
Duration of Run (min)	10 s	1.0	1.0	2.47	1.0	1.0	4.92	1.0	1.0	1.25	1.0	1.0	4.67	1.0	1.0
Chamber Temperature Profile (°C)															
Thermocouple 1	-			290		Chamber									
2	-			540		Profile									
3	-			270		Temperatures									
4	-			167		Eliminated									
Optical Pyrometer (°C)	-	-		1685 Manual			1185 1145 Manual			No Indication < 850			1038		
Thermocouple Reading under the Specimen (°C)	-	-	-	1017	-	-	790			743			815		

Table B-1 (continued)

Run	HF-97					HF-98					HF-99					HF-100				
Specimen Identification	LaB6					LaB_6					LaB_6					LaB_6				
Source	HF-96					HF-97					HF-98					HF-99				
Nozzle Flows																				
Helium (ft^3/min)	3.8	3.6	2.85	3.6	3.8	3.8	3.6	2.7	3.6	3.8	3.8	3.6	2.55	3.6	3.8	3.8	3.6	2.45	3.6	3.8
Fluorine	0.9	1.0	1.7	1.0	0.9	0.9	1.0	1.73	1.0	0.9	0.9	1.0	1.8	1.0	0.9	0.9	1.0	1.9	1.0	0.9
Hydrogen	0.45	0.5	0.85	0.5	0.45	0.45	0.5	0.865	0.5	0.45	0.45	0.5	0.9	0.5	0.45	0.45	0.5	0.95	0.5	0.45
	5.15	5.1	5.40	5.1	5.15	5.15	5.1	5.295	5.1	5.15	5.15	5.1	5.25	5.1	5.15	5.15	5.1	5.30	5.1	5.15
Theoretical Flame Temperature (K)	1700	1830	2450	1830	1700	1700	1830	2535	1830	1700	1700	1830	2615	1830	1700	1700	1830	2690	1830	1700
Duration of Run (min)	1.0	1.0	4.75	1.0	1.0	1.0	1.0	4.75	1.0	1.0	1.0	1.0	4.75	1.0	1.0	1.0	1.0	5.0	1.0	1.0
Optical Pyrometer (°C)			1060					1125					1120					1170		
Thermocouple Reading under the Specimen (°C)			848					842					838					843		

Table B-1 (continued)

Run	HF-101					HF-102				HF-103	HF-108[23]			HF-109[23]	
Specimen Identification	LaB_6					LaB_6				LaB_6	NiAl			NiAl	
Source	HF-100					HF-101				HF-102	HF-29			HF-108	
Nozzle Flows															
Helium (ft^3/min)	3.8	3.6	2.3	3.6	3.8	3.8	3.6	2.15	2.15	2.15	3.8	3.6	3.3	3.0	2.7
Fluorine	0.9	1.0	1.95	1.0	0.9	0.9	1.0	2.0		2.0	0.9	1.0	1.4	1.6	1.73
Hydrogen	0.45	0.5	0.976	0.5	0.45	0.45	0.5	1.0	1.0[24]	1.0	0.45	0.5	0.7	0.8	0.87
	5.15	5.1	5.226	5.1	5.15	5.15	5.1	5.15		5.15	5.15	5.1	5.4	5.4	5.30
Theoretical Flame Temperature (K)	1700	1830	2770	1830	1700	1700	1830	2840	2840+	2840	1700	1830	2215	2400	2535
Duration of Run (min)	1.0	1.0	4.83	1.0	1.0	1.0	1.0	10.75	3.42	3.75	1.0	1.0	4.77	5.33	4.52
Optical Pyrometer (°C)			1193						1375	925			830 Manual		1295
Thermocouple Reading Under the Specimen (°C)			903						1080	842			700		1065

Table B-1 (continued)

Run	HF-110[23]					HF-111[10]		HF-112[25]				HF-113[25]				
Specimen Identification	Ni-270					Y		Al_2O_3				Al_2O_3				
Source	HF-43					Y-12		TRW A10206, HF-84				TRW A10205				
Nozzle Flows																
Helium (ft^3/min)	3.0	2.7	2.55	2.45	2.15	3.0	2.7	3.8	3.6	3.3	3.0	3.8	3.6	3.6	3.6	3.8
Fluorine	1.6	1.73	1.8	1.9	2.0	1.6	1.73	0.9	1.0	1.4	1.6	0.9	1.0	1.2	1.0	0.9
Hydrogen	0.8	0.865	0.9	0.95	1.0	0.8	0.865	0.45	0.5	0.7	0.8	0.45	0.5	0.6	0.5	0.45
	5.4	5.3	5.25	5.30	5.15	5.4	5.3	5.15	5.1	5.4	5.4	5.15	5.1	5.4	5.1	5.15
Theoretical Flame Temperature (K)	2400	2535	2615	2690	2840	2400	2535	1700	1830	2215	2400	1700	1830	2000	1830	1700
Duration of Run (min)	4.25	5.25	3.0	2.0	1.5	2.75	1.12	1.0	1.0	4.08	1.08	1.0	1.0	4.5	1.0	1.0
Optical Pyrometer (°C)	825 Manual	985	1010-1040	1035	1250	965	1280				1280			< 750 Manual		
Thermocouple Reading under the Specimen (°C)	700	800	895	895	1200		1090				863			748		

Table B-1 (continued)

Run	HF-114[25]						HF-115[26]				HF-116[26]				HF-118[10]		HF-119
Specimen Identification	Al_2O_3						MgO (YD)				MgO				Scandium		Scandium
Source	HF-113						TRW				TRW HF-115				Research Chemical (Haselden) Lot Sc-M-3-272D		HF-118
Nozzle Flows																	
Helium (ft^3/min)	3.8	3.6	3.4	3.3	3.6	3.8	3.8	3.6	3.3	3.0	3.8	3.6	2.6	2.45	3.0	2.6	2.45
Fluorine	0.9	1.0	1.3	1.4	1.0	0.9	0.9	1.0	1.4	1.6	0.9	1.0	1.7	1.9	1.6	1.7	1.9
Hydrogen	0.45	0.5	0.65	0.7	0.5	0.45	0.45	0.5	0.7	0.8	0.45	0.5	0.85	0.95	0.8	0.85	0.95
	5.15	5.1	5.35	5.4	5.1	5.15	5.15	5.1	5.4	5.4	5.15	5.1	5.15	5.30	5.4	5.15	5.30
Theoretical Flame Temperature (K)	1700	1830	2120	2215	1830	1700	1700	1830	2215	2395	1700	1830	2550	2690	2400	2550	2690
Duration of Run (min)	1.0	1.0	4.0	2.25	1.0	1.0	1.0	1.0	3.5	4.5	1.0	1.0	3.33	1.92	3.33	2.78	0.77
Optical Pyrometer (°C)				1155					No Indication < 850				No Indication Manual > 1100[27]			1047	1280
Thermocouple Reading under the Specimen (°C)				NA					None				None			675	580

Table B-1 (continued)

Run	HF-120					HF-121					HF-122						
Specimen Identification	Sapphire - Single Crystal					Sapphire - Single Crystal					$LaCrO_3$						
Source	ESPI					HF-120					Y-12						
Nozzle Flows																	
Helium (ft^3/min)	3.8	3.6	3.6	3.6	3.8	3.8	3.6	3.45	3.6	3.8	3.8	3.6	3.3	3.1	3.0	3.6	3.8
Fluorine	0.9	1.0	1.2	1.0	0.9	0.9	1.0	1.3	1.0	0.9	0.9	1.0	1.4	1.5	1.6	1.0	0.9
Hydrogen	0.45	0.5	0.6	0.5	0.45	0.45	0.5	0.65	0.5	0.45	0.45	0.5	0.7	0.75	0.8	0.5	0.45
	5.15	5.1	5.4	5.1	5.15	5.15	5.1	5.40	5.1	5.15	5.15	5.1	5.4	5.35	5.4	5.1	5.15
Theoretical Flame Temperature (K)	1700	1830	2000	1830	1700	1700	1830	2105	1830	1700	1700	1830	2215	2320	2395	1830	1700
Duration of Run (min)	1.0	1.0	5.0	1.0	1.0	1.0	1.0	5.0	1.0	1.0	1.0	1.0	3.83	1.67	4.17	0.83	1.0
Thermocouple Reading under the Specimen (°C)			657					678							740		
Optical Pyrometer (°C)			No Indication Manual Pyrometer - No Indication					No Indication Manual - 818°C							1065		

Table B-1 (continued)

Run	HF-123	HF-124[10]	HF-125					HF-126						
Specimen Identification	$LaCrO_3$	TiAl	La_2O_3-Si_3N_4					Al_2O_3						
Source	HF-122	AFML[28]	Y-12					Coors						
Nozzle Flows														
Helium (ft^3/min)	3.0	3.3	3.8	3.6	3.3	3.6	3.8	3.8	3.3	3.3	3.0	3.3	3.3	3.8
Fluorine	1.6	1.4	0.9	1.0	1.4	1.0	0.9	0.9	1.0	1.3	1.4	1.3	1.0	0.9
Hydrogen	0.8	0.7	0.45	0.5	0.7	0.5	0.45	0.45	0.5	0.65	0.7	0.65	0.5	0.45
	5.4	5.4	5.15	5.1	5.4	5.1	5.15	5.15	4.8	5.25	5.1	5.25	4.8	5.15
Theoretical Flame Temperature (K)	2395	2215	1700	1830	2215	1830	1700	1700	1910	2150	2280	2150	1910	1700
Duration of Run (min)	2.33	3.93	1.0	1.0	4.0	1.0	0.88	1.0	0.58	0.58	2.08	0.67	0.58	1.0
Thermocouple Reading under the Specimen (°C)	700	813			747							680		
Optical Pyrometer (°C)	1048	1435			1360							965		

Table B-1 (continued)

Run	HF-127					HF-128							HF-129[29]	HF-130[22]		
Specimen Identification	Si_3N_4 (MgO Doped 5%)					Al_2O_3							ATJ Graphite	Al_2O_3		
Source	Cerac					Coors							Y-12	Coors		
Nozzle Flows																
Helium (ft^3/min)	3.8	3.6	3.3	3.6	3.8	3.8	3.3	3.3	3.0	3.3	3.3	3.8	3.0	3.8	3.7	3.8
Fluorine	0.9	0.1	1.4	1.0	0.9	0.9	1.0	1.3	1.4	1.3	1.0	0.9	1.4	0.9	1.1	0.9
Hydrogen	0.45	0.5	0.7	0.5	0.45	0.45	0.5	0.65	0.7	0.65	0.5	0.45	0.7	0.45	0.55	0.45
	5.15	5.1	5.4	5.1	5.15	5.15	4.8	5.25	5.1	5.25	4.8	5.15	5.1	5.15	5.35	5.15
Theoretical Flame Temperature (K)	1700	1830	2215	1830	1700	1700	1910	2150	2280	2150	1910	1700	2280	1700	1900	1700
Duration of Run (min)	1.0	1.0	4.0	1.0	1.0	1.0	0.58	0.58	2.67	0.58	0.58	1.0	4.13	1.0	7.25	1.0
Thermocouple Reading under the Specimen (°C)			780						735				750			
Optical Pyrometer (°C)			1335						1220				1280	No Indication Manual Pyrometer ≈ 740°C after 5 min		
Thermocouple Experiment Readings (°C)																
1														687		
2														758		
3														775		
4														768		

Table B-1 (continued)

Run	HF-131[22]			HF-132[22]				HF-133						HF-134				
Specimen Identification	Al_2O_3			Al_2O_3				BeO						BeO				
Source	HF-130			HF-131				National Beryllia, Berlox K-150						Y-12				
Nozzle Flows																		
Helium (ft^3/min)	3.8	3.6	3.8	3.8	3.5	3.3	3.8	3.8	3.6	3.3	3.0	3.6	3.8	3.8	3.6	3.3	3.6	3.8
Fluorine	0.9	1.2	0.9	0.9	1.3	1.4	0.9	0.9	1.0	1.4	1.6	1.0	0.9	0.9	1.0	1.4	1.0	0.9
Hydrogen	0.45	0.6	0.45	0.45	0.65	0.7	0.45	0.45	0.5	0.7	0.8	0.5	0.45	0.45	0.5	0.7	0.5	0.45
	5.15	5.4	5.15	5.15	5.45	5.4	5.15	5.15	5.1	5.4	5.4	5.1	5.15	5.15	5.1	5.4	5.1	5.15
Theoretical Flame Temperature (K)	1700	2000	1700	1700	2090	2215	1700	1700	1830	2215	2395	1830	1700	1700	1830	2215	1830	1700
Duration of Run (min)	1.0	8.0	1.0	1.0	8.33	3.92	1.0	1.0	1.0	6.33	3.33	1.0	1.0	1.0	1.0	3.17	1.0	1.0
Thermocouple Reading under the Specimen (°C)	-			-				805						700				
Optical Pyrometer (°C)	No Indication Manual Pyrometer 820°C after 7 min 20 s			1035				1025						978 980 Manual				
Thermocouple Experiment Readings (°C)																		
1	726			810														
2	798			931														
3	822			981														
4	815			927														

Table B-1 (continued)

Run	HF-135							HF-137					HF-138[22]			HF-139[22]	
Specimen Identification	Al_2O_3							*Single Crystal MgO*[30]					*MgO*			*ATJ Graphite*	
Source	Coors							Materials Research					Research Chemicals (Haselden)			Y-12	
Nozzle Flows																	
Helium (ft^3/min)	3.8	3.3	3.3	3.0	3.3	3.3	3.8	3.8	3.6	2.85	3.6	3.8	3.8	3.6	3.3	3.7	3.7
Fluorine	0.9	1.0	1.3	1.4	1.3	1.0	0.9	0.9	1.0	1.7	1.0	0.9	0.9	1.0	1.4	1.0	1.1
Hydrogen	0.45	0.5	0.65	0.7	0.65	0.5	0.45	0.45	0.5	0.85	0.5	0.45	0.45	0.5	0.7	0.5	0.55
	5.15	4.8	5.25	5.1	5.25	4.8	5.15	5.15	5.1	5.4	5.1	5.15	5.15	5.1	5.4	5.2	5.35
Theoretical Flame Temperature (K)	1700	1910	2150	2280	2150	1910	1700	1700	1830	2450	1830	1700	1700	1830	2215	1810	1900
Duration of Run (min)	1.0	0.58	0.58	4.58	0.58	0.58	1.0	1.0	1.0	2.5	1.0	1.0	1.0	1.0	1.17	7.0	3.37
Thermocouple Reading under the Specimen (°C)				650						735					-	-	-
Optical Pyrometer (°C)				1155						1395					1010	-	1178
Thermocouple Experiment Readings (°C)																(32)	(33)
1															881	752	1149
2															705	652	868
3															830	740	1118
4															880	745	1136

Table B-1 (continued)

Run	HF-140[22,31]	HF-141[22,31]					HF-142[22,31]					HF-143[31]			HF-144[22]
Specimen Identification	Ni-270	LaB_6					LaB_6					LaB_6			ATJ Graphite
Source		Research Chemicals (Haselden)					HF-141					Research Chemicals (Haselden)			HF-139
Nozzle Flows															
Helium (ft^3/min)	3.0	3.6	3.0	2.6	2.45	3.6	3.6	2.6	2.1	2.1	3.6	2.6	2.1	2.6	3.7
Fluorine	1.6	1.0	1.6	1.7	1.9	1.0	1.0	1.7	2.0	2.0	1.0	1.7	2.0	1.7	1.1
Hydrogen	0.8	0.5	0.8	0.85	0.95	0.5	0.5	0.85	1.0	1.073	0.5	0.85	1.0	0.85	0.55
	5.4	5.1	5.4	5.15	5.30	5.1	5.1	5.15	5.1	5.173	5.1	5.15	5.1	5.15	5.35
Theoretical Flame Temperature (K)	2395	1830	2395	2550	2690	1830	1830	2550	2853	2853+	1830	2550	2850	2550	1900
Duration of Run (min)	4.05	1.0	3.75	3.25	3.33	1.15	1.0	3.5	3.33	0.82	1.18	2.33	3.17	1.23	3.1
Thermocouple Reading under the Specimen (°C)	-												925		-
Optical Pyrometer (°C)	1384				1275					1423			1240		1248
Thermocouple Experiment Readings (°C)															
1	1425				1079					1270			-		1188
2	1000				998					1164			-		827
3	1425				1105					Failed			-		1232
4	1425				972 Slipped Out of Position					1346			-		1132

Table B-1 (continued)

Run	HF-145[34]		HF-146[34]	HF-147[22]										HF-148			HF-149[22,31]
Specimen Identification	ATJ Graphite		ATJ Graphite	MgO - Single Crystal[35]										ATJ Graphite			NiAl
Source	Plate		Plate	Materials Research										Y-12			UTRC
Nozzle Flows																	
Helium (ft^3/min)	3.6	3.8	3.7	3.8	3.6	3.7	3.6	3.45	3.3	3.6	3.7	3.6	3.8	3.6	3.3	3.6	3.1
Fluorine	0.85	0.9	1.1	0.9	1.0	1.1	1.2	1.3	1.4	1.2	1.1	1.0	0.9	1.0	1.4	1.0	1.5
Hydrogen	0.43	0.45	0.55	0.45	0.5	0.55	0.6	0.65	0.7	0.6	0.55	0.5	0.45	0.5	0.7	0.5	0.75
	4.88	5.15	5.35	5.15	5.1	5.35	5.4	5.40	5.4	5.4	5.35	5.1	5.15	5.1	5.4	5.1	5.35
Theoretical Flame Temperature (K)	1700	1700	1900	1700	1830	1910	2000	2105	2215	2000	1910	1830	1700	1830	2215	1830	2320
Duration of Run (min)	3.17	2.43	7.42	3.25	1.67	2.0	1.5	2.75	1.75	1.17	1.0	1.0	1.0	2.0	1.58	1.42	3.25
Thermocouple Reading under the Specimen (°C)	535		898												1000		-
Optical Pyrometer (°C)	No Indication		1440					1130							≈ 1280		1350
Thermocouple Experiment Readings (°C)																	
1	-		-				888	1070							-		1255
2	-		-				720	806							-		1004
3	-		-				909	1097							-		1297
4	-		-				750	865							-		1208

Table 6-1 (continued)

Run	HF-150[31]	HF-151				HF-152	HF-153								
Specimen Identification	$TaLaF_3$[36]	$TaLaF_3$				$TaLaF_3$[38]	Poco Graphite Sprayed with Nominal 7-mil Coat of LaB_6[39]								
Source	Y-12	HF-150[37]				Y-12									
Nozzle Flows															
Helium (ft^3/min)	3.8	3.6	3.7	3.6	3.3	3.8	3.8	3.7	3.3	3.1	3.0	3.1	3.3	3.7	3.8
Fluorine	0.9	1.0	1.1	1.2	1.4	0.9	0.9	1.1	1.4	1.5	1.6	1.5	1.4	1.1	0.9
Hydrogen	0.45	0.5	0.55	0.6	0.7	0.45	0.45	0.55	0.7	0.75	0.8	0.75	0.7	0.55	0.45
	5.15	5.1	5.35	5.4	5.4	5.15	5.15	5.35	5.4	5.35	5.4	5.35	5.4	5.35	5.15
Theoretical Flame Temperature (K)	1700	1830	1910	2000	2215	1700	1700	1900	2215	2320	2395	2320	2215	1900	1700
Duration of Run (min)	3.1	2.67	1.58	2.06	1.03	5.12	1.0	2.33	2.25	1.25	2.25	1.0	1.0	1.0	1.25
Thermocouple Reading under the Specimen (°C)	650	-	-	-	777	650					823				
Optical Pyrometer (°C)	1400				1545	1253						1230			
Thermocouple Experiment Readings (°C)															
1	-				-	-					None				
2	-				-	-									
3	-				-	-									
4	-				-	-									

Table B-1 (continued)

Run	HF-154					HF-155[34]		HF-156[34]	HF-157[34]			HF-158[34]	HF-159[34]	HF-161	
Specimen Identification	Poco Graphite Sprayed with Nominal 28-mil Coat of LaB_6[39]					MgO Plate		ATJ Graphite Plate with Slots	Ni-200 Plate			ATJ Graphite Plate with Slots	Alumina Plate	SrB_6 LaB_6 Mixture	
Source						Norton			Y-12			Y-12	Coors	Y-12	
Nozzle Flows															
Helium (ft^3/min)	3.8	3.7	3.3	3.7	3.8	3.8	3.6	3.7	3.8	3.7	3.45	3.8	3.8	3.3	3.1
Fluorine	0.9	1.1	1.4	1.1	0.9	0.9	1.0	1.1	0.9	1.1	1.3	0.9	0.9	1.4	1.5
Hydrogen	0.45	0.55	0.7	0.55	0.45	0.45	0.5	0.55	0.45	0.55	0.65	0.45	0.45	0.7	0.75
	5.15	5.35	5.4	5.35	5.15	5.15	5.1	5.35	5.15	5.35	5.40	5.15	5.15	5.4	5.35
Theoretical Flame Temperature (K)	1700	1900	2215	1900	1700	1700	1830	1900	1700	1900	2105	1700	1700	2215	2320
Duration of Run (min)	1.0	1.0	2.25	1.0	1.0	3.25	0.9	2.27	3.0	2.08	3.32	6.25	5.65	3.5	3.82
Thermocouple Reading under the Specimen (°C)			764				585	561			772	595	580		840
Optical Pyrometer (°C)			1235				≈ 1275	1327			1137	1280	1117		1505

Table B-1 (continued)

Run	HF-162		HF-163			HF-164		HF-165					HF-166	HF-167				
Specimen Identification	Y_2O_3		Y_2O_3			Ni-270 Sprayed with Nominal 18-mil Coat LaB_6		CaB_6					CaB_6	CaB_6				
Source	Ceradyne		Ceradyne			Y-12		Ceradyne					Ceradyne	HF-165				
Nozzle Flows																		
Helium (ft^3/min)	3.8	3.6	3.6	3.7	3.6	3.6	3.6	3.8	3.7	3.6	3.45	3.3	3.3	3.8	3.7	3.45	3.1	2.6
Fluorine	0.9	1.0	1.0	1.1	1.2	0.9	1.2	0.9	1.1	1.2	1.3	1.4	1.4	0.9	1.1	1.3	1.5	1.7
Hydrogen	0.45	0.5	0.5	0.55	0.6	0.45	0.6	0.45	0.55	0.6	0.65	0.7	0.7	0.45	0.55	0.65	0.75	0.85
	5.15	5.1	5.1	5.35	5.4	5.15	5.4	5.15	5.35	5.4	5.4	5.4	5.4	5.15	5.35	5.4	5.35	5.15
Theoretical Flame Temperature (K)	1700	1830	1830	1900	2000	1700	2000	1700	1900	2000	2100	2215	2215	1700	1900	2100	2320	2550
Duration of Run (min)	3.33	1.88	7.0	4.25	1.18	2.67	4.6	3.0	2.25	2.25	1.25	3.58	34 s	1.75	2.42	2.75	2.58	2.2
Thermocouple Reading under the Specimen (°C)		617			676		723					771	-					840
Optical Pyrometer (°C)		1268			1193		1160					1247	-					1620

Table B-1 (continued)

Run	HF-168			HF-169					HF-170			HF-171				
Specimen Identification	Poco Graphite Sprayed with Nominal 14-mil Coat LaB_6			CaB_6					W-Ni-Fe Alloy Sprayed with LaB_6[33]			LaB_6[41]				
Source	Y-12			Ceradyne					Y-12			Research Chemicals (Haselden)				
Nozzle Flows																
Helium (ft^3/min)	3.8	3.7	3.45	3.8	3.7	3.46	3.7	3.8	3.8	3.7	3.3	3.0	2.6	2.1		2.0
Fluorine	0.9	1.1	1.3	0.9	1.1	1.3	1.1	0.9	0.9	1.1	1.4	1.6	1.7	2.0		1.6
Hydrogen	0.45	0.55	0.65	0.45	0.55	0.65	0.55	0.45	0.45	0.55	0.7	0.8	0.85	1.0		1.0
	5.15	5.35	5.4	5.15	5.35	5.4	5.35	5.15	5.15	5.35	5.4	5.4	5.15	5.1	→	4.6[42]
Theoretical Flame Temperature (K)	1700	1900	2100	1700	1900	2100	1900	1700	1700	1900	2215	2395	2550	2853	→	2853+
Duration of Run (min)	2.17	2.0	3.0	1.42	1.83	3.75	1.17	1.0	1.92	2.33	4.18	2.42	1.75		6.83	
Thermocouple Reading under the Specimen (°C)			753			738					775					Failed at 1341
Optical Pyrometer (°C)			1217			1233					1137					1730

Table B-1 (continued)

Run	HF-172[43]	HF-173[34]		HF-174[34]		HF-175[34]			HF-176[43]	HF-178[44]	
Specimen Identification	ATJ Graphite	LaB_6 Plasma-Sprayed Plate[45]		LaB_6 Plasma-Sprayed Disc[46]		Plate HF-173 Rerun			ATJ Graphite	LaB_6	
Source	Y-12	Y-12		Y-12		Y-12			Y-12	Research Chemicals (Haselden)	
Nozzle Flows											
Helium (ft^3/min)	3.7	3.8	3.7	3.8	3.7	3.8	3.7	3.45	3.7	3.8	3.8
Fluorine	1.1	0.9	1.1	0.9	1.1	0.9	1.1	1.3	1.1	0.9 →	0.7
Hydrogen	0.55	0.45	0.55	0.45	0.55	0.45	0.55	0.65	0.55	0.45 →	0.7
Tetrafluoromethane	800 cm^3/min	-	-	-	-	-	-	-	1600 cm^3/min	-	-
		5.15	5.35	5.15	5.35	5.15	5.35	5.4	5.35	5.15	5.2
Theoretical Flame Temperature (K)	1900	1700	1900	1700	1900	1700	1900	2100	1900	1700→≈3033 Calculated	
Duration of Run (min)	6.5	2.92	1.8	3.17	4.28	2.5	1.83	4.0	6.75	(47)	6.33
Thermocouple Reading under the Specimen (°C)	752 Max	738 Max[48]		840 Max[48]				1060	1042 Max		873
Optical Pyrometer (°C)	1270 Max	1260		No Indication				1190	1130 Max		1117

Table B-1 (continued)

Run	HF-179[44]									HF-180[44]	HF-187[34]	
Specimen Identification	LaB_6, Dense									LaB_6, HF-178[49]	Ni-200 Plate	
Source	Research Chemical (Haselden)									Research Chemical (Haselden)	Y-12	
Nozzle Flows												
Helium (ft^3/min)	3.8	3.6	3.4	3.2	3.0	2.8	2.8	2.5	2.2	3.7	3.8	3.6
Fluorine	0.9	1.1	1.35	1.35	1.5	1.5	1.65	1.65	1.65	0.75	0.9	1.0
Hydrogen	0.45	0.45	0.45	0.45	0.5	0.5	0.55	0.55	0.55	0.75	0.45	0.5
	5.15	5.15	5.20	5.00	5.0	4.8	5.00	4.70	4.40	5.20	5.15	5.1
Theoretical Flame Temperature (K)	1700								1383 Calculated	3158 Calculated	1700	1830
Duration of Run (min)	1.08	1.08	1.08	1.25	1.5	1.25	0.75	1.0	1.5	6.75	5.83	2.17
Thermocouple Reading under the Specimen (°C)									689	910	822	
Optical Pyrometer (°C)									815	1200	835[50]	

Table B-1 (continued)

Run	HF-188[34]	HF-200[34]		HF-201		HF-202		
Specimen Identification	LaB_6 Plate, Dense	LaB_6 Plate, Dense		Yttria Doped Nickel[23]		Yttria Doped Nickel[23]		
Source	Ceradyne	Ceradyne		UTRC		UTRC		
Nozzle Flows								
Helium (ft^3/min)	3.8	3.8	3.6	3.8	3.6	3.8	3.7	3.6
Fluorine	0.9	0.9	1.2	0.9	1.0	0.9	1.1	1.2
Hydrogen	0.45	0.45	0.6	0.45	0.5	0.45	0.55	0.6
Theoretical Flame Temperature (K)	1700	1700	2000	1700	1830	1700	1900	2000
Duration of Run (min)	2.38	3.08	1.92	1.67	7.33	2.83	4.0	2.67
Thermocouple Reading under the Specimen (°C)	487	555		893		855		
Optical Pyrometer (°C)	No Indication	1290		1150		1375		

(1) Distance from nozzle tip to specimen was 4 in. Fluorine-to-hydrogen ratio of two unless noted otherwise. Includes sight port window and mirror (if any) corrections and represents the highest temperature observed during the hot-test portion of the run.
(2) $F_2/H_2 = 1.16$.
(3) $F_2/H_2 = 1.75$.
(4) $F_2/H_2 = 1.85$.
(5) Heat cleaned at 1800°C for 20 min.
(6) Uncorrected readings. Lower temperature limit of automatic optical pyrometer is 850°C.
(7) The Marquardt Company, subsidiary of CCI Corporation, Van Nuys, California.
(8) Atlantic Research Corporation, Alexandria, Virginia.

(9) Specimen reached the temperature only within the last few seconds of the cycle.
(10) Specimen mounted on alumina wafer and ATJ graphite support.
(11) Rocketdyne Division of Rockwell International Corporation, Canoga Park, California.
(12) Probably a low reading since sight glass was dirty.
(13) Nozzle inadvertently moved to 3.3 in from specimen. Condition probably existed from Run HF-24 to HF-29.
(14) United Technology Research Center (UTRC), East Hartford, Connecticut.
(15) Nozzle was repositioned and rotameter was installed to control hydrogen flow.
(16) Temperature readings are unaccountably low.
(17) Optical pyrometer recalibrated prior to run.
(18) Specimen was scrubbed and washed with TF Freon.
(19) Apparent breakpoint temperature.
(20) TRW Defense and Space Systems Group, Redondo Beach, California.
(21) Physmet Corporation Division of Manufacturing Laboratories (Manlabs), Cambridge, Massachusetts.
(22) Thermocouple experiment.
(23) Specimen rested on alumina wafer and nickel support.
(24) The fluorine flow was reduced in stages to 1.4, 1.25, and 1.0 ft^3/min when flameout occurred.
(25) Alumina grit was sprinkled under specimen at support points.
(26) The MgO powder used at specimen support points.
(27) Temperature rose rapidly near end of run.
(28) Air Force Materials Laboratory (AFML), Wright-Patterson Air Force Base, Ohio.
(29) To check flame alignment.
(30) Specimen was previously exposed to the HF flame for periods of 8.5 and 13 min; the flame was not operating properly, however, and the runs were not considered valid.
(31) Alumina grit under the specimen.
(32) Before film left specimen.
(33) After film left specimen.
(34) Configuration chamber experiment.
(35) Specimen had been previously exposed to a 1700 K flame for 3.75 min and a 1830 K flame for 1.52 min; run was aborted because the flame was off-center; specimen developed cracks but did not fall apart.
(36) With 33 vol % LaF_3; 67 vol % Ta.
(37) White coating was brushed off leaving a black specimen with visible metallic flakes on surface.
(38) Estimated density 90% of theoretical; LaF_3 may have left the mixture during fabrication of specimen.
(39) Top center area of specimen had bump on it.
(40) Nominal 7-mil coat on tip and 15-mil coat on side.
(41) Specimen rested on plasma-sprayed LaF_3 wafer and LaB_6 powder.
(42) Due to low fluorine supply pressure, fluorine flow had decreased near end of run.
(43) The CF_4 experiment in configuration test chamber.
(44) Specimen rested on nickel specimen support and plasma-sprayed LaB_6 chips.
(45) At 81.1% of theoretical density.
(46) At 84.2% of theoretical density.
(47) It took 1.87 min to go from initial to final flows.
(48) Recorder apparently malfunctioned.
(49) Fluoride coating was removed by belt sanding.
(50) Incorrect reading - dirty sight glass.

APPENDIX C

OBSERVATIONS ON TEST SPECIMENS EXPOSED TO A HYDROGEN FLUORINE FLAME

Table C-1

OBSERVATIONS ON TEST SPECIMENS EXPOSED TO A HYDROGEN/FLUORINE FLAME

Run	Material	Theoretical Flame Temperature (K)	Duration of Run (min)	Sample Surface Temperature[1] (K)	Loss (%)			Measured Loss in Height (mm)
					Weight	Diameter	Height	
P-14	CeO_2	≈ 2400	3	1850	NM	NM	NM	-
P-19	Y_2O_3	2250	1.25	1138	NA	NA	NA	-
P-20	WC:HfC (65:35)	2000	1.75	1493	NA	NA	NA	
		2100	2	1676	NA	NA	≈ 9%	≈ 1.02
P-23	Al_2O_3	1650	1	Modified Heat Up Cycle to Minimize Thermal Stress	NM	NM	NM	
		1850	0.5					
		2035	0.5					
		2080	2					
			4					
P-24	Al_2O_3	1650	1.5	1706	27.9	6.9	16.7	2.2
		1915	1					
		2150	0.75					
		2280	2					
			5.25					
P-25	Natural Flake Graphite	2280	2	1766	NM	NM	NM	
P-27	Fibrous Carbon-Carbon Composite	2280	2.50	1747	11.4	NM	NM	-
P-29	CeS	2280	< 1	1980	NA	NA	10.4 to 62.7	NA
P-30	Tungsten	2280	< 1	> 1726 K	NA	NA	1.9	0.25
P-31	Calcium Aluminate Cement	1650	1.2	1671	NA	NA	20 to 65.5	NA
		1915	0.5					
		2150	0.7					
		2280	2.3					
			4.7					
P-33	Carbon-Carbon Composite (Marquardt A)	2280	2	1850	13.3	1.8	7.5	0.9
P-34	Carbon-Carbon Composite (Marquardt B)	2280	2	1931	12.9	2.4	4.9	0.66
P-35	CeO_2	1650	1	1596	40.7	1.9	38.4	5.1
		1915	0.58					
		2150	0.75					
		2280	2.17					
			4.5					
P-36	Y_2O_3	1650	0.25	NA	NA	NA	NA	-
P-37	Fibrous Carbon-Carbon Composite	2280	2	1727	NM	NM	NM	
		2280	2	1747	14.7	NM	NM	

HX C

AME

1

D TO A HYDROGEN/FLUORINE FLAME

Loss (%) Diameter	Loss (%) Height	Measured Loss in Height (mm)	Remarks
NM	NM	-	Cracked in several places. Some material loss. Holder kept sample intact.
NA	NA	-	Disintegrated on heat up from thermal shock.
NA	NA		Small pieces spalled from side on heat up.
NA	≈ 9%	≈ 1.02	Cracked into five large pieces on heat up from thermal shock.
NM	NM		Appeared intact. Decision made to run again. Sample not removed from chamber.
6.9	16.7	2.2	Surface cracking but generally intact.
NM	NM		Survived with fast heat up without thermal shock. Some erosion. Sparking on heat up. Coating burned away at ≈ 1323 K.
NM	NM	-	Coating formed at lower temperature which burned away at ≈ 1323 K. Considerable sparking below 1173 K.
NA	10.4 to 62.7	NA	Immediate reaction on heat up. Molten phase on surface flowed freely. Run terminated.
NA	1.9	0.25	Sample holder and supports melted. High conductivity of sample requires holder modification.
NA	20 to 65.5	NA	Extensive corrosion, fused to support.
1.8	7.5	0.9	No shape distortion. Maintained configuration. Coating burned away at 1323 K. Sparking < 1173 K.
2.4	4.9	0.66	No shape distortion. Maintained configuration. Coating burned away at 1323 K. Sparking < 1173 K.
1.9	38.4	5.1	Severely corroded.
NA	NA	-	Disintegrated to powder on heat up.
NM	NM		Cycled through heat up twice to prove that film
NM	NM		formation and dissolution occurred on each step. Lost ≈ 3.3% on second run.

Table C-1 (continued)

Run	Material	Theoretical Flame Temperature (K)	Duration of Run (min)	Sample Surface Temperature[1] (K)	Loss (%)			Mean
					Weight	Diameter	Height	
P-38	Natural Flake Graphite	2280	2	1757	7.9	1.2	3.6	0.4
HF-1	Pyrolytic Graphite (Atlantic Research)	2280	2	1866	7.9	0.7 0.9	5.4	0.4
HF-2	BeO	1650	0.25	1611	NM	NM	NM	
HF-3	ATJ Graphite	2280	2	1696	8.0	1.3	3.2	0.4
HF-4	Poco Graphite	2280	2	1732	8.1	1.3	3.2	0.4
HF-5	Al_2O_3	1650 1915 2150 2290	1 0.58 0.58 2 4.16	1646	19.9	5.6 to 4.5	10.8	1.1
HF-6	WC:HfC (65:35)	1650 1915 2150 2290	1 0.5 0.5 2.17 4.17	1888	27.4	5.0	16.7 to 12.2	1.1 Ave
HF-7	MgO	1650 1915 2160 2280	1 0.67 0.67 2.42 4.76	1233	2.1 Top 1.3 Bot	No Change	No Change	0.0
HF-8	Isotropic Carbon	2280	2	1858	16.5	2.8	7.8	0.0
HF-9	MgO	1650 1915 2160 2280	1 0.58 0.67 1 3.25	2038	NA	NA	NA	
HF-10	Anisotropic Carbon	2280	2	1656	14.0	1.7	5.6	0.
HF-11	ATJS Graphite	2280 2280	2 2	NA NA	NM 15.7	NM 3.1	NM 7.2	0
HF-12	BN	1650 1950 2160 2280	1 0.92 0.92 2.17 5.01	1908	NA	NA	NA	1
HF-13	Glassy Carbon	2280	2	1928	36.7	4.8	26.2 6.6 for 12.7-mm-Thick Specimen	1

Table C-1 (continued)

ple face sure(1) K)	Loss (%) Weight	Diameter	Height	Measured Loss in Height (mm)	Remarks
	7.9	1.2	3.6	0.46	Maintained configuration. Coating burned away at ≈ 1323 K.
	7.9	0.7 0.9	5.4	0.64	Maintained original square configuration. Coating burned off at 1323 K.
	NM	NM	NM		Reacted immediately on heat up in flame. Viscous molten phase flowed freely.
	8.0	1.3	3.2	0.41	Sparks at low temperature. Film burn-off at ≈ 1323 K. Good configurational stability.
	8.1	1.3	3.2	0.41	Specimen texture change on top and sides. Film burn-off at ≈ 1323 K.
	19.9	5.6 to 4.5	10.8	1.37	Good configurational stability.
	27.4	5.0	16.7 to 12.2	1.96 Average	White residue on bottom. Obvious corrosion. Texture change on top and sides.
	2.1 Top 1.3 Bot	No Change	No Change	0.0	Two thin samples stacked.
	16.5	2.8	7.8	0.99	Very slight amount of sparking compared to previous graphite specimens. White residue remained on bottom of the specimen. Specimen changed texture.
	NA	NA	NA		Two thin samples reacted and melted.
	14.0	1.7	5.6	0.71	Specimen changed texture. Bottom of specimen did not react.
3A	NM	NM	NM	0.91	Cycled through heat up twice. Specimen had a
3A	15.7	3.1	7.2		white residue on the bottom. Specimen changed texture.
	NA	NA	NA	NA	Severely corroded. Nickel from the support melted onto the specimen.
	38.7	4.8	26.2 8.6 for 12.7-mm-Thick Specimen	0.84	Thin wafer specimen. No sparking or whitish formation noted during run. Underside of specimen retained its shiny appearance; top had a bluish coloration and had changed texture. Specimen had not cracked.

Table C-1 (continued)

Run	Material	Theoretical Flame Temperature (K)	Duration of Run (min)	Sample Surface Temperature[1] (K)	Loss (%) Weight	Diameter	Height	Measured Loss in Height (mm)
HF-14	SrO	1650 1950 2160 2280	1 0.75 0.75 2 4.5	1636	NA	NA	NA	
HF-15	W	2280	2.75	1493[2]	12.0	2.1	6.2	0.79
HF-16	Mo with CM 500 coat (Rocketdyne) W-WC Composite	2280	2	1870	15.1	1.9	5.1	0.66
HF-17	ATJ Graphite	> 1650	2	1390	6.3	0.8	2.2	0.30
HF-18	Mo with W coat (Rocketdyne)	2160	2.17	1717	15.2	1.8	6.2	≈ 0.79
HF-19	TaC:HfC[80:20 molar]	2160	0.25 - 0.5	≈ 1626	5.6	-	-	-
HF-20	TaC:HfC[80:20]	1650 1915 2160	1 1.25 2 4.25	1861	19.3	3.4	7.5	1.02
HF-21	Coors Alumina	1650 1915	3.25 3 6.25	< 1138	0.02	0.0	0.0	0.0
HF-22	Coors Alumina from HF-21	1775 2080	2.5 2.25 2.75	1575	5.9	≈ 0.4	3.15 Average	- -1.22 to +0.
HF-23	Poco Graphite AFX-5Q-Z	> 1775	2.75	< 1138	0.3	0.0	0.0	0.0
HF-24	Coors Alumina	1775 1900 2200+	2.83 3.42 1.75 8.0	NA	13.3	2.0	7.5	0.97
HF-25	Graphite (Y-12) MP 11 B-1	1775 2000	2.75 2.08 4.83	1653	16.2	2.5	7.5	0.97
HF-26	NiAl	≈ 1775	3.25	1088 Visual	+0.004	0.0	+0.18	+0.03
HF-27	Same Specimen from HF-26	1890 1970 2026	3 3 2 8	1218	0.18	0.1 to 0.4	0.0	0.0
HF-28	ATJ Graphite	≈ 1775	2.17	1463	4.83	0.3	2.0	0.26
HF-29	NiAl	2120 2150	2.67 2 4.67	1203	0.08	0.1	0.22	0.03
HF-30	ATJ Graphite	2000	2.17	1088 Visual	0.09	0.1	+0.2	+0.03

ued)

ter	Height	Measured Loss in Height (mm)	Remarks
A	NA		Specimen cracked and a portion of it melted; melted material was greenish. Specimen reached temperature only within seconds of completing the cycle.
	6.2	0.79	Specimen showed signs of corrosion and reaction with graphite holder.
	5.1	0.66	Specimen showed some signs of corrosion.
	2.2	0.30	Specimen changed texture; underside had whitish coat on it.
	6.2	≈ 0.79	Corrosion on top of specimen was slightly uneven.
	-	-	Specimen cracked; run was terminated.
	7.5	1.02	Specimen turned from brown to black on top and sides. Vapor evolved from specimen during run.
	0.0	0.0	No change in specimen.
	3.15 Average	- -1.22 to +0.23	Specimen not fully covered by flame; corrosion confined to 2/3 of top surface; some flow took place. Some cracks noted.
	0.0	( )	Specimen not fully covered by flame; portions not touched had a whitish coat; 2/5 was covered.
	7.5	0.97	Flame slightly off center. Lost process He during third cycle; specimen cracked as temperature quickly rose.
	7.5	0.97	Bottom of specimen did not react and had a bit of whitish coating; other surfaces changed texture.
	+0.18	+0.03	Specimen had darkened on top and sides; blue and greenish coloration evident.
.4	0.0	0.0	Specimen dark gray on top. Side and bottom had a nonadherent whitish coat.
	2.0	0.25	Specimen changed texture on sides and top. Low density specimen.
	0.22	0.03	Whitish coating on top flaked off. Whitish coat also on sides.
	+0.2	+0.03	White coating on top and side.

Table C-1 (continued)

Run	Material	Theoretical Flame Temperature (K)	Duration of Run (min)	Sample Surface Temperature[1] (K)	Loss (%) Weight	Diameter	Height	Mean Loss Height (mm)
HF-31	ATJ Graphite	2215	2.5	1418	7.4	0.9	3.2	0.4
HF-32	ATJ Graphite	2120	2.25	1375	5.4	0.8	1.8	0.2
HF-33	ATJ Graphite	2045	2	1330	4.6	0.6	1.8	0.2
HF-34	ATJ Graphite	2000	2.37	1310	4.7	0.5	2.6	0.2
HF-35	ATJ Graphite	1900	4	1305	3.8	0.4	2.0	0.2
HF-36	ATJ Graphite	1810	5	1088 Visual	0.24	0.2	0.14	0.0
HF-37	ATJ Graphite with a 1 μm Coat of CaF_2	2000	2.37	1310	4.4	0.4	1.8	0.2
HF-38	Coors Alumina	1700 1830 2000	1 1.2 4 6.2	1223	6.1	0.8	-	-1.35 to
HF-39	Coors Alumina	1700 1830 1900	1 1.15 4 6.15	< 1138	0.18	0.1	0.12	0.0 Aver
HF-40	CVD W on Mo	2000	2.07	1473	9.5	1.2	3.4	0.4 (0.38 to Aver
HF-41	Y_2O_3 Doped Ni	1900	2.37	< 1138	0.003	0.0	0.0	0.0
HF-42	Y_2O_3 Doped Ni	2000	4.17	< 1138	-	0.0	0.0	0.0
HF-43	Ni 270	2000	4.17	< 1138	0.02	0.0	0.0	0.0
HF-44	Ni 270	2280	4.03	1300	0.75	0.0	0.4	0.0
HF-45	Ni 200 5-mil-Thick Foil	2280	2.35	1438	100.0		-	0.1
HF-46	BeO	1700 1830 2000	1.27 1.35 4.38 7.00	≈ 1108	+0.7	+0.96	+1.3 to +3.0	+0.13 t
HF-47	SrO	1700 1830 2000	1 1 4 6.0	1198	+0.2	+0.1	+0.96 to +0.42	+0.1 +0.
HF-48	CaO	1700 1830 2000	1 1 4.5 6.5	1158	1.03	+0.5	+0.96	+0.1

Height	Measured Loss in Height (mm)	Remarks
3.2	0.41	Specimen changed to a black texture except on the bottom.
1.8	0.23	Specimen changed to a black texture except on the bottom.
1.8	0.23	Specimen changed to a black texture except on the bottom.
2.6	0.33	Specimen changed to a black texture except on the bottom.
2.0	0.25	Specimen changed to a black texture except on the bottom.
0.14	0.02	Entire specimen except for a portion on the bottom had a white coating.
1.8	0.23	Specimen changed to a black texture except on the bottom.
-	-1.35 to +0.03	Specimen corroded unevenly; had slight cracks on top and side.
0.12	0.02 Average	Specimen had fine cracks on top and side.
3.4	0.43 (0.38 to 0.53) Average	Golden coloration on side. Top had a grayish appearance.
0.0	0.0	Specimen turned dark gray on top and partially on the side. Top and bottom layers seemed to be separating.
0.0	0.0	Top layer and portion of side became dark gray. Bonding of layers seemed OK.
0.0	0.0	Specimen became light gray on top and side.
0.4	0.05	Specimen turned to a light grayish appearance on top and side.
-	0.13	Foil burned away within 2 min.
+1.3 to +3.0	+0.13 to +0.33	Specimen had film built up on it which seemed flaky; specimen had a big crack.
+0.96 to +0.42	+0.1 to +0.05	Specimen cracked in several places; top had a rough texture.
+0.95	+0.13	Specimen was cracked and chipped.

Table C-1 (continued)

Run	Material	Theoretical Flame Temperature (K)	Duration of Run (min)	Sample Surface Temperature[1] (K)	Loss (%) Weight	Diameter	Height	Measured Loss in Height (mm)
HF-49	YN	1700	10 s	-	-	-	-	-
HF-50	Yttrium	2280	4	1148	+0.1	0.0	0.0	0.0
HF-51	$CaAl_4O_7$	1700	1	1350	12.5	1.5	13.6	1.73
		1830	1					
		2000	4					
			6.0					
HF-52	CeO_2	1700	1	1333	33.8	4.2	17.7	2.44
		1830	1					
		2000	4					
			6.0					
HF-53	Y_2O_3	1700	1	No	-	-	-	-
		1830	1	Indication				
		2000	4	< 1138				
			6.0					
HF-54	Y_2O_3	1700	14 s	-	-	-	-	-
HF-55	CeS	1700	1	1566	21.6	1.5	8.0 to 23.5	0.97 to 2.8
		1830	1					
		2000	1.5					
			3.5					
HF-56	Alumina	1700	1	No	0.9	1.0	0.4	0.05
		1830	1	Indication				
		2000	5	<1138				
		1830	1					
		1700	≈ 1					
			9.0					
HF-59	Alumina	1700	1	1438	25.0	NA	NA	NA
		1830	1		est			
		2000	2.5					
		2110	3.0					
		1830	1					
		1700	1.17					
			9.67					
HF-60	Tantalum	2000	4	1596	22.4	4.9	11.8	1.5
HF-61	CeO_2	1700	4	1245	8.2	+0.98	3.3	0.38
HF-62	BeO	1700	4	No Indication < 1138	+0.6	+0.3	0.2	0.025
HF-63	SrO	1700	1	1143	+0.2	+1.0	+1.74 to +1.99	+0.2 to +0.25
		1910	4					
		1700	1					
			6.0					
HF-67	MgO	1700	1	No	+0.07	0.2	est'd 0	0.08 Average
		1830	1	Indication				
		2000	4.5	< 1138				
		1830	1					
		1700	1					
			8.5					

ight	Measured Loss in Height (mm)	Remarks
-	-	Specimen fell apart into eight pieces during test.
0.0	0.0	Shiny top of specimen turned gray; rest of specimen also turned gray.
3.6	1.73	Flame burned with a yellowish color. Specimen turned gray and was surrounded by a whitish melted layer.
7.7	2.44	Specimen was cracked. There was a light tan coating on the top and side with a darker tan on the bottom.
-	-	Specimen broke into ≈ 10 pieces.
-	-	Specimen broke apart.
to 23.5	0.97 to 2.6	Run terminated; corrosion quite evident. Light gray coating on specimen.
0.4	0.05	There was some white residue on the bottom; very fine visible cracks.
NA	NA	Specimen corroded; broke into two pieces.
11.8	1.5	Side had a silver coat plus some bluish gray corroded areas; top looked bluish gray. Alumina support wafer cracked.
3.3	0.38	Coating flakes off.
0.2	0.025	White coating flakes off.
1.74 to +1.99	+0.2 to +0.25	Specimen had cracks and fell apart after handling. Surface had changed texture.
est'd 0	0.08 Average	Specimen seemed to be intact; had dark brown coloration on the underside.

Table C-1 (continued)

Run	Material	Theoretical Flame Temperature (K)	Duration of Run (min)	Sample Surface Temperature[1] (K)	Loss (%)			Mea Lo Hei (m
					Weight	Diameter	Height	
HF-68	SiC	1700	1	1548	27.2	4.3	11.9 to 20.5	1.6 to
		1830	1					
		2000	4.5					
		1830	1					
		1700	1					
			8.5					
HF-69	LaB_6	1700	1	< 1138	0.08	0	0.0	0.0
		1830	1					
		2000	4.5					
		1830	1					
		1700	1					
			8.5					
HF-70	ATJ Graphite	2000	6	1468	-	-	-	-
	Rerun	1700	3.83	1473	31.5	5.6	17.3	2.4
		1830	2.78					
			6.61					
HF-72	MgO - Rerun of HF-67	1700	1	1138	0.001	+0.05	+0.2	+0.4
		1830	1					
		2120	4.5					
		1830	1					
		1700	1					
			8.5					
HF-73	MgO - Rerun of HF-72	1700	1	1158	+0.016	+0.15	0.04	0.0
		1830	1					
		2215	4.5					
		1830	1					
		1700	1					
			8.5					
HF-74	MgO - Rerun of HF-73	1700	1	1757	NA	NA	NA	N
		1830	1					
		2320	5					
		1830	1					
		1700	1					
			9.0					
HF-75	LaB_6 - Rerun of HF-69	1700	1	1260	0.1	0.1	0.4	0.0
		1830	1				Average	
		2120	4.5					
		1830	1					
		1700	1					
			8.5					
HF-76	LaB_6 - Rerun of HF-75	1700	1	1238	0.08	0	0.4	0.
		1830	1					
		2215	4.67					
		1830	1					
		1700	1					
			8.67					
HF-77	ATJ Graphite	2280	4	1566	14.3	2.5	6.6	0.

ntinued)

ss (%) Diameter	Height	Measured Loss in Height (mm)	Remarks
	11.9 to 20.5	1.6 to 2.7	Specimen was gray on top and on the sides; was black on the bottom. Corrosion was evident.
	0.0	0.0	Tested specimen had a white film on top, the side and partially on the bottom.
-	-	-	Specimen showed signs of corrosion.
	17.3	2.2	
55	+0.2	+0.02	Specimen had white coating on top; brownish coloration on the bottom.
15	0.04	0.01	Specimen still had white coating; fine cracks were visible which may be in the film itself; brownish coloration on the bottom.
NA	NA	NA	Specimen failed after approximately 5 min and 50 s; temperatures rose when this took place. Specimen was coated with what had been molten material. Apparent breakpoint was 1248 K.
1	0.4 Average	0.05	Top of specimen had a brownish spot in the center which was surrounded by a white coating.
	0.4	0.05	Top of specimen had a brownish spot in the center which was surrounded by a white coating.
5	6.6	0.84	Specimen changed texture except on the bottom side.

Table C-1 (continued)

Run	Material	Theoretical Flame Temperature (K)	Duration of Run (min)	Sample Surface Temperature[1] (K)	Loss (%) Weight	Diameter	Height	Measured Loss in Height (mm)
HF-78	LaB_6 - Rerun of HF-76	1700	1	1350	0.07	≈ 0	+0.34	+0.04
		1830	1					
		2320	4.5					
		1830	1					
		1700	1					
			8.5					
HF-79	Al_2O_3	1700	1	1646	42.4	-	-	-
		1830	1					
		2280	4.5					
		1830	1					
		1700	1					
			8.5					
HF-80	Al_2O_3 (TRW)	1700	1	< 1138	-	-	-	-
		1830	1					
		2000	4.25					
		1830	0.58					
			6.83					
HF-81	$CaZrO_3$	1700	1	< 1138	-	-	-	-
		1830	1					
		2000	4.42					
		1830	1					
		1700	1					
			8.42					
HF-82	Boride V	1700	1	1443	28.1	5.1	11.9	1.78
		1830	1					
		2000	4.33					
		1830	1					
		1700	1					
HF-83	Al_2O_3 (TRW)	1700	1	Visual	0.04	Length	Width	0.0
		1830	1	< 888-988		0.0	0.0	
		2000	4.33					
		1830	1					
		1700	1					
			8.33					
HF-84	Al_2O_3 (TRW)	1700	1	Visual	0.1	Length	Width	0.0
		1830	1	< 888-988		0.0	0.0	
		2000	4.33					
		1830	1					
		1700	1					
			8.33					
HF-85	Al_2O_3 (TRW)	1700	1	1088	0.18	Length	Width	0.0
		1830	1	Manual		0.0	0.0	
		2000	4.5					
		1830	1					
		1700	0.97					
			8.47					
HF-86	Vitreous Carbon (TRW)	1700	1	< 1038	0.02	Diagonal	Width	0.0
		1830	1	Manual		0.38	0.79	
		2000	4.17					
		1830	1					
		1700	1					
			8.17					

d)

er	Height	Measured Loss in Height (mm)	Remarks
	+0.34	+0.04	Brownish area on top had increased; some grayish area exists on the bottom; balance of specimen had white coating.
	-	-	Specimen had corroded in nonuniform fashion and had split into three pieces.
	-	-	Specimen cracked early in the run.
	-	-	Specimen cracked and broke apart into several pieces.
	11.9	1.78	Specimen appeared to be corroded; top had a whitish coating.
	Width 0.0	0.0	Specimen appeared to be intact.
	Width 0.0	0.0	Specimen appeared to be intact.
	Width 0.0	0.0	Specimen appeared to be intact except for a corroded section on the edge pointed toward the flame.
	Width 0.79	0.0	Center area contacted by flame was dark, adjacent areas had a light white coating.

Table C-1 (continued)

Run	Material	Theoretical Flame Temperature (K)	Duration of Run (min)	Sample Surface Temperature[1] (K)	Loss (%)			Meas Loss Heig (m
					Weight	Diameter	Height	
HF-87	CaB_6	1700	10 s	-	-	-	-	-
HF-88	SrO	1700	1	2015	-	-	-	-
		1830	1					
		2320	2.47					
			4.47					
HF-90	Al_2O_3	1700	1	1478	11.3	1.4	3.1 to 12.8	0.4 to
		1830	1					
		2000	4.92					
			6.92					
HF-93	Sc_2O_3	1700	1	No				
		1830	1	Indication				
		2000	1.25	< 1138				
			3.25					
HF-96	LaB_6, HF-78	1700	1	1328	0.07	0.0	0.0	0.0
		1830	1					
		2400	4.67					
		1830	1					
		1700	1					
			8.67					
HF-97	LaB_6, HF-96	1700	1	1350	0.04	0.0	0.0	0.0
		1830	1					
		2450	4.75					
		1830	1					
		1700	1					
			8.75					
HF-98	LaB_6, HF-97	1700	1	1416	0.06	0.0	0.0	0.0
		1830	1					
		2535	4.75					
		1830	1					
		1700	1					
			8.75					
HF-99	LaB_6, HF-98	1700	1	1410	0.05	0.0	0.0	0.0
		1830	1					
		2615	4.75					
		1830	1					
		1700	1					
			8.75					
HF-100	LaB_6, HF-99	1700	1	1463	0.02	0.0	0.4	0.0
		1830	1					
		2690	5					
		1830	1					
		1700	1					
			9.0					
HF-101	LaB_6, HF-100	1700	1	1486	0.2	0.0	0.4	0.0
		1830	1					
		2770	4.83					
		1830	1					
		1700	1					
			8.83					

(continued)

Loss (%) Diameter	Loss (%) Height	Measured Loss in Height (mm)	Remarks
-	-	-	Specimen cracked and fell apart.
-	-	-	Specimen melted.
1.4	3.1 to 12.8	0.4 to 1.65	Dishing effect and fine crack lines were evident. Center thermocouple hole became visible.
			Specimen appeared to be cracked after 1 min; broke apart after approximately 2-1/2 min.
0.0	0.0	0.0	Brownish area on top lessened.
0.0	0.0	0.0	Brownish area still visible.
0.0	0.0	0.0	Brownish area still visible.
0.0	0.0	0.0	Brownish area still visible.
0.0	0.4	0.05	Brownish area faint.
0.0	0.4	0.05	Brownish area increased.

Table C-1 (continued)

Run	Material	Theoretical Flame Temperature (K)	Duration of Run (min)	Sample Surface Temperature[1] (K)	Loss (%) Weight	Diameter	Height	Measured Loss in Height (mm)
HF-102	LaB_6, HF-101	1700	1	1672	0.96	0.2	+1.8 to -1.6	+0.23 to -0.20
		1830	1					
		2840	10.75					
		2840+	3.42					
			16.17					
HF-103	*LaB_6, HF-102*	2840	3.75	1213	0.06	0	0.1	0.3
HF-108	NiAl, HF-27	1700	1	Manual	0.13	0.0	0.0	0.0
		1830	1	1138				
		2215	4.77					
			6.77					
HF-109	NiAl, HF-108	2400	5.33	1591	34.3	4.1	29.8	4.1
		2535	4.52					
			9.85					
HF-110	Ni-270, HF-43	2400	4.25	1544	-	-	-	-
		2535	5.25					
		2615	3.0					
		2690	2.0					
		2840	1.5					
			16.00					
HF-111	Yttrium	2400	2.75	1576	-	-	-	-
		2535	1.12					
			3.87					
HF-112	Al_2O_3 (TRW), HF-84	1700	1	1576	-	-	-	-
		1830	1					
		2215	4.08					
		2400	1.08					
			7.16					
HF-113	Al_2O_3 (TRW), A-10205	1700	1	Manual	0.45	Length	Width	Width
		1830	1	< 1068		0.0	0.39	0.03
		2000	4.5				0.62	0.03
		1830	1					
		1700	1					
			8.5					
HF-114	Al_2O_3, HF-113	1700	1	1447	39.7	Length	26.0	1.7
		1830	1			0.0	51.6	2.1
		2120	4					
		2215	2.25					
		1830	1					
		1700	1					
			10.25					
HF-115	MgO (TRW)	1700	1	< 1138	0.16	Length	0.4	0.03
		1830	1			0.0	0.0	0.0
		2215	3.5					
		2395	4.5					
			10.0					
HF-116	MgO (TRW), HF-115	1700	1	Manual	-	-	-	-
		1830	1	> 1410				
		2560	3.3					
		2690	1.92					
			7.22					

ter	Height	Measured Loss in Height (mm)	Remarks
	+1.8 to -1.6	+0.23 to -0.20	Partial melting of the fluoride layer took place. Specimen had a glazed appearance.
	0.1	0.3	Coating on specimen turned from gray to white after exposure to room air.
	0.0	0.0	No change.
	29.8	4.1	Melting and corrosion of a specimen took place. Melting on specimen surface per manual pyrometer appeared at 1488 K.
	-	-	Specimen corroded and fused to Ni specimen support. Reaction at top surface started at 1390 K.
	-	-	Specimen melted. Melting and film burn-off started at 1365 K.
	-	-	Specimen corroded; one small section left. Extensive corrosion noticed at 1478 K.
	Width 0.39 0.62	Width 0.03 0.03	Little change.
	26.0 51.6	1.7 2.1	Specimen corroded and thinned down.
	0.4 0.0	0.03 0.0	Top edge slightly rounded.
	-	-	Specimen corroded; appeared to burn in two parts.

Table C-1 (continued)

Run	Material	Theoretical Flame Temperature (K)	Duration of Run (min)	Sample Surface Temperature[1] (K)	Loss (%) Weight	Diameter	Height	Measured Loss in Height (mm)
HF-118	Scandium	2400 2550	3.33 2.78 6.11	1336	+4.4	+2.1	+10.8	+1.4
HF-119	Scandium HF-118	2690	0.77	1576	-	-	-	-
HF-120	Sapphire Single Crystal	1700 1830 2000 1830 1700	1 1 5 1 1 9.0	No Indication < 1138	0.5	0.5	0.6	0.08
HF-121	Sapphire HF-120	1700 1830 2105 1830 1700	1 1 5 1 1 9.0	Manual 1126	7.4	0.4 Average	5.4 Average	0.69 Average
HF-122	$LaCrO_3$	1700 1830 2215 2320 2395 1830 1700	1 1 3.83 1.67 4.17 0.83 1.0 13.5	1493	1.4	+2.0	+3.4	+0.43
HF-123	$LaCrO_3$, HF-122	2395	2.33	1338	0.3	0.0	0.0	0.0
HF-124	TiAl, (AFML)	2215	3.93	1732	10.0	1.5	3.9	0.51
HF-125	La_2O_3·Si_3N_4	1700 1830 2215 1830 1700	1 1 4 1 0.88 7.88	1656	13.5	+0.4	+0.4	0.05
HF-126	Al_2O_3	1700 1910 2150 2280 2150 1910 1700	1 0.58 0.58 2.08 0.67 0.58 1.0 6.49	1254	2.4	0.0	3.7 Average	0.48 Average
HF-127	Si_3N_4, MgO Doped	1700 1830 2215 1830 1700	1.0 1.0 4.0 1.0 1.0 8.0	1631	39.3	6.1 to 6.6	13.9	1.78

C-1 (continued)

Loss (%)		Measured Loss in Height (mm)	Remarks
Diameter	*Height*		
+2.1	+10.8	+1.4	White coating on side of specimen.
.	.	.	Specimen melted. Started to go at 1395 K.
0.5	0.6	0.08	Specimen appeared to be etched all over.
0.4 Average	5.4 Average	0.69 Average	Specimen had cracks in it, but did not fall apart.
+2.0	+3.4	+0.43	Specimen had white coating all over except for small area on the bottom; almost one-half of top surface had a glaze and showed evidence of melting. Apparent breakpoint 1355 K.
0.0	0.0	0.0	Some cracking evident in the coating layer; condition of basic structure not visible.
1.5	3.9	0.61	Specimen had a black nonadherent coating.
+0.4	+0.4	0.05	Specimen cracked almost immediately upon flame ignition; white coating did form on main portion of specimen. Apparent breakpoint 1493 K.
0.0	3.7 Average	0.48 Average	Specimen corroded unevenly.
6.1 to 6.6	13.9	1.75	Apparent breakpoint 1365 K.

Table C-1 (continued)

Run	Material	Theoretical Flame Temperature (K)	Duration of Run (min)	Sample Surface Temperature[1] (K)	Loss (%) Weight	Diameter	Height	Measured Loss in Height (mm)
HF-128	Al_2O_3	1700 1910 2150 2280 2150 1910 1700	1.0 0.58 0.58 2.67 0.58 0.58 1.0 6.99	1514	11.7	2.2 to 1.7 Average	8.3 Average	1.1 Average
HF-130	Al_2O_3	1700 1900 1700	1.0 7.25 1.0 9.25	1048[3]	0.07	0.0	0.0	0.0
HF-131	Al_2O_3, HF-130	1700 2000 1700	1.0 8.0 1.0 10.0	1095[3]	0.39	0.0	0.2	0.03
HF-132	Al_2O_3, HF-131	1700 2090 2215 1700	1.0 8.33 3.95 1.0	1325	5.99	1.4	10.1 Max	1.3 Max
HF-133	BeO National Beryllia	1700 1830 2215 2395 1830 1700	1.0 1.0 6.33 3.33 1.0 1.0 13.66	1315	53.3	12.4 Average	32.6 Average	3.2
HF-134	BeO (Y-12)	1700 1830 2215 1830 1700	1.0 1.0 3.17 1.0 1.0	1267 1288 Manual	18.6	2.8 Average	10.3 Average	1.2 Average
HF-135	Al_2O_3	1700 1910 2150 2280 2150 1910 1700	1.0 0.58 0.58 4.58 0.58 0.58 1.0 4.32	1446	17.6	4.0 Average	8.1 Average	1.0 Average
HF-137	Single Crystal MgO	1700 1830 2450 1830 1700	1.0 1.0 2.5 1.0 1.0 6.5	1692	NA	+0.9	9.9	1.3
HF-138	MgO	1700 1830 2215	1 1 1.17 3.17	1299	0.02	0.0	0.0	0.0

Height	Measured Loss in Height (mm)	Remarks
8.3 Average	1.1 Average	Flame apparently off-center; uneven corrosion; visible crack lines.
0.0	0.0	Thermocouple experiment. No apparent effect on specimen.
0.2	0.03	Thermocouple experiment. Several whiskers appeared at top outer edge of specimen.
10.1 Max	1.3 Max	Thermocouple experiment. Two-thirds of top surface was corroded; center thermocouple hole became visible, some cracks observed.
32.6 Average	3.2	Specimen corroded.
10.3 Average	1.2 Average	Specimen corroded; stuck to support because of melting.
8.1 Average	1.0 Average	Specimen corroded unevenly.
9.9	1.3	Specimen melted on top and cracks developed.
0.0	0.0	*Thermocouple experiment specimen cracked vertically in plane passing through drilled thermocouple holes in about 3 min.*

Table C-1 (continued)

Run	Material	Theoretical Flame Temperature (K)	Duration of Run (min)	Sample Surface Temperature[1] (K)	Loss (%) Weight	Diameter	Height	Measured Loss in Height (mm)
HF-139	ATJ Graphite	1810 1900	7 3.37 10.37	1471	10.7	1.5 Average	5.6	0.71
HF-140	Ni 270	2395	4.05	1680	-	-	-	-
HF-141	LaB_6	1830 2395 2550 2690 1830	1 3.75 3.25 3.33 1.15 12.48	1571	0.16	+0.1	+0.1	+0.01
HF-142	LaB_6, HF-141	1830 2550 2853 2853+ 1830	1 3.5 3.33 0.82 1.18 9.83	1720	+0.12	0.0	0.4	0.05 At Center Only
HF-143	LaB_6	2550	2.33 3.17 1.23 6.73	1534	0.096	0.0	0.0	0.0
HF-144	ATJ Graphite, HF-139	1900	3.1	1543	6.1	0.8	5.9	0.7
HF-145	ATJ Graphite	1700	5.6	No Indication	+0.24	-	-	-
HF-146	ATJ Graphite	1900	7.42	1752	5.8	0.0	16.3 Max	0.64 Max
HF-147	MgO Single Crystal	1700 1830 1910 2000 2105 2215 2000 1910 1830 1700	3.25 1.67 2.0 1.5 2.75 1.75 1.17 1.0 1.0 1.0 17.09	1421	-	-	-	-
HF-148	ATJ Graphite	1830 2215 1830	2.0 1.58 1.42 5.00	1576	10.9	1.6	4.4 to 6.6	0.84 Max

ntinued)

Loss (%)		Measured Loss in Height	
Diameter	Height	(mm)	Remarks
.5 erage	5.6	0.71	Thermocouple experiment; specimen surface changed to a black velvet texture.
-	-	-	Thermocouple experiment; specimen melted; nickel sheathed thermocouples fused to the specimen. Apparent breakpoint 1418 K.
.1	+0.1	+0.01	Thermocouple experiment. Top surface of specimen became grayish; bottom had a white coat.
.0	0.4	0.05 At Center Only	Thermocouple experiment; specimen was gray on top with a white film on the bottom.
.0	0.0	0.0	Specimen turned gray on top and had a white layer on the bottom.
.8	5.9	0.7	Thermocouple experiment; specimen corroded; two top thermocouple holes became visible.
-	-	-	Test chamber run. There was a white coating on both sides of the test plate in area containing the holes. Rest of assembly appeared to be untouched.
.0	16.3 Max	0.64 Max	Test chamber run; area around holes in test plate corroded. Chamber assembly appeared to be untouched. Holes increased from 1.016- to 2.26-mm and up to 2.79-mm diameter in center of plate. Breakpoint temperature reached after approximately 4.3 min in the run.
-	-	-	Thermocouple experiment. A portion of the specimen melted; corrosion was uneven. Center thermocouple hole became visible. Apparent breakpoint 1279 K.
.6	4.4 to 6.6	0.84 Max	Flame calibration run. Specimen corroded.

Table C-1 (continued)

Run	Material	Theoretical Flame Temperature (K)	Duration of Run (min)	Sample Surface Temperature[1] (K)	Loss (%) Weight	Loss (%) Diameter	Loss (%) Height	Measured Loss in Height (mm)
HF-149	NiAl	2320	3.25	1646	3.4[4]	0.97	1.5	0.2
HF-150	Ta-LaF_3	1700	3.1	1697	16.9	0.3	-	-
HF-151	Ta-LaF_3, HF-150	1830 1910 2000 2215	2.67 1.58 2.05 1.03 7.33	1845	37.9	-	-	-
HF-152	Ta-LaF_3	1700	5.12	1548	19.9	+2.0 to -1.0	+0.21	+0.03
HF-153	Graphite Sprayed with LaB_6	1700 1900 2215 2320 2395 2320 2215 1900 1700	1.0 2.33 2.25 1.25 2.25 1.0 1.0 1.0 1.25 13.33	1524	4.98	0.4	1.4	0.18
HF-154	Graphite Sprayed with LaB_6	1700 1900 2215 1900 1700	1.00 1.00 2.25 1.0 1.0 6.25	1529	1.6	0.0	1.3	0.2
HF-155	MgO Plate	1700 1830	3.25 0.9 4.15	≈ 1583	+0.5	-	+0.7	-
HF-156	ATJ Graphite Plate	1900	2.27	1635	0.97	0.0	9.9	0.38
HF-157	Ni 200 Plate	1700 1900 2105	3.0 2.08 3.32 8.40	1437	0.17	0.0	0.8	0.03
HF-158	ATJ Graphite Plate	1700	6.25	1587	1.49	0.0	11.2	0.43
HF-159	Alumina Plate	1700	5.65	1416	-	-	-	-
HF-161	SrB_6 LaB_6 Mixture	2215 2320	3.5 2.82 6.32	1802	6.24	0.6	1.8	0.26

Height	Measured Loss in Height (mm)	Remarks
1.5	0.2	Thermocouple experiment; the TC3 nickel sheathed thermocouple and nickel specimen support reacted with the specimen. Bluish coloration on top of specimen.
-	-	A white, thick, flaky, nonadherent coating formed.
-	-	White, soft, nonadherent coating formed; some evidence of melting.
+0.21	+0.03	White nonadherent coating formed approximately 0.33 to 0.51 mm (13 to 20 mil thick).
1.4	0.18	White nonadherent coating formed.
1.3	0.2	White LaF_3 layer appeared to be adherent; bottom of specimen not having a LaB_6 coating reacted.
+0.7	-	Test chamber run; specimen cracked into several pieces. Holes in plate were enlarged. Apparent breakpoint 1247 K.
9.9	0.38	Test chamber run. Slots were widened in test plate to 1.016 to 1.778 mm (40 to 70 mil). Breakpoint temperature reached in approximately 38 s.
0.8	0.03	Test chamber run; slight corrosion around center of plate with an increase in some of the hole diameters from 1.016 to 1.067 mm and to 1.219 mm.
11.2	0.43	Test chamber run; slots were widened from 0.46 to 1.499 mm and to 1.981 mm. Corrosion had occurred, particularly in center of the plate. Breakpoint temperature reached in approximately 4.3 min.
-	-	Test chamber run; plate cracked and portion of it was lost. Some corrosion had occurred.
1.8	0.26	Fluoride layer thick on top but porous; some indication of melting.

Table C-1 (continued)

Run	Material	Theoretical Flame Temperature (K)	Duration of Run (min)	Sample Surface Temperature[1] (K)	Loss (%) Weight	Diameter	Height	Measured Loss in Height (mm)
HF-162	Y_2O_3	1700 1830	3.33 1.88 5.21	1563	+0.3	0.0	3.0	0.28
HF-163	Y_2O_3	1830 1900 2000	7.0 4.25 1.18 12.43	1486	-	-	-	-
HF-164	Ni 270 Sprayed with LaB_6	1700 2000	2.67 4.6 7.27	1452	0.16	+0.29	+0.19	+0.03
HF-165	CaB_6	1700 1900 2000 2100 2215	3.0 2.25 2.25 1.25 3.58 12.33	1542	6.1	0.2	0.8	0.08
HF-166	CaB_6	2215	34 s	-	-	-	-	-
HF-167	CaB_6, HF-165	1700 1900 2100 2320 2550	1.75 2.42 2.75 2.58 2.2 11.7	1924	4.1	0.8	-7.5 to +2.1	0.74
HF-168	Poco Graphite Sprayed with LaB_6	1700 1900 2100	2.17 2.0 3.0 7.17	1510	0.3	0.1	0.6	0.08
HF-169	CaB_6	1700 1900 2100 1900 1700	1.42 1.83 3.75 1.17 1.0 9.17	1527	4.5	2.0	0.8	0.08
HF-170	W-Ni-Fe Sprayed with LaB_6	1700 1900 2215	1.92 2.33 4.18 8.43	1428	0.5	0.1	0.2	0.03
HF-171	LaB_6	2395 2550 2853 2853+	2.42 1.75 6.83 11.0	2041	9.2	2.2	3.3	0.46
HF-172	ATJ Graphite Plate with 1.016-mm (38- to 40-mil)-Diameter Holes	1900	6.5	1577 Max	2.02	-	5.8	0.23

ed)

ter	Height	Measured Loss in Height (mm)	Remarks
	3.0	0.28	Specimen split, melting occurred to weld the two pieces together.
	-	-	Specimen cracked into three pieces after breakpoint. Apparent breakpoint 1340 K.
	+0.19	+0.03	LaF_3 coating on side had cracks; coating on top separated.
	0.8	0.08	Specimen had a white adherent film except in area of vertical support posts.
	-	-	Specimen broke into three pieces.
	−7.5 to +2.1	0.74	Fluoride film had mostly melted off the top surface; some melt adhered to the side. Apparent breakpoint 1661 K.
	0.6	0.08	Fluoride layer cracked on top in a ring approximately 1.59 mm (1/16 in) from OD; probably occurred during cooldown.
	0.8	0.08	Specimen had white adherent coat on it, except on bottom.
	0.2	0.03	Top LaF_3 was cracked and was peeling off. Bottom may have reacted since it had not been sprayed.
	3.3	0.46	Droplets were seen before breakpoint was recorded. Specimen support and thermocouple melted. No LaF_3 obvious on specimen. Specimen had metallic and copper-colored lumps on it. Apparent breakpoint 1738 K.
	5.8	0.23	CF_4 experiment in graphite configuration test chamber. Holes in plate increased from 1.016- to 1.778-mm (40- to 70-mil)- diameter. Breakpoint temperature reached after approximately 5 min in the run. Apparent breakpoint 1143 K.

Table C-1 (continued)

Run	Material	Theoretical Flame Temperature (K)	Duration of Run (min)	Sample Surface Temperature[1] (K)	Loss (%)			Measured Loss in Height (mm)
					Weight	Diameter	Height	
HF-173	LaB_6 Plasma-Sprayed Plate with 1.016-mm (36- to 40-mil)-Diameter Holes	1700 1900	2.92 1.8 4.72	1567	0.78	-	+2.5	+0.1
HF-174	LaB_6 Plasma-Sprayed Disk with 1.016-mm (36- to 40-mil) Diameter Holes	1700 1900	3.17 4.28 7.45	No Indication	-	-	-	-
HF-175	Plate from HF-173	1700 1900 2100	2.5 1.83 4.00 8.33	1493	1.14	+0.007 to -0.02	3.1 to 6.1	0.13 to 0.26
HF-176	ATJ Graphite Plate with 1.016-mm (36- to 40-mil)-Diameter Holes	1900	6.75	1429 Max	1.3	0	5.7	0.23
HF-178	LaB_6, Dense	1700 to ≈ 3300	1.67 6.33 8.00	1416	0.03	0	+0.18	+0.025
HF-179	LaB_6, Dense	1700 to ≈ 1383	11.0	1103	0.13	0	0.18	0.025
HF-180	LaB_6, HF-178	≈ 3158	6.75	1493	0.35	0	0.0	0.0
HF-187	Ni-200 Plate	1700 1830	5.83 2.17 8.00	(5)	-	-	-	-
HF-188	Dense LaB_6 Plate	1700	2.38	No Indication	-	-	-	-
HF-200	Dense LaB_6 Plate	1700 2000	3.08 1.92 5.00	1586	-	-	-	-
HF-201	Yttria Doped Nickel	1700 1830	1.67 7.33 9.00	1442	1.08	0	0.41	0.05
HF-202	Yttria Doped Nickel	1700 1900 2000	2.83 4.00 2.67 9.50	1671	16.3	-	-	-

(1) Window corrections added range from 15 to 40°C.
(2) Low reading due to dirty sight glass.
(3) Highest thermocouple reading in center of specimen at point nearest the top surface.
(4) Includes tip of thermocouple.
(5) Plate showed signs of melting; nickel melting point is 1728 K.

	Height	Measured Loss in Height (mm)	Remarks
	+2.5	+0.1	Configuration test chamber experiment: graphite chamber was plasma sprayed with LaB_6. A crack developed in the plate and holes enlarged to approximately 1.09 mm (43 mil). A portion of LaB_6 coating in chamber peeled off; LaB_6 coating on deflection ring separated.
	-	-	Specimen cracked in about 4 min and some pieces fell to bottom of reactor. Conducted in plasma-sprayed graphite test chamber.
02	3.1 to 6.1	0.13 to 0.25	Configuration test chamber experiment—unsprayed graphite chamber. Vapors observed inside chamber during run. Crack had increased in size. Holes increased in size to 1.17-mm (46-mil)-diameter.
	5.7	0.23	CF_4 experiment with graphite configuration test chamber. After 5.75 min, a slow burn-off of the white film was seen. Hole diameters increased to an average of 1.17 mm (46 mil). Apparent breakpoint 1195 K. Chamber had cracked; sapphire window had etched; chamber looked as if it had reacted with gases.
	+0.18	+0.025	Specimen had a thin, light grey coating except for two areas on the bottom where it rested on LaB_6 chips.
	0.18	0.025	Specimen had a white coating except for two unreacted areas on the bottom.
	0.0	0.0	Specimen had a thin, light grey coating except for two unreacted areas on the bottom.
	-	-	The 1.016-mm (40-mil)-diameter holes were enlarged to 2.29- to 2.41-mm (90- to 95-mil)-diameter; corrosion and some melting of the plate occurred. Plasma-sprayed LaB_6 liner in chamber had cracked but remained in position. LaF_3 layer on deflection ring cracked.
	-	-	Plate appeared to crack immediately and had several cracks; one crack originated at a bolt hole. The LaB_6 liner had additional cracks.
	-	-	Plate split into two almost immediately. Cracked LaB_6 liner remained in position.
	0.41	0.05	Flame was off-center. A small area on the top surface had probably been molten and slightly ran over the edge of specimen. Top surface became gray with large grains evident.
	-	-	Specimen melted at 1561 K, drops were rolling over the edge of specimen; onset of fluidity approximately 1289 K.

APPENDIX D

TABLES, FIGURES, AND BIBLIOGRAPHY

Table D-1

SUMMARY OF PHYSICAL AND CHEMICAL PROPERTIES OF LANTHANUM HEXABORIDE[1]

Property	Units	Temperature	Value	Remarks
Formula Weight	g	-	203.78	
Color	-	-	-	Purple, metallic-like.
Density	g/cm^3	298	4.079	By X-ray.
Structure	-	-	-	Cubic, space group Pm3m.
Lattice Parameter	A	298	4.1573 ± 0.001	
Heat of Formation, $\Delta H^\circ_{f,298}$	kcal/mol	298	30.7	
Heat Capacity, Cp	cal/(mol-K)	298	23.22	See Figure D-1.
Thermal Conductivity, K	cal/(s-cm-K)	300	0.114 ± 0.01	See Figure D-2.
Thermal Diffusivity, α	cm^2/s	300	0.177	See Figure D-1.
Average Coefficient of Linear Thermal Expansion, α	K^{-1}	-	$6.4 \pm 0.5 \times 10^{-6}$ (293 to 1073 K)	By X-ray, see Figure D-3.
			$7.4 \pm 0.5 \times 10^{-6}$ (293 to 873 K)	By X-ray, see Figure D-3.
Melting Point	K	-	2988	
Vapor Pressure of La over LaB_6	Pa	1993	9.07×10^{-3}	
Vapor Pressure of B over LaB_6	Pa	1993	4.97×10^{-3}	
Rate of Evaporation	$g/(cm^2/s)$	1993	1.54×10^{-6}	
Crystal Lattice Energy U	kcal/mol	-	1770	
Debye Temperature, Θ	K	-	886	
Root-mean-square Amplitude of Thermal Vibrations of Atom Complexes, $(\bar{\mu}^2_{291})^{1/2}$	A	291	0.042	
Electrical Resistivity	Ω-cm	293	7×10^{-6}	
Thermal Coefficient of Electrical Resistance	K^{-1}		$+2.68 \times 10^{-3}$ (273 to 373 K)	
Coefficient of Thermal EMF	μV/K	-	7.0	
Electronic Work Function	eV	-	2.68	
Richardson Constant	$Amps/cm^2\text{-}K^2$	-	29	
Coefficient of Secondary Emission	-	-	0.95	
Hall Constant, R	cm^3/coulomb	-	-4.96×10^4	
Magnetic Susceptibility	mol^{-1}	-	60×10^{-6} (293 to 673 K)	
Effective Magnetic Moment	Bohr magnetons	-	9.0	
Normal Spectral Emittance at $\lambda = 0.65$ μm	-	-	0.82 (1073 to 1973 K)	
Microhardness	kg/mm^2	-	2065 (100-g load)	

Hall Constant, R	cm^3/coulomb	-	-4.56 X 10^{-4}	
Magnetic Susceptibility	mol^{-1}	-	60 X 10^{-6} (293 to 873 K)	
Effective Magnetic Moment	Bohr magnetons	-	9.0	
Normal Spectral Emittance at λ = 0.65 μm	-	-	0.82 (1073 to 1973 K)	
Microhardness	kg/mm^2	-	2065 (100-g load)	
Modulus of Elasticity	kg/mm^2 (msi)	-	41.0 to 48.8 (58.3 to 69.4)	Maximum values reported.
Bending Strength, MOR	kg/mm^2 (ksi)	-	12.9 to 35.0 (19.3 to 49.8)	Maximum values reported.
Reagent Resistance	-	293	-	Nearly insoluble in 1:1 concentrated acid: H_2O dilution HCl, H_2SO_4, and 15% NaOH solution; completely soluble in 1:1 dilution HNO_3 or HNO_3 mixed with HCl or H_2SO_4.
Machining Techniques				1. Diamond-tool grinding, sawing, or polishing. 2. Electrical discharge machining. 3. Electrochemical machining. 4. Electrochemical grinding. Electrolytes for latter two techniques suggested are 2.5N NH_4NO_3 or NH_4NO_3 mixed with Na_3PO_4.

(1) Data from primary lanthanum hexaboride reference, Table D-2.

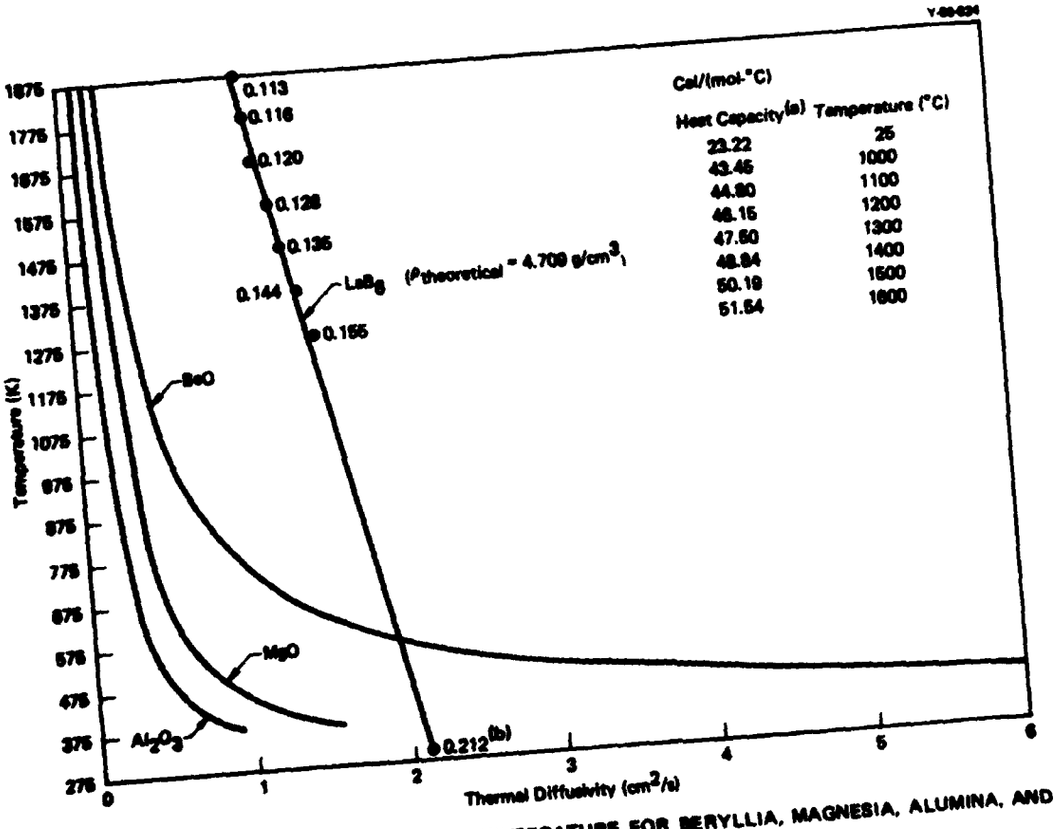

Figure D-1. THERMAL DIFFUSIVITY VERSUS TEMPERATURE FOR BERYLLIA, MAGNESIA, ALUMINA, AND LANTHANUM HEXABORIDE.

[a]See Gerdienko, S. P., Gusova, E. A., and Fesenko, V. V. in Bibliography.
[b]See L'vov, S. N. in Bibliography.

Source: Reference 18 for LaB6 except as noted in footnotes a and b.

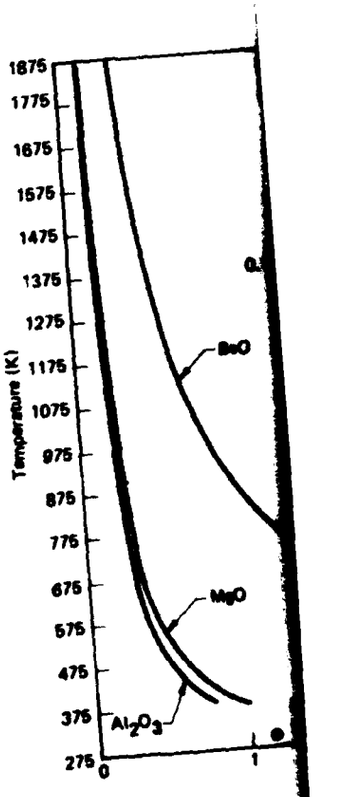

Figure D-2. THERMAL CONC
LANTHANUM HEXABORIDE

[a]See L'vov, S. N. in Bibliograp

Source: Reference 18 for LaB

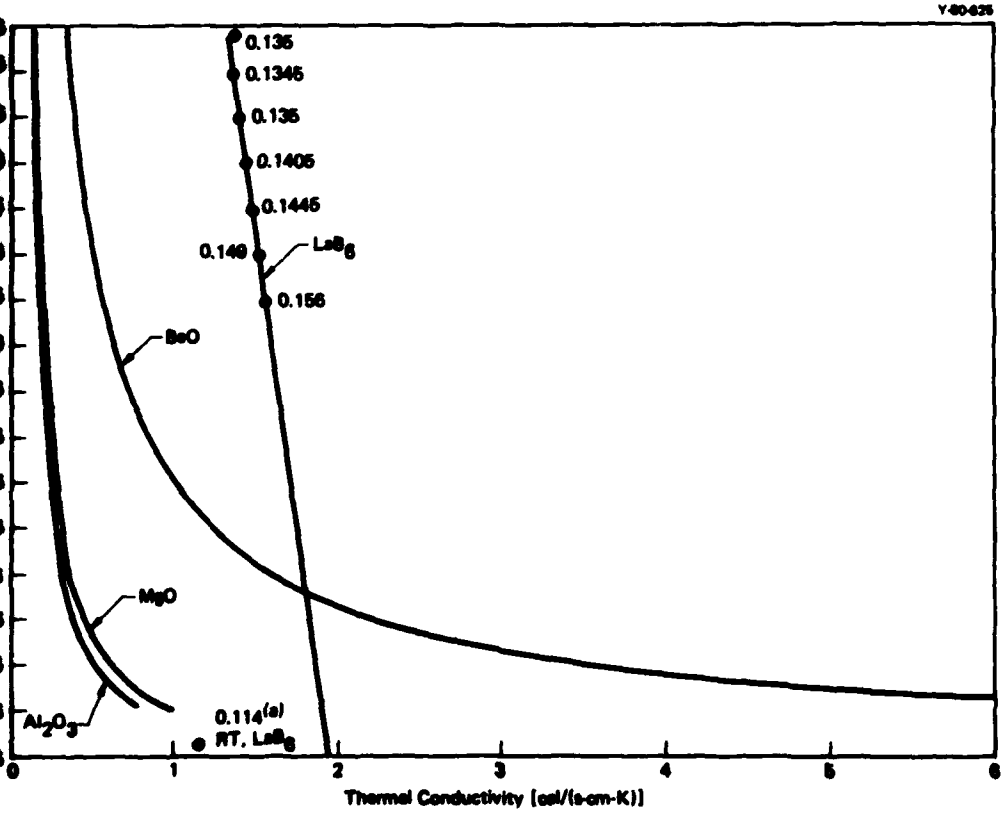

D-2. THERMAL CONDUCTIVITY VERSUS TEMPERATURE FOR BERYLLIA, MAGNESIA, ALUMINA, AND ANUM HEXABORIDE.

'vov, S. N. in Bibliography.

Reference 18 for LaB_6 data except as noted in footnote a.

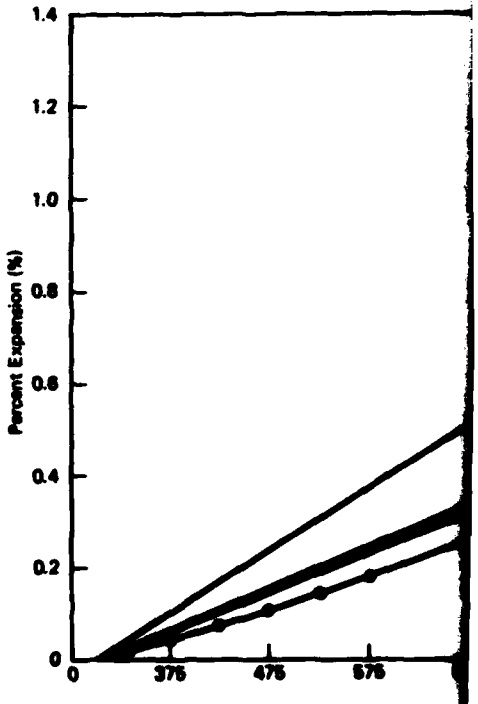

Figure D-3. THERMAL EXPANSION VERSUS LANTHANUM HEXABORIDE.

Source: Reference 17 for LaB_6 data.

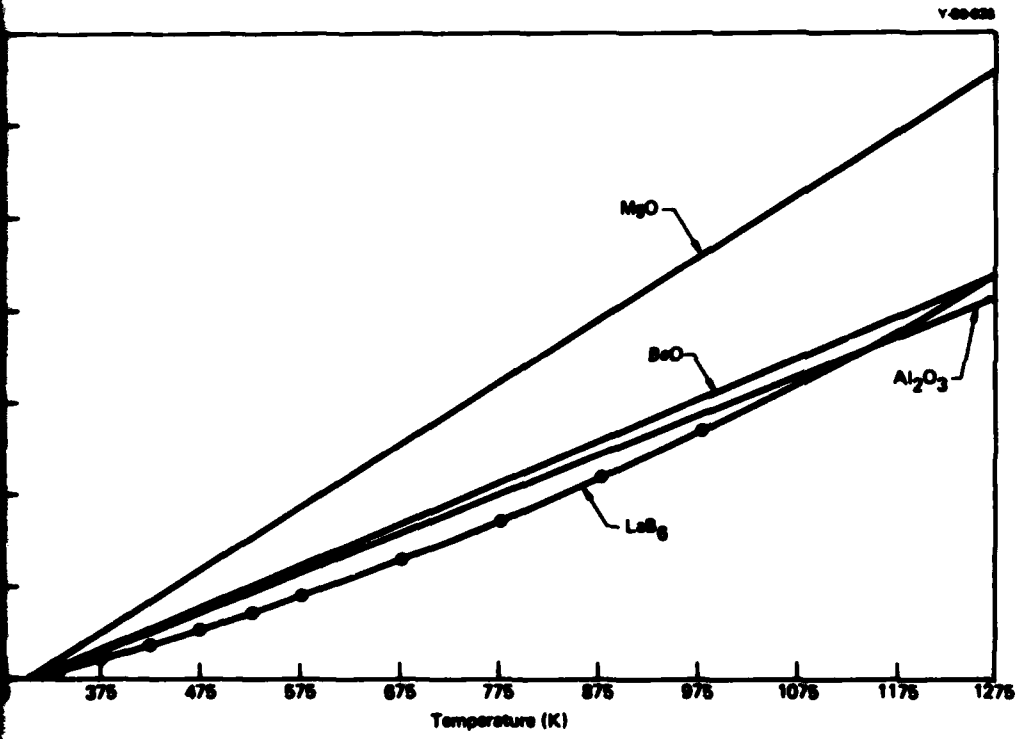

D-3. THERMAL EXPANSION VERSUS TEMPERATURE FOR BERYLLIA, MAGNESIA, ALUMINA, AND ANUM HEXABORIDE.

Reference 17 for LaB_6 data.

Table D-2

BIBLIOGRAPHY

Ames, L. L. and McGrath, L.; "Vaporization Studies on the Rare Earth Hexaborides," ***High Temperature Science***, 7, pp 44 - 54 (1975).

Arabei, B. G., Shtrom, E. N., and Lapitskii, Yu. A.; "Characteristics of the Manufacturing Technology of Dense Parts from, and the Mechanical Properties of, Some Hexaborides of the Rare-Earth Metals," ***Powder Metallurgy*** (***Poroshkovaya Met***, Russian translation), 5 (23), pp 406 - 490 (1964).

Binder, F.; "Contribution to the Knowledge of Cubic Hexaborides," ***Radex-Rundschau***, 1, pp 52 - 71 (1977).

Curtis, B. J.; "The Precipitation of Graphite from the Hexaborides of Some Rare Earth Elements and Yttrium," ***Carbon***, 4, pp 483 - 488 (1966).

Dutchak, Ya. I., Fedyshin, Ya. I., and Paderno, Yu. B.; "Thermal Properties of Metallic Hexaborides," ***Inorganic Materials*** (***Neorg Matl***, Russian translation), 8 (12), pp 1877 - 1880 (1972).

Fesenko, V. V. and Bolgar, A. S.; "Evaporation Rate and Vapor Pressure of Carbides, Silicides, Nitrides, and Borides," ***Powder Metallurgy*** (***Poroshkovaya Met***, Russian translation), 1 (13), pp 11 - 17 (1963).

Gordienko, S. P., Guseva, E. A., and Fesenko, V. V.; "Thermodynamic Properties of Lanthanum Hexaboride," ***High Temperature*** (***Teplofizika Vysokikh Temp***, Russian translation), 6, pp 785 - 789, 821 - 825 (1968).

Gordienko, S. P., Samsonov, G. V., and Fesenko, V. V.; "The Evaporation of Lanthanum Hexaboride," ***Powder Metallurgy*** (***Poroshkovaya Met***, Russian translation), 8 (32), pp 661 - 663 (1965).

Kapyrina, V. Ya., Prilepskii, V. N., Timofeev, V. A., Timofeeva, E. N., and Trubitsyn, A. Ya.; "Enthalpy and Heat Capacity of Lanthanum Hexaboride at Temperatures of 1100 - 2200 K," ***High Temperature*** (***Teplofizika Vysokikh Temp***, Russian translation), 6, pp 188 - 189 (1968).

Kosolapova, T. Ya. and Domasevich, L. T.; "Chemical Properties of Lanthanoid Boride Powders," ***Powder Metallurgy*** (***Poroshkovaya Met***, Russian translation), 5 (89), pp 353 - 356 (1970).

Kuznetsova, G. M., Kudintseva, G. A., Khacheva, T. K. L., and Suchkov, L. K.; "Production of Large-Sized Lanthanum Hexaboride Parts," ***Ibid.*** 10 (118), pp 810 - 814 (1972).

Lafferty, J. M.; "Boride Cathodes," ***Journal of Applied Physics***, 22 (3), pp 299 - 309 (1951).

Lavrenko, V. A., Glebov, L. A., Lugovskaya, Y. S., and Frantsevich, I. N.; "Investigation of High-Temperature Oxidation of Lanthanum Hexaboride in Oxygen and the Effect of Internal Oxidation on the Protective Properties of the Scale," ***Oxidation of Metals***, 7 (2), pp 131 - 139 (1973).

L'vov, S. N., Nemchenko, V. F., and Paderno, Yu. B.; "The Thermal Conductivity of Alkaline Earth and Rare Earth Metal Hexaborides," translation from ***Dokl Akad Nauk USSR***, 149 (6), pp 353 - 354 (1963).

Meerson, G. A. and Mamedov, F. G.; "Investigation of Sintering Conditions for Lanthanum Hexaboride," ***Inorganic Materials*** (***Neorg Mat***l, Russian translation), 3, pp 844 - 850 (1967).

Meerson, G. A., Manelis, R. M., and Telyukova, T. M.; "Peculiarities of the Production of Objects from Lanthanum and Yttrium Hexaborides by Sintering Under Vacuum," ***Ibid.*** 2, pp 250 - 255 (1966).

Meerson, G. A., Nurmukhamedov, V. Kh., and Manelis, R. M.; "Thermodynamics of LaB_6 Formation by the Borothermal Reaction," ***Ibid.*** 9 (12), pp 1884 - 1885 (1973).

Mordovin, O. A. and Timofeeva, E. N.; "Rare-Earth Element Hexaborides," ***Russian Journal of Inorganic Chemistry***, 13 (12), pp 1627 - 1629 (1968).

Samsonov, G. V.; ***High-Temperature Compounds of Rare Earth Metals***; Consultants Bureau, New York (1965).

Samsonov, G. V.; ***High-Temperature Materials, No 2, Properties Index***; Plenum Press, New York (1967).

Samsonov, G. V., Paderno, Yu. B., and Fomenko, V. S.; "Hexaborides of the Rare Earth Metals," ***Powder Metallurgy*** (***Poroshkovaya Met***, Russian translation), 6 (18), pp 449 - 454 (1963).

Samsonov, G. V., Paderno, Yu. B., and Kreingold, S. U.; "Preparation of Lanthanum Hexaboride," ***Journal of Applied Chemistry of USSR*** (***Zhur Prikl Khim***, Russian translation), 34 (1), pp 8 - 13 (1961).

Shlyuko, V. Ya. and Chernyak, L. V.; "Investigation of the Sintering Conditions of Parts Made of Lanthanum Hexaboride," ***Powder Metallurgy*** (***Poroshkovaya Met*** Russian translation), 12, pp 969 - 972 (1967).

Tanaka, T.; "The Thermal and Electrical Conductivities of LaB_6 at High Temperatures," ***Journal of Physics***, 7, pp 177 - 180 (1974).

Timofeeva, I. I. and Timofeeva, E. N.; "Physicochemical Properties of Lanthanide Hexaborides," ***Inorganic Materials*** (***Neorg Matl***, Russian translation), 4, pp 1559 - 1561 (1968).

Zhuravlev, N. N., Belousova, I. A., Manelis, R. M., and Belousova, N. A.; "X-ray Determination of the Expansion Coefficients of Lanthanum and Yttrium Borides," ***Russian Crystallography*** (***Kristallografiya***, Russian translation), 15 (4), pp 723 - 724 (1971).

Zhuravlev, N. N., Stepanova, A. A., Paderno, Yu. B., and Samsonov, G. V.; "X-ray Determination of the Expansion Coefficients of Hexaborides," ***Ibid.*** 6 (5), pp 636 - 638 (1961).

Distribution

AFOSR/NE
Simmons, W. S., Major

Air Force Materials Laboratory - Wright-Patterson Air Force Base
Graham, H. C. (2)
Mazdiyasni, K. S.

Air Force Weapons Laboratory - Kirtland Air Force Base
Olson, D. (2)
Pchelkin, N. (2)

Altantic Research Corporation
MacPherson, J. R.

AMMRC
Katz, R.

Babcock and Wilcox
Davis, H. H.

Battelle-Columbus Laboratory
Willis, R.

Bell Aerospace Company
Anthony, F.
Conn, P. K.
Solomon, W.

Bendix - Kansas City
Kessler, R. E.

Carborundum Company
Coppola, J.
Weber, G. W.

Chemetal Corporation
Holzl, R. A.

Defense Advanced Research Projects Agency Material Sciences
Bement, A.
Ruby, S.
Winsor, H. (2)

Defense Documentation Center - Cameron Station

Department of Energy - Albuquerque
Meyer, H. N., Jr./Whiteman, A. E.

Department of Energy - Oak Ridge
Hickman, H. D.
Poteat, R. M.

Department of Energy - Washington
Hoover, W. W.
Sander, S. M.

Deposits and Composites, Inc.
Engdahl, R.

IIT Research Institute
Larsen, D. C.

Jet Propulsion Laboratory
Leipold, M.

Lawrence Livermore National Laboratory
Arnold, W. F.
Carr, R. B./Wraith, C. L.
Craig, R. J.
Dittman, G. L./Jepson, J. O.
Hoenig, C. L.
Humphrey, J. R.
Landingham, R. L.
Ludwig, E. R.
Olander, D.
Rizzo, H. F.
Robbins, J. L.
Root, G. S.
Seilheimer, R. A.
Staehle, G. G./Lyle, J. W.
Stock, R. P./Golopol, H. A.
Woodruff, R. D./Grissom, M. L.
Technical Information Division

Lehigh University
Spriggs, R. M.

Los Alamos National Laboratory

Aragon, J.
Baker, R. D.
Deinken, H. P.
Eyster, E. H./Wechsler, J. J.
Feber, R. C., Jr.
Hockett, J. E.
Hoyt, H. C.
Larson, T. E.
Library Services
Sandford, T. A.
Sandstrom, D. J./Catlett, D. S.
Skaggs, S. R.
Stoddard, S. D.
Wagner, P.
Wallace, T. C.

Monsanto-Mound Facility

Records Management

NASA-Lewis Research Center

Ashbrook, R. L.
Probst, H.

National Bureau of Standards - Maryland

Wachtman, J.

National Bureau of Standards - Washington, D.C.

Wiederhorn, S. M.

National Science Foundation - Arlington

Wilcox, B. A.

Naval Air Systems Command

Machlin, I.

Naval Research Laboratory

Rice, R. W.

Oak Ridge Gaseous Diffusion Plant

Armstrong, R. C.
Barber, E. J.
Hale, C. F.
Merriman, J. R.
Stief, S. S.
Wilcox, W. J., Jr.

Oak Ridge National Laboratory

Brynestad, J.
Hopkins, C. C.
Weir, J. R., Jr.

Oak Ridge Y-12 Plant

Burditt, R. B.
Condon, J. B.
Dodson, W. H./Googin, J. M.
Dow, N.
Duerksen, W. K.
Fraser, R. J.
Haeusler, K. R.
Holcombe, C. E., Jr. (15)
Jessen, N. C., Jr.
Keith, A.
Kite, H. T.
Koger, J. W.
Mills, J. M., Jr.
Montgomery, C. D.
Morrow, G. B.
Tewes, W. E.
Y-12 Central Files (master copy)
Y-12 Central Files (route copy)
Y-12 Central Files (Y-12RC)
Y-12 Central Files (5)

Paducah Gaseous Diffusion Plant

Bewley, H. D.

Rice University

Margrave, J. L.

Rocketdyne

Carpenter, H.

Rocket Propulsion Laboratory

Dean, J.

Rockwell International - California

Lange, F.

Rockwell International - Rocky Flats

Floyd, D. R.
O'Brien, M.
Weidner, C. W.
Wiederecht, D. A.

SAMSO

Doughty, J. R.

Sandia National Laboratories - Albuquerque

Claassen, R. S.
Heilman, L. J.
Hillman, J. T.

Sandia National Laboratories - Livermore

Adolphson, D. R.
Schuster, D. M.
Spencer, W. J.
Technical Library

Savannah River Laboratory

Turno, D. H.

Stanford Research Institute

Hildenbrand, D. L.

TRW/DSSG

Ackerman, R.
Mace, J.

Union Carbide Corporation - New York

Tinsley, S. W.

United Technologies Research Center

Chalfante, A.
Decresenti, M.
Grose, R.

U.S. Army Missile Research and Development Command - DRDMI - HAL

Clapp, S.
Walters, J.

U.S. Army Research Office - Durham

RDRD-IP

Yale University

Nordine, P. C.

In addition, this report is distributed in accordance with the Category UC-25, Materials, as given in the *Standard Distribution for Unclassified Scientific and Technical Reports*, DOE/TIC-4500.

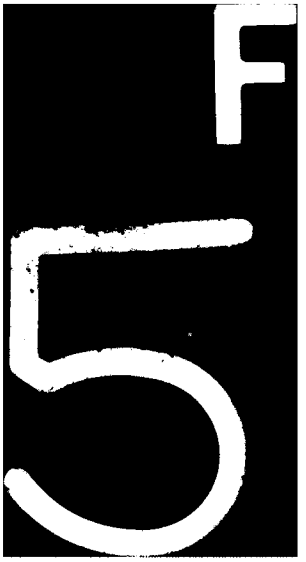
5F